# A study of secondary winding designs for the two-coil Tesla transformer

Richard Miles Craven

A Doctoral thesis submitted in partial fulfilment of the requirements for the award of Doctor of Philosophy of Loughborough University

I certify that I am responsible for the work submitted in this thesis, and that the original work is my own except as specified in acknowledgements or footnotes. Neither the submission nor the original work contained therein has been submitted for an award of this or any other degree awarding body.

Signed:

Date: 20th March 2014

**Abstract**

The multi-order response of the tuned secondary circuit of a Tesla transformer, following impulse excitation from its tuned primary circuit, is presented and analysed at the fundamental resonant frequency and at higher-order mode frequencies. A novel way of modifying the frequency response of the secondary coil is then investigated by utilising a technique normally applied to the design of a certain type of filter known as a helical filter. In general, these are used in radio and microwave frequency circuits in order to pass certain frequencies with little attenuation whilst significantly attenuating other frequencies. Design techniques, developed over several decades, modify and optimise the performance of such filters. The frequency response of the helical filter is modified by altering the geometry of the helical resonator component therein, which is typically in the form of an air-cored single-layer solenoid. A Tesla transformer whose secondary is constructed to be some form of single-layer solenoidal winding resonates at its designed frequency - its fundamental mode - but also at non-integer harmonics (higher-order "anharmonic" frequencies, also known as overtones). Those multi-order oscillatory voltages and currents energised in the secondary circuit have been identified and measured and research has determined the fundamental and higher-order mode frequencies and amplitudes for various experimental secondary winding configurations derived from helical filter design techniques. Applied to the Tesla transformer secondary winding, such techniques lead to a new design

with a performance that is improved by the suppression of higher-order anharmonic frequencies whilst imparting little change to the fundamental response. It is anticipated that this feature will lead to Tesla transformers which exhibit enhanced spectral purity and which will be better suited to use in certain pulsed power applications than conventionally wound designs.

Acknowledgements

I would like to thank my supervisor Professor I.R. Smith for his initial suggestion that I embark on a part-time doctorate, and for his continuous encouragement, unstinting patience, advice and guidance throughout. Invaluable assistance was afforded to me regarding my learning of Linux and writing of “Bash” scripts by my good friend David J. Singer who was, and continues to be, relentlessly patient. In a similar vein, Paul Nicholson extended excellent assistance and advice to me regarding his TSSP software programs, as did Neoklis Kyriazis who helped me by modifying his NEC software, and David Knight for extremely useful email correspondence. A number of former and present colleagues assisted with suggestions, computer resources, and loans of components and test and measurement equipment mentioned in chapter five. Along similar lines, Carl Bradbury of Tektronix UK and Simon Coleby of Agilent UK have been superlatively helpful in assisting with equipment loans and repair. My wife Jane, a virtual PhD widow, has exhibited endless patience whilst we have moved house twice during this period of part-time study, and she has had to endure parts of our house becoming a laboratory. My parents, who have tolerated various high voltage experiments in their house during the last thirty or more years, must take ultimate credit for allowing me the opportunity to develop these interests.

# Contents

# List of Figures

# List of Tables

# Glossary

| | |
|---|---|
| $\mathcal{H}$ | the height of a vertically mounted resonant structure e.g. a helix in a cavity or a Tesla transformer secondary winding |
| $f_1$ | frequency of the fundamental response (mode) of a helical resonator |
| $f_3$, $f_5$ | frequencies of the next two anharmonic responses (modes) of a helical resonator |
| $Q$ | Q factor, quality factor |
| anharmonic | non-integer multiple of the $f_1$ (fundamental) resonant frequency of a resonator; see *overtone* |
| Bash | Bourne again shell, a command-line interpreter (shell) which provides a user interface for the Linux operating system |
| E | vector field quantity representing electric field strength |
| EMI | electromagnetic interference |
| ESA | electrically small antenna |

| | |
|---|---|
| FSS | frequency selective surface |
| GUI | graphical user interface |
| H | vector field quantity representing magnetic field strength |
| helical filter | a filter which employs a helical resonator inside a conducting cavity as a high Q factor element |
| heliconical | a cylindrical cross-section helix whose diameter tapers from one end to the other |
| helix | helical resonator, coil: a three dimensional structure consisting of a conductor wound at a fixed radius about an axis. |
| ITU | international telecommunications union |
| Linux | a Unix-like computer operating system |
| modes | wavelength-related spatial patterns of field maxima and minima, associated with alternating currents driving resonant transmission lines |
| NEC | numerical electromagnetics code, a free and open-source numerical modelling code |
| OLTC | off-line Tesla coil |
| overtone | non-integer multiple of the fundamental frequency of a system; see *anharmonic* |

| | |
|---|---|
| PEC | perfect electrical conductor, a theoretical electrical conductor which exhibits zero impedance at all frequencies |
| resonator | a physical structure which supports standing waves of alternating current and voltage. In this thesis, the term is used synonymously to mean an air-cored solenoid (simply, a coil) or helix |
| RFI | radio frequency interference |
| s-parameter | scattering parameter; matrix elements which describe the response of a linear electrical network when it is subjected to steady-state electrical currents |
| solenoid | a single layer of wire, wound onto a cylindrical cross-section former, to make a conducting helix |
| SSTC | solid state Tesla coil, using semiconductors rather than thermionic valves or spark gaps as the primary switch |
| Tesla | the SI unit of magnetic flux density in webers per square metre, named after Nikola Tesla (1856-1943) |
| topload | a conducting surface with a large radius of curvature, designed to act as an electric field grading structure to prevent electrical breakdown |
| toroid | an annular solid described by a cylinder whose long axis is bent into a circle such that the cylinder's open ends become joined to one another |

| | |
|---|---|
| TSSP | Tesla secondary simulation project |
| VNA | vector network analyser |
| Wine | a compatibility layer which allows Windows executables to run in a Linux environment |

# Chapter 1

# Thesis aims and methodology

The aim of this thesis is to investigate and analyse the application of helical filter design techniques to Tesla transformers. The proposition is that a new design of Tesla transformer will evolve whose performance is improved by suppressing modes at overtone frequencies whilst leaving the fundamental unaffected, thus developing an improvement in the spectral purity of the transformer output. Such designs may find utility in those applications where harmonic purity is advantageous. For example, substantial pulsed power research within the UK Ministry of Defence's research body, the Defence Science and Technology Laboratory [Dstl], may benefit.

The background and theory of operation of a conventional two-coil Tesla transformer was studied. Alterations were made to the secondary coil of the transformer in the form of its winding sense, whereby a proportion of turns were wound in a clockwise direction whilst the remainder were wound in a counterclockwise direction. It is proposed that reversing the secondary winding sense for some

proportion of turns will modify the distribution of currents in the secondary winding, in itself causing a change in the response of this winding to any stimulus from the coupled primary. A program of comparison measurements and modelling was implemented to qualify developed theories and to test their validity. A variety of software modelling programs supporting aspects of this work are discussed later.

Chapter seven of Vizmuller [1] demonstrates methods by which standing waves can be suppressed on structures which have electrical dimensions of a quarter of a wavelength. His approach exploits changes in the winding sense of a resonant helical coil. Having studied this work, it was decided that aspects of winding sense should be considered as a candidate for modifying the frequency response of the Tesla transformer secondary. This approach sets the basis for the study and measurement reported in this thesis.

The following assertions were of great value in the development and experimental work of the thesis:

- The quality factor ($Q$) of a circuit or circuit element is a description of the energy stored in it compared with the energy lost by it, per unit time.
- The $Q$ of an equivalent resonant circuit determines the voltage across the reactive parts of the secondary winding and determines the current circulating in the reactive parts.
- For an air-cored single-layer solenoid, $Q$ varies with frequency (and may even increase as frequency increases, over a limited bandwidth).

- If $Q$ is unchanged at the fundamental frequency but reduced at overtone frequencies, the current and voltage waveforms associated with the output power from a Tesla transformer experience a corresponding reduction in overtone frequency content.

- Construction and characterisation of a typical air-cored single-layer solenoidal inductor (e.g. a Tesla transformer secondary winding), in comparison with similar coils constructed using helical filter design techniques, will enable differences in frequency response to be investigated.

- Modelling of both standard and experimental coils alongside a literature investigation pertaining to currents flowing in helically wound conductors allows design parameters to be discerned.

## 1.1 Software modelling

During the initial stages of this thesis it became apparent that a variety of numerical modelling tools could add significant insight and hopefully veracity to support the numerous measurements that would need to be made. However, the cost of some of the modelling software was identified as prohibitively expensive*, and an interesting notion arose†: could useful modelling results be achieved during this research, solely by the use of zero-cost software?

*HFSS, a commercial electromagnetic (EM) structure modelling package from Ansys, costs in excess of £10,000 (February 2013) with an annual maintenance fee of several thousand pounds

†suggestion by author's wife, 2011

One source of free software [2] utilised the GNU/Linux operating system (abbreviated for the purposes of this thesis as “Linux”). Given that Linux is a free operating system, it became apparent that a variety of other programs, if they could be run under Linux, could form the basis of an entirely free yet comprehensive suite of applications to aid in the understanding of helical resonators and their behaviour when used as a Tesla transformer secondary winding. A brief discussion follows of the main software packages that were used; all are zero-cost.

### 1.1.1 4nec2, xnec2c, nec2c, nec2c-rxq

The Numerical Electromagnetics Code (NEC) (p. 397 of [3]) employs a boundary element method of solution known as the Method of Moments (MoM) which is discussed in appendix (A). MoM is valid for the analysis of thin, perfectly conducting wires in any arbitrary 3D arrangement, such as resonant single-layer solenoidal coils wound from conductors where the length of the conductor is very much greater than the conductor diameter. Various electrical properties can be determined such as the complex input impedance of a conducting structure subjected to an alternating current source, or its near-field (or far-field) electric and magnetic field distributions.

4nec2 [4] is a free NEC2-based modelling and analysis program which, via a comprehensive graphical user interface, allows easy programming of the NEC2 core. It can generate models of 3D conducting structures and simulate and display numerous properties such as near-field and far-field electric/magnetic radiation patterns. 4nec2 is written to be run on a Microsoft Windows operating system (OS). Wine, a free application written for Linux, allows Windows-based

programs (e.g. 4nec2) to be run on Linux.

nec2c [5] runs in a Linux terminal session, where the executable code is presented with a pre-compiled input file and generates an output file. In contrast, xnec2c [6] is a graphical and interactive equivalent of nec2c which also runs on Linux; xnec2c reads input files as per nec2c but does not produce an output file, instead generating graphs or field plots as output results.

nec2c-rxq [7] is derived from nec2c but is capable of being run on numerous CPU cores in parallel, enabling solutions to large problems to be found rapidly.

Frequency-domain modellers such as the NEC-based solvers mentioned or FEKO [8] represent free and costly packages respectively which utilise the MoM solution method. For completeness, a variety of other computation methods that exist are mentioned in appendix (A).

### 1.1.2 Gnuplot

Gnuplot [9] is a command-line driven graphing utility, available for and often included in Linux distributions[‡] (such as Linux Mint, see section (1.1.3)). Gnuplot was originally written (1986) to enable easy and interactive visualisation of mathematical functions and data. It is used as Octave's plotting engine (see section (1.1.5)). Gnuplot is also available on Windows operating systems.

[‡]a distribution is a Linux OS which includes a range of free software applications such as word processors, spreadsheets and so on

### 1.1.3 Linux ("Mint" distribution)

Linux Mint [10] (version 13, LM13) is a distribution based on a version of the GNU/Linux OS. It provides a familiar graphical user interface, built on a Linux kernel and utilising a family of libraries and utilities. A distinct advantage of Linux is the command-line "shell" which contains a substantial set of commands, enabling easy scripting and processing of text-based or numerical data. Included with Linux-based operating systems are numerous free software applications for authoring of documents, designing graphical images and diagrams etc.

### 1.1.4 LTSpice

LTSpice [11] (version IV as of February 2013) is a free SPICE[§] lumped component modelling tool released by Linear Technology (LT), a U.S. semiconductor manufacturer. LT describe their tool as a high performance simulator which allows schematic capture, circuit analysis and results, all implemented via a GUI. LTSpice is designed to run on a Microsoft Windows OS but can be run in a Linux operating system via Wine.

### 1.1.5 Octave

Octave (strictly, GNU Octave) [12] is an interpreted high-level mathematical programming language which runs on Linux and Microsoft Windows operating systems. It can numerically solve linear and nonlinear problems and provides extensive graphics capabilities

[§]SPICE (Simulation Program with Integrated Circuit Emphasis) was developed in the 1970s to simulate lumped component circuits

for data visualisation via Gnuplot (see section (1.1.2)).

### 1.1.6 QUCS

Qucs [13], a "Quite Universal Circuit Simulator", is a Linux open-source circuit simulator which utilises graphical schematic capture and enables a range of circuit simulations such as transient response, swept frequency response and s-parameter analysis to be undertaken. Simulation results can be displayed via a number of graph types, or via tables, or the results can be exported as numerical data for processing via Gnuplot or Octave.

### 1.1.7 RFSim99

RFSim99 [14] is a (now unsupported) tool, originally written for Microsoft Windows OS, which implements linear s-parameter based circuit simulation and analysis via graphical schematic capture, simulation, and manipulation of 1 port and 2 port s-parameter data. Again, Wine is used to run RFSim99 in Linux.

### 1.1.8 TSSP

TSSP [2], the "Tesla Secondary Simulation Project", is a toolkit of programs, designed to be compiled for Linux, which work together via plain ASCII data files to model accurately a single-layer solenoid operating perpendicular to a ground plane i.e. a configuration typically used as a resonating secondary coil in a Tesla transformer.

### 1.1.9 LyX and JabRef

For completeness and noting that this subsection discusses software which is not used for modelling, LyX [15] is an advanced open source document processor running on a Linux OS. It automates formatting according to predefined rules, resulting in typesetting consistency. LyX produces a high quality output suitable for academic publication using LaTeX which is an open source typesetting language. JabRef [16] is an open-source reference database manager used in conjunction with LyX to keep track of the numerous citations used throughout this work.

## 1.2 Author's publications

Arising directly from the work reported in this thesis, the following papers have either been published or submitted for publication or are in preparation:

- R.M. Craven, I.R. Smith and B.M. Novac. A study of resonator designs for the two-coil Tesla coil. *UK Pulsed Power Symposium*. Loughborough University, UK, P.3, March 2011.
- R.M. Craven, I.R. Smith and B.M. Novac. Optimizing the secondary coil of a Tesla transformer to improve spectral purity. *IEEE Transactions on Plasma Science*, 42(1) pp. 143–148, 2014.
- R.M. Craven, I.R. Smith and B.M. Novac. Quality factor measurements of air-cored solenoids. *Electronics Letters*. In preparation.
- R.M. Craven, I.R. Smith and B.M. Novac. Novel secondary windings for Tesla transformers. *UK Pulsed Power Symposium*. Loughborough University, UK, accepted for inclusion, March 2014.
- R.M. Craven, I.R. Smith and B.M. Novac. Improvements to secondary windings of Tesla transformers. *IEEE International*

*Power Modulator and High Voltage Conference (IPMHVC)*. Santa Fe, New Mexico, USA, submitted for inclusion, June 2014.

Other publications by the author are:

- R.M. Craven. Design improvements in Tesla coil performance. *Pulsed Power '97, IEE Colloquium on*. London, UK, pp. 38/1–38/3, 1997.
- P. Sarkar, B.M. Novac, I.R. Smith, R.A. Miller, R.M. Craven and S.W. Braidwood. A high rep-rate UWB source. *Proceedings of the Megagauss XI Conference*. London, UK, pp. 324-327, 2005.
- P. Sarkar, B.M. Novac, I.R. Smith, R.A. Miller, R.M. Craven and S.W. Braidwood. Compact battery-powered 0.5 $MV$ Tesla-transformer based fast-pulse generator. *IEE Pulsed Power Symposium*. London, UK, pp. 3/1-3/5, 2005.
- P. Sarkar, S.W. Braidwood, I.R. Smith, B.M. Novac, R.A. Miller and R.M. Craven. A Compact battery-powered 500 $kV$ pulse generator for UWB radiation. *IEEE Pulsed Power Conference.* Monterey, California, USA, pp. 1306-1309, 2005.
- P. Sarkar, S.W. Braidwood, I.R. Smith, B.M. Novac, R.A. Miller and R.M. Craven. A compact battery-powered half-megavolt transformer system for EMP generation. *IEEE Transactions on Plasma Science.* 34(5) pp. 1832–1837, 2006.
- P. Sarkar, I.R. Smith, B.M. Novac, R.A. Miller and R.M. Craven. A high-average power self-break closing switch for high repetition rate applications. *IET Pulsed Power Symposium*. Warrington, UK, pp. 62–65, 2006.
- P. Sarkar, B.M. Novac, I.R. Smith, R.A. Miller, R.M. Craven and S.W. Braidwood. A high repetition rate battery-powered 0.5 $MV$ pulser for ultrawideband radiation. *IEEE 27th International Power Modulator Symposium*. Washington, DC, USA, pp. 592–595, 2006.

# Chapter 2

# Introduction to Tesla transformers

> "Is there, I ask, can there be, a more interesting study than that of alternating currents?" (p.81 of [17])

A Tesla transformer (or Tesla coil*) is a type of high voltage air-cored resonant pulse transformer (p. 104-109 of [18], [19] and p. 276-296 of [20]) named after Nikola Tesla who was born in Smiljan, Croatia, in July 1856 (p. 13 of [21] and p. 91 of [22]). Tesla suffered tragedy at an early age when in 1861 his older brother died in a horse-riding accident, prompting a change in Tesla's behaviour which led to a degree of reclusiveness that was to remain with him for the rest of his life. Soon afterwards the family moved to a nearby town, Gospic, as a result of a promotion for Tesla's father, a clergyman (p. 6-7 of [23]).

As a young boy, Tesla developed a way of imagining ideas vividly; in later interviews for newspapers he recalled building a toy waterwheel in a stream near his home after a dream of great clarity and insight (p.

*Tesla coils are a typical colloquialism meaning an air-cored Tesla transformer

39 of [22]). Interestingly, Tesla may have suffered from a neurological condition now known as "synaesthesia", whereby stimulation of one sense (e.g. hearing) is translated to an involuntary experience in another sense (e.g. vision). For example, Tesla is quoted in an interview (p. 93 in [22]) as saying

" ... when I drop little squares of paper in a dish filled with liquid, I always sense a peculiar and awful taste in my mouth".

In 1870, Tesla was sent to further his education at the higher Real Gymnasium in Gospic, Croatia. During this phase of his life, he suffered from malaria which left him weakened in sharp contrast to his earlier boyhood. During his time at the Gymnasium, he envisaged a huge ring, built around the Earth's equator, and rotating at a synchronous velocity, which could be used as a global rapid transport mechanism. In 1873, Tesla returned home and, instead of following his father's wishes and entering the clergy, he stated his wish to pursue a career in electrical engineering. In 1875 he enrolled in the Polytechnic School in Graz (Austria), the intervening period being blighted with ill-health due to cholera and a period of time in the Croatian mountains to avoid military conscription (p. 14 of [23]).

In 1880, he attended the University of Prague but, due to a variety of problems at the university compounded by the 1879 death of his father, Tesla moved to Budapest in 1881 at the encouragement of a relative to take up his first job in Budapest's telegraph engineering department at the Central Telegraph Office. During 1882, whilst walking in Budapest's City Park he conceived the AC induction motor (p. 23-24 of [21]). Tesla described the realisation by saying that he observed the sunset and recalled a poem from Goethe's "Faust". The

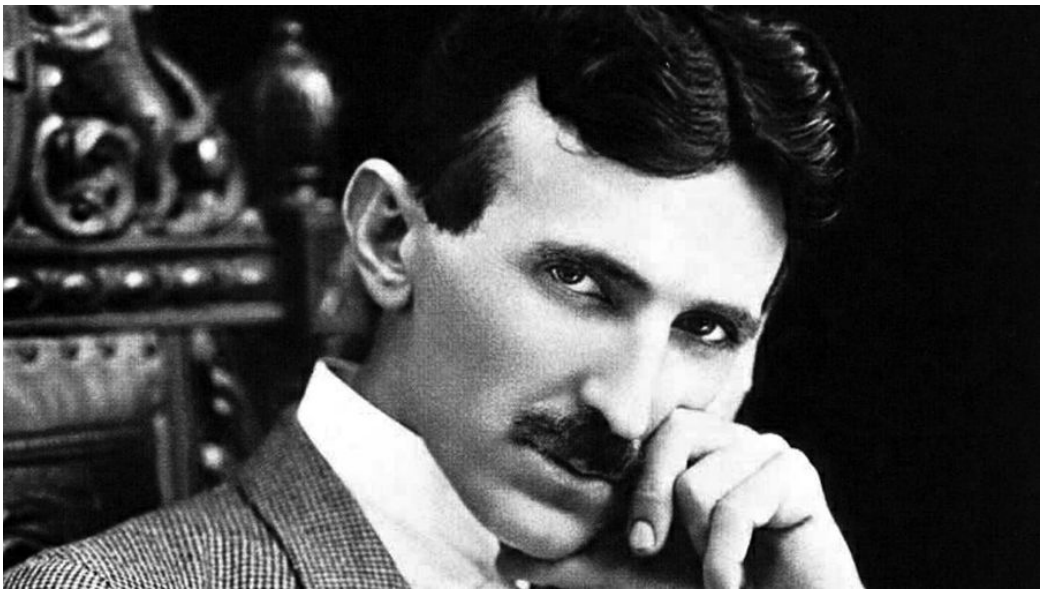

Figure 2.1: Nikola Tesla, 1856-1943 (from [24] )

idea of a rotating magnetic field, without moving parts, appeared to him abruptly; he sketched a diagram of the motor in the soil he was walking upon.

In April 1882 Tesla went to work in Paris for the Edison Company and in the spring of 1884, he emigrated to USA with a letter of introduction to Edison himself. He started working directly for Edison but conflicts soon arose. In May 1885, George Westinghouse, head of the Westinghouse Electric Company in Pittsburgh, bought the patent rights to Tesla's polyphase system of alternating-current dynamos, transformers, and motors. In 1887 Tesla established his own laboratory in New York, experimenting on various types of lighting which eventually led him to invent fluorescent lighting. In 1895, when Röntgen announced his discovery of X-ray radiation, Tesla contacted Röntgen to demonstrate his discovery of X-rays many years earlier but he had not published the work (p. 147 of [21]). Later that year, a

fire destroyed Tesla's entire New York laboratory and he then began to concentrate his research effort on wireless power transmission via high voltage resonant circuits.

Between 1899-1900 [25] Tesla worked in his laboratory in Colorado Springs (figure (2.2)) where he developed radio communication, wireless remote control and certain types of air-cored high voltage resonant transformers, now known as Tesla transformers or Tesla coils.

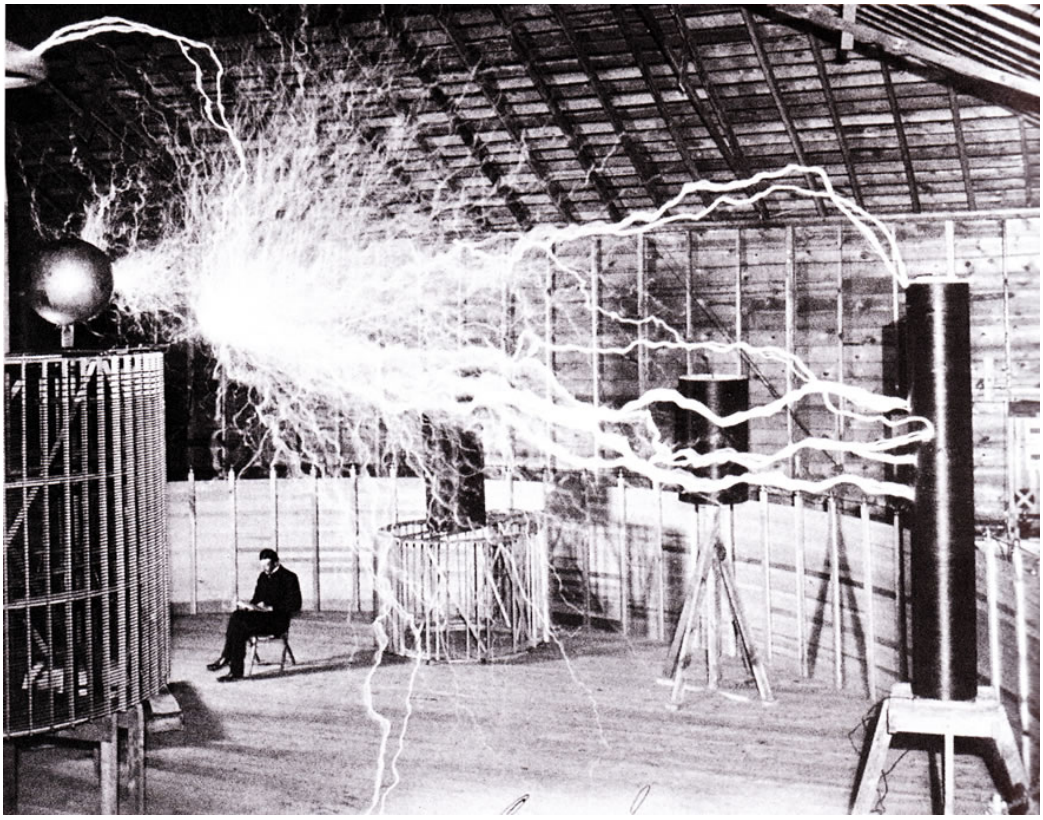

Figure 2.2: Tesla's Colorado Springs experiments (from [26])

Tesla returned to New York in 1900 and endeavoured without success to raise funds to develop his theories for the wireless transmission of electrical power (p. 184ff. of [21]). For example, in 1901 he sold to the J.P. Morgan bank a controlling share interest in his

numerous patents and inventions relating to wireless telegraphy for a comparatively small sum. He used the funds to start development of "Wardenclyffe" on Long Island, New York, which was intended to be a wireless electrical power transmitting station as well as a radio broadcasting station. However, J.P. Morgan lost confidence and withdrew additional funding, causing the project to cease.

In spite of his eccentricities and shy nature, Tesla was socially popular in high society circles in New York. He was frequently courted by press reporters and held something of a celebrity status. However, in later years Tesla's technical proclamations became more and more extravagant and he attracted notoriety which eventually replaced the fame and high standing reputation that he had won during the latter years of the 19th century. He still generated numerous patents but died in poverty, 8th January 1943 (p. 234 of [21]).

Two years after his death, the US Supreme Courts asserted Tesla over Marconi as the inventor of radio communication in *Marconi Wireless Telegraph Co. of America v. United States, 320 U.S.1* (1943) (p. 238 of [21], p. 373 of [23] and p. 197-199 of [27]).

## 2.1 Tesla transformer theory: lumped circuit model

By way of introduction and for the purposes of this thesis, a Tesla transformer is considered to be a two-coil[†], doubly-resonant air-cored

[†]three-coil Tesla transformers are sometimes known as "magnifiers" and were developed by Tesla in Colorado Springs, USA [25] [28] [29]

transformer (p. 104-109 of [18] and p. 276-296 of [20]) where the two resonant circuits, primary and secondary, are tuned to equal frequencies (when decoupled from one another). A typical circuit comprises a primary inductor of a few turns capable of conducting large peak currents of several hundred amperes and loosely coupled to a secondary inductor in the form of a single-layer solenoid having numerous turns and capable of conducting peak currents of a few amperes. The secondary solenoid is typically cylindrical but can be conical, and the length is typically greater than its diameter. The windings are invariably constant in both their pitch and winding sense (i.e. completely clockwise or counter-clockwise).

The primary inductor is tuned by an external lumped capacitance, i.e. a high voltage pulse capacitor, to form a circuit whose resonant frequency is typically several hundred kilohertz or higher. The secondary coil is similarly tuned by capacitance but this is usually the self-capacitance of the coil, plus a high voltage terminating electrode, plus its surroundings, i.e. it is a distributed capacitance. The secondary coil is usually grounded at its bottom end with, as already mentioned, a terminating load of some kind, or a high voltage terminal (variously described as a corona nut, toroid, bung or capacity-hat) affixed to its top, possibly via a sharpening gap[‡]. Appendix (B) is based on work found in several references ([30], [31], p. 327ff. of [32] and p. 135ff. of [33]) and summarises the main analysis from a lumped component standpoint.

In some practical systems the load capacitance connected to the secondary winding output (typically a pulse forming line (PFL)) may

[‡]a spark gap designed to hold off a high voltage, often by the use of pressurised gas as a dielectric, and then rapidly breakdown to present a fast rising edge to a load

be sufficiently high to lower the LC oscillation frequency to well below the self-resonant frequency associated with the distributed reactance of the unloaded coil. As a result, the lumped element assumption is generally adequate in predicting the Tesla transformer's performance. On this basis, numerous analyses exist which discuss the general sets of coupled "resonance networks" [34] [35] [36], of which the Tesla transformer is a specific named case.

## 2.2 Tesla transformer theory: distributed circuit model

Lumped circuit theory and analysis considers the components in a circuit to be represented by structures through which currents are assumed to flow at infinite velocity, such that the current measured entering a component can be measured at that same instant flowing out of it, and whose dimensions are extremely small compared to the free-space dimensions (p. 390 of [37], p. 379 of [38] and p. 354 of [39]). Every part of a lumped-component circuit is assumed to interact instantaneously with every other part and electrical energy is assumed to follow the conductors which make up the circuit, rather than being distributed in the fields surrounding them. Concise discussions are presented in chapter two of [40], chapter four of [41] and p. 589ff. of [42]. This lumped assumption may result in discrepancies between observations based on lumped-component circuit theory and actual measurements of a distributed circuit. For example, the current flowing in an inductor is considered as uniform per turn and hence the electric and the magnetic fields surrounding the inductor uniformly

link one turn to the next: “currents flowing in lumped circuit elements do not vary spatially over the elements and no standing waves exist” (p. 379 of [38]). Formulae for the self inductance and mutual inductance of windings are common book [43] and technical paper [44] topics, with most assuming that the current is uniformly distributed throughout the winding.

Skin and proximity effects in a solenoid coil are usually included as loss mechanisms derived from the effects of steady state sinusoidal currents (p. 180ff. of [41]). However when transient currents flow, the difference in RF resistance is underestimated by using such formulae [45] and the approach fails to describe accurately the complex current distribution in coils. More sophisticated techniques are needed (e.g. filamentary modelling [46], or MoM analysis [47] as described in subsection (1.1.1)). A detailed examination of skin effect and inductance is given in [48].

A more exact physical model treats the circuit described via a transmission line analysis [49] [50], with the perceived self-capacitance of the secondary coil comprised of distributed values. Voltage and current distributions within a transmission line are a function of both time *and* position. The Tesla transformer’s secondary winding is not a pure inductance and cannot be considered as such; instead it forms a distributed structure which indeed has inductance per unit turn but also possesses resistance per unit turn, as well as capacitance and conductance. This distributed nature means that an alternative analysis of the Tesla transformer’s secondary winding, being a form of transmission line resonator, can be performed.

Numerous analyses discuss the nature of a resonant transmission

line on which exists the superposition of propagating waves in the forward direction and reverse direction (for example p. 515ff. of [39], p. 254ff. of [41], p. 215ff. of [42] and p. 468ff. of [51]). An additional, useful and graphical analysis of the process is known as a Bergeron diagram [52]. Appendix (C) identifies a number of engineering formulae which can be used in the design of a Tesla transformer secondary winding, namely a specific form of a helical transmission line resonator.

## 2.3 Coupling in Tesla transformers

Tesla transformers of differing types can be classified in a variety of ways. This section discusses designs whereby the degree of magnetic coupling differs between tight and loose coupling.

Tesla transformers, used for the generation of extremely high voltages, by necessity require significant insulation between and within the coil windings, and high primary currents and fast pulses often preclude the use of ferromagnetic materials in the transformer core. Under these design conditions, achieving high magnetic coupling between primary and secondary circuits becomes extremely difficult (it is difficult to establish a geometry which causes all of the magnetic flux due to primary currents to couple into the secondary winding). Generally, transformers operating with low magnetic coupling coefficients result in low energy transfer efficiencies. This design aspect impinges on the total power efficiency, the peak voltage observed in the secondary, the complexity of the primary switch[§] and

[§]usually some form of spark gap which discharges the energy stored in the primary capacitor into the primary inductor

the overall system losses. The type of primary switch, whether a spark gap, a solid state component or a thermionic device, is determined primarily by the degree of coupling $k$ sought in the design process and also the peak and average powers to be switched, and ultimately governs the performance of the Tesla transformer.

In more tightly-coupled Tesla transformers, the degree of efficiency of energy transfer from primary to secondary is high. Coupling coefficient values of 0.6 are often employed (e.g. [30] [53] [54]). Appendix (B) provides a discussion of the primary:secondary energy transfer mechanism and chapter nine of [20] provides a succinct summary, demonstrating that various specific values of $k$ (1, 0.6, 0.385 etc.) enable the completion of energy transfer from the primary to the secondary. The time taken for this transfer of energy to occur is short compared with that of a loosely-coupled Tesla transformer and the power developed by the secondary when discharged into a load is comparatively high. The design of the primary switch is constrained to be complex compared with an equivalent device in a loosely coupled Tesla transformer (where values of $k$ may be < 0.3). Effective design of the primary switch governs the ultimate voltage developed by the secondary. This is because during the time that the secondary is free to ring down[¶], the primary should look ideally like an open circuit. This assumes that the primary switch ceases conducting at the exact point at which all the primary energy has been transferred into the secondary and the primary current has fallen to zero. Under such circumstances the secondary ring down process is unimpeded by any impedance reflection from the primary circuit, since this appears as an

[¶]exponential energy loss from a resonant system, see appendix (B)

open circuit when the switch has ceased conducting. If the primary switch does not perform like a perfect component, the primary circuit will have some finite impedance value which couples into the secondary circuit. This generates out-of-phase currents in the secondary, the result of which is to prevent the secondary from developing its intended output voltage. It can be said that the secondary is loaded by the close proximity of the primary if the primary switch is non-ideal and the switch performance is a governing factor in the degree of coupling that can be utilised in the Tesla transformer.

However, in more loosely-coupled Tesla transformers such as the experimental test-bed which will be discussed in chapter (5), the coupling coefficients may be as low as $k$ = 0.1 - 0.2 (a range of typical values). In this case, the degree of damping that the secondary suffers due to the presence of the primary is lower and the secondary winding may achieve a higher voltage, since the secondary $Q$ in the presence of a loosely-coupled primary is likely to be higher than in a tightly coupled case. To summarise, a tightly coupled Tesla transformer will generate a higher average power output but at a lower ultimate voltage, whereas a loosely coupled Tesla transformer design will provide a higher output voltage at the expense of a lower power transfer efficiency [55] [56]. However, efficiency can be restored by designing the transformer to operate in the pulsed resonant mode discussed in subsection (2.3.3). In this manner, maximum energy transfer to the load is achieved only after a number of resonant frequency half-cycles have been completed, starting from the time the primary circuit is closed.

Loosely coupled Tesla transformers are often of an “open” design using simple geometry and unpressurised air insulation (an example of

which is discussed in chapter (5)). This is in contrast to tightly coupled transformers which frequently employ an "enclosed" design of the type discussed in subsection (2.3.1), utilising metal pressure vessels within which the primary and secondary windings are housed in a pressurised insulating gas atmosphere.

### 2.3.1 Tightly coupled designs

The winding geometry in tightly coupled Tesla transformers can be significantly different from that of loosely coupled Tesla transformers. Tightly coupled transformers usually conform to one of three winding topologies; the two most common being the cylindrical and the heliconical shapes, with the third type being a flat spiral design.

In a cylindrical design, the secondary is wound on a cylindrical former as a single-layer solenoid and the primary is wound coaxially as a coarse helix around the secondary. Layers of high dielectric strength material, or a high dielectric strength fluid such as transformer oil, insulate the primary from the secondary. Coupling coefficients can be high ($k \leqslant 0.7$ using ferrite loading of the solenoid core, or $k \leqslant 0.9$ using a metallic core) but voltage grading and insulation strength issues are then problematic.

In one heliconical design the secondary takes the form of a single-layer solenoid but the primary has a conical cross-section, tapering outwards. The voltage grading and insulation problems experienced by a cylindrical form are eased, but the maximum coupling coefficient that can be achieved is reduced.

Another heliconical approach is to make the primary coil from one or two turns of copper sheet, which couple into the bottom of a

heliconical secondary (a secondary wound in the form of a circular cross-section cone, with a base similar in diameter to the primary and whose apex is 10% of the starting diameter). The distributed capacitance of such a conical winding is lower than that of a standard cylindrical single-layer solenoidal winding.

In a spiral design, both the primary and secondary are wound as flat spirals from copper sheet, with the secondary wound directly on top of the primary. In this instance higher coupling coefficients can be achieved than when using the other geometries mentioned, and without the use of core materials, but the electric stresses generated by the copper edges, and the insulation coordination needed to hold off the high secondary voltage, usually prove very difficult to implement successfully.

Higher coupling requires closer spacing between coils, which must necessarily be separated by materials of high dielectric strength. This is usually realised by housing both the primary and secondary windings within a container filled with a fluid insulator such as transformer oil, or a gas at sufficiently high pressure (e.g. sulphur hexafluoride ($SF_6$)). In addition, if the walls of the transformer housing are metallic then a high degree of shielding is given to surrounding equipment from the high electric fields that can be generated. Detailed examples of this type of design can be found in [19] and [57], which describe transformer windings housed in a large cylindrical pressure vessel and filled with $SF_6$ gas for high voltage insulation. It was noted that the conductive walls of the pressure vessel had an effect on the value of the circuit parameters, resulting in a slight reduction in the expected resonant frequency and coupling coefficient.

The transformer designs assessed by Abramyan [58] used heliconical primary coils wound from several turns of copper strip, with the secondary coils wound from several hundred turns of copper wire in the form of a single-layer solenoid. Operation with coupling coefficient $k \cong 0.6$ gave maximum efficiency, which can achieve 95% (according to [59] [60] and cited on p. 287 of [20]). The Tesla transformer resonated at frequencies of tens of $kHz$; hydrogen thyratron switches (chapter seven of [20] and p. 335ff. of [61]) were used instead of spark gaps in the primary circuit and ran at PRFs of several hundred per second.

Another Tesla transformer described in [54] used a heliconical primary winding, chosen to separate the primary winding from the high voltage end of the secondary winding. This reduced capacitive coupling and associated voltage stress between the output terminal and the relative ground of the primary winding. At the output end of the secondary winding, a toroidal "corona ring" was added ($d_{minor}$= 9.5 $mm$ and $d_{major}$=178 $mm$, made from copper tube) to act as a field grading structure which contributed additional capacitance of approximately 6 $pF$.

An additional example is the Tesla transformer produced by Loughborough University by Sarkar et al. [62] and shown in figure (2.3). To ensure good insulation and to maximise the coupling with the primary winding, which set $k$ to 0.54, the secondary coil was wound on a conical mandrel made from polyethylene and immersed in transformer oil contained in a cylindrical aluminium housing.

In general, primary switch performance is heavily influenced by its design and construction [63]. A number of factors such as peak current and required repetition rate govern the type of switch utilised.

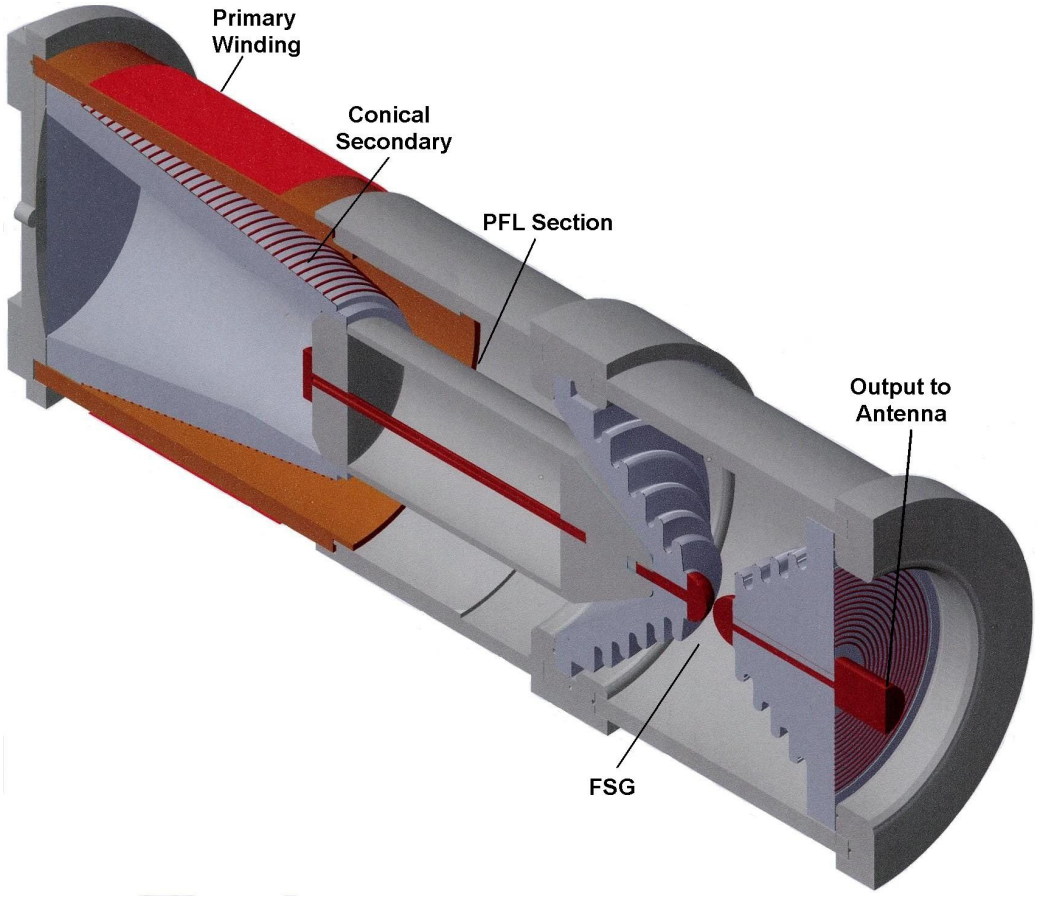


Figure 2.3: A compact battery-powered half mega-volt transformer system for electromagnetic pulse (EMP) generation (from [62], © 2005, Loughborough University)

Furthermore, use of a tightly-coupled dual-resonant Tesla transformer implies a requirement for a fast opening switch. A switch can be designed to perform in a tightly coupled design but the design is likely to need careful consideration in terms of quenching, especially if it is to operate at rep rates of hundreds of $Hz$ or more. To expand on this, a tightly-coupled Tesla transformer needs to extinguish the current flowing in the primary due to the primary gap firing, and it needs to do so at a point when complete transfer of energy from primary to secondary has been completed. The time taken for this completion is sometimes referred to as the filling time (appendix page v-3 of [50]) and is given by :

$$t_s = \frac{1}{(2\Delta f)} \tag{2.1}$$

where $\Delta f$ is the beat frequency resulting from the two tuned circuits beating together. Tighter coupling shortens the filling time and the requirements for gap quenching become more stringent. A variety of methods can be used and these refer to two-terminal self-breaking gaps, trigatrons or other designs such as field distortion gaps and rail gaps (p. 294ff. of [61] and p. 43ff. of [64]). For example, air blast cooling minimises thermal electron emission, which also sweeps out uncombined electron-ion pairs to rapidly deionise the air dielectric. Another technique involves the mechanical separation of electrodes (e.g. rotary spark gaps, p. 275ff. of [61]) which increases the breakdown channel length and promotes channel collapse of the conducting arc, forcing it to extinguish and return the gap to an off state. Additionally, operation in a pressurised gaseous medium such as hydrogen or $SF_6$, depending on the gas pressure used, either increases electron-ion mobility such that rapid recombination is enabled, or

decreases mobility such that the conduction channel self-extinguishes rapidly.

### 2.3.2 Loosely coupled designs

Loosely coupled transformer designs can also take a cylindrical or spiral form of secondary winding but the proportions and geometry of the primary and secondary windings change to suit the required values of coupling coefficient. A typical geometry for a loosely-coupled Tesla transformer primary winding is a flat Archimedean spiral starting at an inner radius $r_1$ and finishing at an outer radius $r_2$, orientated horizontally with the secondary coil standing vertically at the spiral's centre. The base of the secondary coil can be in the same plane of the helix, or raised above it or depressed below it as a method of tuning $k$. The value of $r_1$ is usually adjusted to be larger than the radius of the secondary former so as to enable the primary to be adjusted vertically along the secondary coil's axis (usually positioned within the bottom 15% of the secondary's height). The aspect ratio (height $\mathcal{H}$ / diameter $d$) of the secondary winding typically lies between 4 and 6, which gives the best compromise of $Q$, wire diameter for a given design inductance, self-capacitance and voltage grading. A short, large diameter coil where the aspect ratio equals 0.5 may give the highest $Q$ for a given inductance, but the high voltage end of the winding may not be physically separated sufficiently far from the grounded end and hence breakdown across the coil windings is a risk. Likewise, a coil whose aspect ratio is set to approximately 0.4 has maximum inductance [31], thus using the minimum amount of copper wire (and hence minimum conductor losses). Again the height is prohibitively

short and breakdown is a hazard. Immersion of such coil forms in a gas dielectric, for example pressurised nitrogen or $SF_6$, is one solution. An alternative configuration is to use a heliconical primary similar to that of a tightly-coupled design, where the secondary again takes the form of a single-layer solenoid. The primary has a circular cross-section, with its diameter changing in a conical manner tapering outwards and upwards. The voltage grading and insulation problems are again minimised because separation of the larger diameter uppermost turns of the primary from those of the secondary prevent excessive voltage stressing. Higher coupling coefficients can be achieved than with the flat spiral approach but mechanical design considerations make construction more difficult.

In cases where a design is optimised for maximum spark length, a "topload" in the form of a conductive toroid is connected to the high voltage end of the secondary winding. This fulfils two purposes: it provides an electric field grading structure which controls the electric field in the vicinity of the secondary coil so as to minimise corona formation on the secondary, and also forms a charge storage area which allows rapid conduction of the accumulated charge into a spark as it is forming. A loosely-coupled Tesla transformer design has to take into account the capacitance of such a topload when implementing the secondary winding, such that the secondary inductance and self-capacitance, when operated in conjunction with the topload, achieves resonance at the design frequency.

### 2.3.3 Tesla transformers using solid-state switching

Alongside the professional scientific and engineering community, an active internet group [65] has developed a number of types of Tesla transformer along with associated terminology. Solid-state Tesla transformers, also termed solid state Tesla coils (SSTCs), use semiconductor switches as the primary switch. Well established switched-mode power supply (SMPS) technology is used as a basis for developing switch topologies and associated driver electronics. Half-bridge or full-bridge ("H-bridge") drivers can be used, typically employing MOSFET or IGBT devices with each of the four devices in an H-bridge configuration needing to be able to hold off the full voltage supplied to the bridge. Affordable MOSFET and IGBT modules available off-the-shelf can switch peak currents of several hundred amperes, and the hold-off voltages in single devices can be as high as 1600V. Assembled modules with integral voltage balancing resistors are available up to voltages of several tens of $kV$. The performance of such devices approaches that of an ideal switch with on-resistances usually less than hundreds of milliohms, and off-resistances practically open-circuit. The ability to command the switch to turn rapidly from the on state to the off state means that these devices find use in tightly-coupled circuits. Disadvantages include the complexity of the gate driving electronics, the susceptibility of the gate and driving circuit to damage from electromagnetic interference (EMI), the relatively high cost of the switching devices compared with a simple spark gap switch, and power handling limitations and dV/dt limitations.

There are specific varieties of SSTCs. For example, OLTCs are Off-Line Tesla Coils. Domestic mains power ("line" power) is full-

wave rectified and smoothed and then processed to provide a power supply for the primary coil (and so power is thus taken "off" the "line" supply). The primary coil is not tuned by use of a storage capacitor but is driven by the switching circuitry at the resonant frequency of the secondary. CWSSTCs are SSTCs run in a Continuous-Wave mode, where there is zero or small difference between the peak power delivered to the TC primary and the RMS power measured at the same point. This mode delivers a medium average power and causes minimum stresses to be experienced by the primary switch. Again, the primary is usually untuned. Pulsed SSTCs are run in a "burst" mode where some percentage of a number of cycles of power delivered to the primary coil are significantly higher than the RMS power developed for the remainder of the cycles. This mode delivers a slightly lower average power but the peak power is higher, thereby generating higher peak voltages at the transformer's output. DRSSTCs [66] are dual resonant SSTCs whereby the primary is a tuned circuit whose resonant frequency is set to be that of the secondary to which it couples. The power developed in the secondary is higher and both RMS and peak voltages are higher.

## 2.4 Tesla transformer uses

Electrical pulse generators capable of very high-voltage (HV) output (> 100 $kV$) are essential for a range of physical research activities, particularly in studies associated with particle and plasma physics. Some examples of applications that directly utilise such pulse power sources include:

- pollution control via plasma/corona techniques
- X-ray radiography
- high power lasers
- electron beam generators
- high power microwave (HPM) generation
- ultra wideband (UWB) electromagnetic radiation (EM) generation

The potential use of HPM sources in defence applications for enhancing radar and electronic warfare (EW) capabilities has attracted increasing interest over recent years. Transferring such technology from the laboratory to the field imposes additional engineering performance requirements on the pulsed power system, especially as these also typically specify efficiency and reliability alongside long life, e.g. pulse power systems with long lifetimes (>$10^8$ shots) [62] [67]. Microwave and RF sources are increasingly utilised in technology areas such as communication systems and wideband impulse radar and in the detection of buried explosive munitions [68]. The advantages of wide bandwidth waveforms for radar include improved positional resolution, better signal-to-noise ratio of reflected signals and a lower probability of signals being intercepted than with narrowband signals. Semiconductor-based equipment can be susceptible to high-power EMP radiation and in some circumstances it is necessary to investigate any vulnerabilities, and to then design hardening techniques to prevent or minimise temporary or permanent damage to electronic equipment subjected to EMP. It is essential in the development of such techniques

to be able to generate suitable test signals and [57] demonstrates a potential candidate. Other uses include the generation of high electric fields for materials study and processing [69] and the generation of long arc lightning simulation [70]. In this latter case it is important to note that, as a function of spark formation, an ultimately high voltage is not the sole key to the production of long sparks. Other factors that contribute to maximising spark length [71] include average power, pulse repetition rate and output impedance.

An early use for the Tesla transformer was in high voltage testing of domestic and industrial electrical power insulation and switchgear. Such use fell out of favour; in 1954 Craggs and Meek (p. 109 of [18]) stated that "Tesla coils are now little used **...** their complex waveforms often introduce difficulties" and Denicolai [72] noted that "it is difficult to control the generated wave-shapes" of Tesla transformers. Perhaps, if the output waveform's complexity could be sufficiently controlled, Tesla transformers may again be put to such relatively mundane use.

# Chapter 3

# Introduction to helical filters

Zverev (in chapter nine of [73]) thoroughly describes helical filters, design guidelines for which were published in 1959 [74]. A helical filter is typically constructed as a thick-walled highly conductive cavity (made from copper and often silver plated), which is usually cylindrical (sometimes square) in cross-section, with a resonant helical structure positioned along the central axis of the cavity and grounded at one end [74] as shown in figure (3.1). Figure (3.2) illustrates the orientation of a helix, positioned vertically on the $z$ axis and operating with a ground $(x, y)$ plane at $z = 0$. At lower frequencies (typically VHF and below) the helix is often in the form of an air-cored single-layer solenoid. Helical filters are high-$Q$ devices similar to coaxial lines with helical inner conductors [74], and they are used in radio frequency applications [75] such as filtering of radio receiver inputs (p. 65 of [76]), and the transmitter outputs of cellular phone base stations [77]. Typical helical filters (see figure (3.3)) are capable of providing both high stopband attenuation and low passband attenuation. Cascading a series of helical resonators allows the overall response to be tailored

to suit a specific application.

The ratio of helix diameter (equivalent to the inner conductor of a coaxial transmission line) to the cavity diameter (effectively, the inside diameter of the "outer" of the coaxial line) is discussed [75]. The helix has an electrical length slightly less than a quarter-wavelength of the resonant frequency, and is brought into resonance by the addition of the "top" capacitance, illustrated in figure (3.1) by the "T" shaped structure at the top of the helix. The helix and its distributed capacitance stores slightly less electric than magnetic field energy, with the shortfall made up by the top capacitance so that the overall arrangement is resonant.

Several filter elements tuned to slightly different frequencies can be series-connected to create a filter whose passband and stopband are tightly controlled. RF signal coupling into the first cavity and out of the last cavity can be achieved in a number of ways, including direct link coupling, loop coupling or capacitive coupling (p. 498 of [73], p. 114 of [76]). Inter-cavity coupling can be similarly achieved; an alternative method is to employ aperture coupling, whereby an opening in the adjoining walls of a cavity acts as an iris through which coupling can occur. The degree of coupling between cavities, and the centre frequency of each cavity, allows the response of the filter to be tuned to pass a specific band whilst stopping frequencies away from that band.

It has been shown (chapter seven of [1]) that a helical filter resonating at its fundamental frequency exhibits a minimum electric field strength at its grounded end and a maximum at the other end, whilst for the magnetic field it is a maximum at the grounded end and a minimum at the opposite end. Since the spatial separation between the two field maxima is a quarter wavelength at the resonant frequency, a

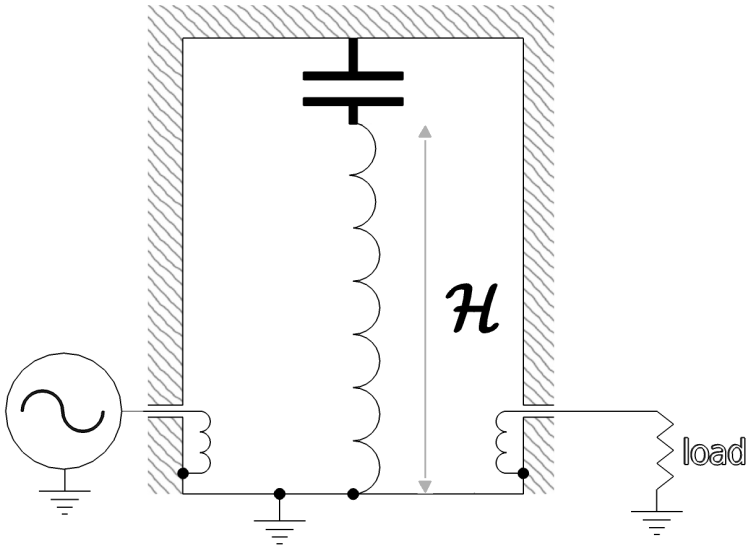


Figure 3.1: Element of a single coaxial cavity helical filter

standing wave of length $\lambda$ is set up along the resonant winding at both this wavelength and a series of related wavelengths when the electrical length of the helix is equivalent to (p. 61 of [1])

$$1\frac{\lambda}{4}, 3\frac{\lambda}{4}, 5\frac{\lambda}{4}, \ldots \frac{(2n+1)\,\lambda}{4}, n = 0, 1, 2, \ldots \tag{3.1}$$

which corresponds to a series of frequencies of

$$f, 3f, 5f, \ldots, (2n+1)f, n = 0, 1, 2, \ldots \tag{3.2}$$

These standing wave terms represent a series of modes which describe the frequencies of currents flowing in the winding. The frequency of the fundamental mode is denoted by $f_1$, with $f_3$ being the frequency of the next mode (whose electrical length is $3\frac{\lambda}{4}$) and so on.

Figure (3.4) shows that at the resonator's fundamental resonant mode frequency $f_1$, the helix appears to be electrically one quarter-

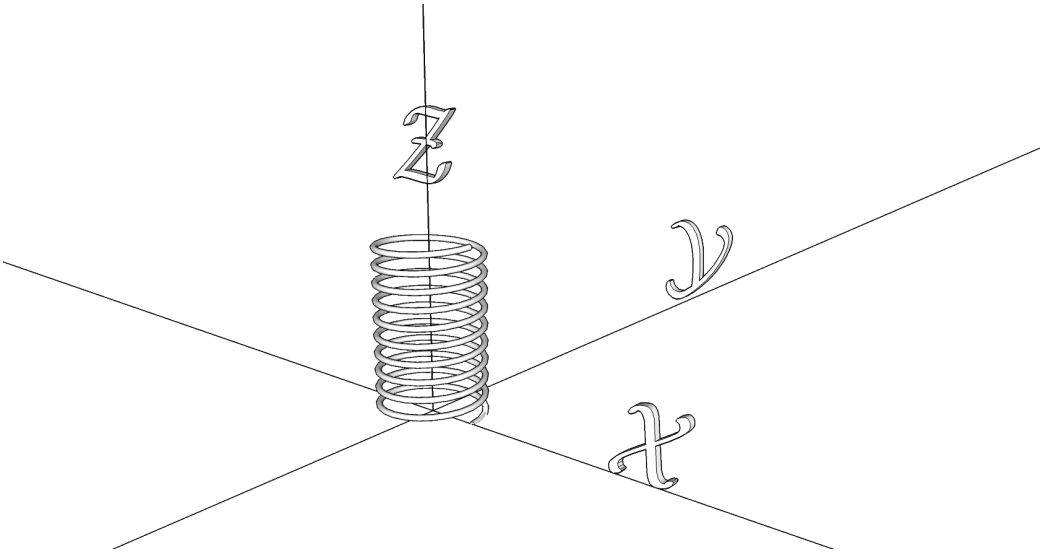


Figure 3.2: A vertical helix, orientated on the $z$ axis, standing on the $xy$ plane

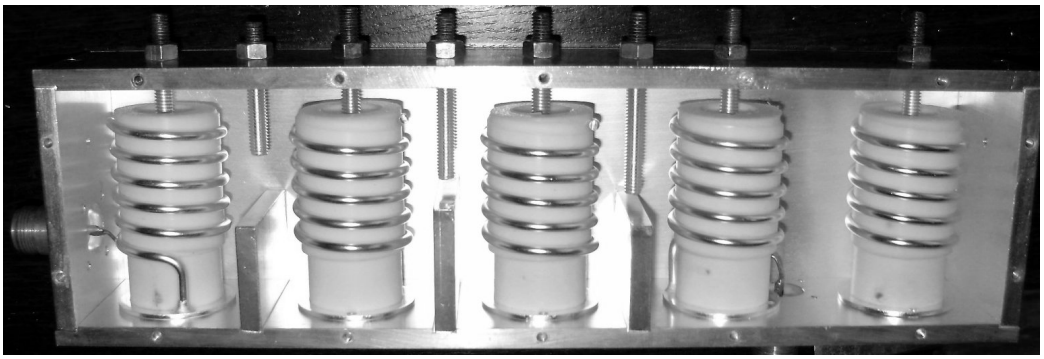

Figure 3.3: Photograph showing a typical helical filter (from [78])

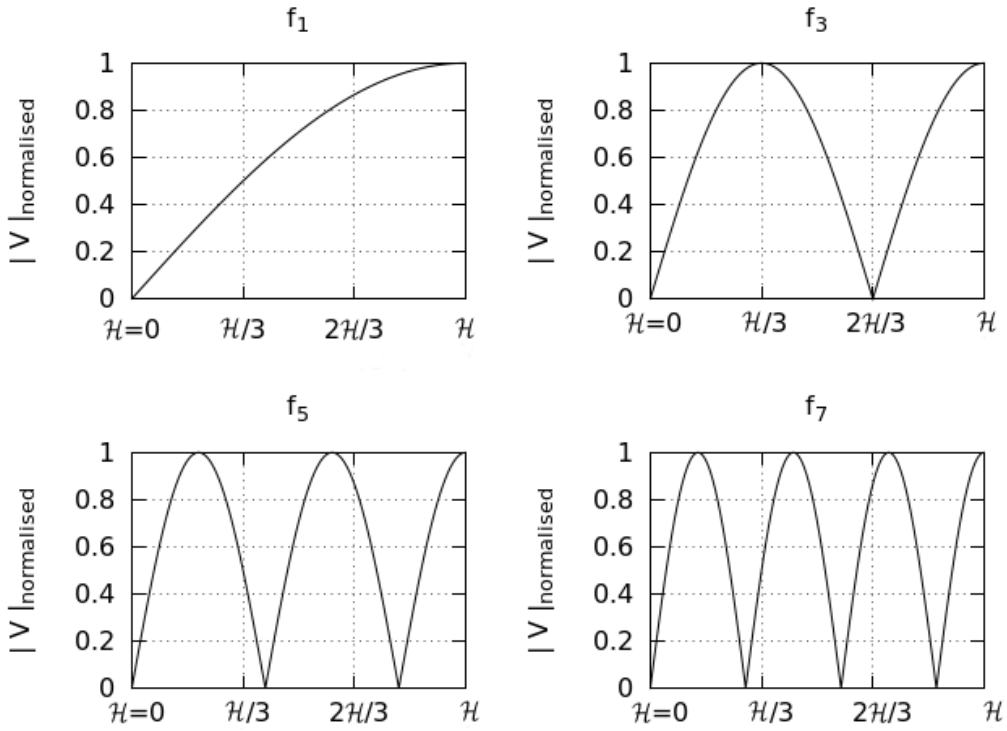


Figure 3.4: Sinusoidal voltage distributions of the first four modes

wavelength tall ($\mathcal{H} = \frac{\lambda}{4}$) and a voltage node $V_{min}$ appears at its grounded base ($\mathcal{H} = 0$). A voltage anti-node $V_{max}$ appears at $\mathcal{H}$ (the top of the resonator). At the next resonant mode $f_3$, a voltage node $V_{min}$ is again present at the base ($\mathcal{H} = 0$) but now a voltage anti-node $V_{max}$ is located at position $\frac{\mathcal{H}}{3}$. Another $V_{min}$ node occurs at $\frac{2\mathcal{H}}{3}$ and finally a $V_{max}$ anti-node is present at $\mathcal{H}$. The structure now appears to be, *electrically*, three quarters of a wavelength tall such that $\mathcal{H} = \frac{3\lambda}{4}$. At the next resonant mode $f_5$ there is again a $V_{min}$ voltage node at the base ($\mathcal{H} = 0$), with additional $V_{min}$ voltage nodes located at $\frac{2\mathcal{H}}{5}$ and $\frac{4\mathcal{H}}{5}$. There are $V_{max}$ voltage anti-nodes located at $\frac{\mathcal{H}}{5}$, $\frac{3\mathcal{H}}{5}$and $\mathcal{H}$ (the top). The structure now appears to be, *electrically*, five quarters of a wavelength tall such that $\mathcal{H} = \frac{5\lambda}{4}$.

In general, for any odd-numbered mode $n$:

a $V_{min}$ node is always established at position

$$0, \frac{2\mathcal{H}}{n}, \frac{4\mathcal{H}}{n}, \frac{6\mathcal{H}}{n}, \dots \left(\frac{n-1}{n}\right)\mathcal{H} \tag{3.3}$$

and a $V_{max}$ node is always established at position

$$\frac{\mathcal{H}}{n}, \frac{3\mathcal{H}}{n}, \frac{5\mathcal{H}}{n}, \dots \mathcal{H} \tag{3.4}$$

The frequencies of the resonances higher than the fundamental mode frequency are called "overtones" rather than "harmonics". A harmonic is a special case of an overtone whose frequency is an *integer* multiple of the fundamental and for a *non*-dispersive resonator, the fundamental mode is termed the $1^{st}$ harmonic, the first overtone is the $2^{nd}$ harmonic, the second overtone the $3^{rd}$ harmonic and so on. However, a helix is a *dispersive* resonator because the velocity factor

$\mathbb{V}$, defined as the speed of a wavefront along the longitudinal ($z$) axis of the helix as a proportion of the speed of light ([74] [75] and p. 260 of [76]), is not a linear function of frequency (see appendix (C) equation (C.8)). Therefore the overtone modes of the resonator are not necessarily integer multiples of the fundamental and are denoted as being anharmonic i.e. non-harmonic. Reference [79] defines anharmonic as

> "physics of or concerned with an oscillation whose frequency is not an integral factor or multiple of the base frequency"

Vizmuller [1] expanded on the earlier work by Zverev and described a new class of resonator, namely one which addresses the problem of filter "reresonance". Reresonance is the property whereby a helical resonator shows such anharmonic resonant responses at higher frequencies instead of just at the wanted fundamental response.

## 3.1 Comparison of Tesla transformers and helical filters

Historically, Sloan [53] developed Tesla's original transformer into a cavity-bound "resonance transformer", which he described as "a large radio oscillator ... sends high frequency power into a 50 meter wavelength antenna which is coiled up without insulation, and enclosed in a metal vacuum tank".

He further referred to Tesla transformers, commenting that "the most useful class of resonance transformers **...** cannot be treated usefully by mathematics" and also confirmed that the resonance

transformer “only has one frequency of oscillation (aside from harmonics)”, thus illustrating that higher frequency harmonic content was known to exist in the transformer output. Additional discussions by Sloan concern descriptions of resonance transformers as separable into three classes, namely “lumped constants” (i.e. lumped circuit components), “evenly distributed constants” and “unevenly distributed constants”, noting that “only the latter two types are of practical value for generating high voltage”.

Similarities are observed when comparing Tesla transformer secondaries (working as grounded and toploaded resonators) with helical resonators whose “open” ends are forshortened as per helical filters:

- A Tesla transformer secondary with a “corona nut” (e.g. a toroidal topload) is brought into resonance in just the same way as a capacitively toploaded helical resonator.
- In both cases, the helix has an electrical length slightly less than a quarter - wavelength of the resonant frequency, and is brought into resonance by the addition of the “top” capacitance.
- In both cases, the helix stores slightly less electric than magnetic field energy, with the shortfall made up by the top capacitor so that the overall arrangement is resonant.

Clear parallels exist between a Tesla transformer secondary coil responding as a quarter-wave resonator and a helical filter’s shortened helix, since a Tesla transformer’s secondary coil is brought into resonance by the additional capacitance of some form of electric field grading structure (such as a corona shield or nut, p. 30 of [18] or metal

toroid) in the same way as the winding in a helical filter is brought into resonance by additional capacitance at its high voltage end.

It is thus apparent that there are considerable similarities between Tesla transformer secondary coils and helical filters with foreshortened ends. These similarities were illustrated by Terman (p. 273 of [33]) and by Sloan [53] who discussed the helical resonator in its cavity and evolved the description to that of an "open" helical resonator operating against a ground plane, with boundary conditions for the resonator removed.

## 3.2 Helical filter improvements and Tesla transformers

Vizmuller (p. 68ff. of [1]) investigated methods by which standing waves are suppressed on $\frac{\lambda}{4}$ resonant structures by counter winding the uppermost portion of a resonant helix as shown in figure (3.5). He showed that a helix of fixed height $\mathcal{H}$=$\mathcal{H}_1$+$\mathcal{H}_2$ can be constructed whereby $\mathcal{H}_1$ is that portion of the helix wound in a normal direction and the remainder, $\mathcal{H}_2$, is counter-wound (i.e. the winding direction is reversed for portion $\mathcal{H}_2$ compared with that for portion $\mathcal{H}_1$).

The fundamental resonant frequency of the helix corresponds to $\frac{\lambda}{4} = \mathcal{H}_1 + \mathcal{H}_2$ rather than $\frac{\lambda}{4} = \mathcal{H}_1$ alone (p. 68 of [1]). However, the frequencies and magnitudes of the responses corresponding to the $f_3$ mode and above are particularly sensitive to the ratio of $\mathcal{H}_2$ to $\mathcal{H}_1$. Thus a mechanism exists whereby the higher-frequency mode responses can be significantly altered while the fundamental mode remains largely unaltered.

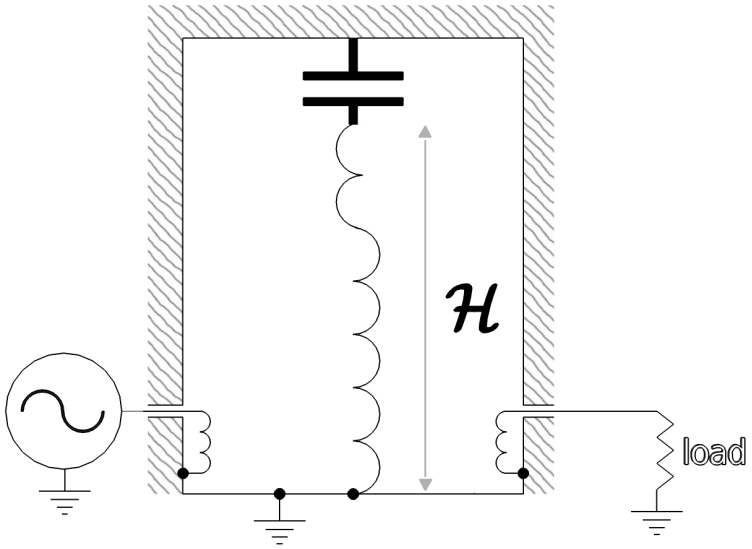


Figure 3.5: Element of a single coaxial cavity helical filter, illustrating counter-wound portion

Although the application of helical filter design to high power pulse generation is not immediately obvious, it is apparent that striking similarities exist between the geometry of a helical filter and the secondary coil of a Tesla transformer. This raises the possibility of applying Vizmuller's helical filter design techniques to Tesla transformer secondary windings in order to examine any potential for enhanced performance*.

*author's original argument submitted to [65], June 1996, see http://www.pupman.com/listarchives/1996/june/msg00342.html

# Chapter 4

# Theory and modelling of secondary coils

A "model" is a mathematical description which accounts for the known properties of a component or system of components. This chapter discusses contributions from different modelling techniques used to analyse and design both the Tesla transformer and the range of experimental secondary windings used in the thesis. In addition, a theoretical overview assisted in formulating a theory of operation for the experimental (partially counter-wound) coils. Simple numerical analysis was used to set initial circuit parameters for the Tesla transformer. Then, SPICE modelling was used firstly to establish the primary/secondary coupling coefficient $k$ for the Tesla transformer and secondly to determine the spectra of currents flowing in a simple model of the reference secondary coil, in which none of the turns were counter-wound and it is referred to as the "0%" coil. TSSP modelling was employed to assess and identify a range of values of counter winding percentages to test. Finally, NEC modelling was used to investigate

the E and H field distributions of a range of coils to help develop, and contribute to, the initial theory of operation.

Simple, approximate modelling of a conventionally wound Tesla transformer secondary coil can be implemented via various formulae which assume that the inductance of the single-layer solenoid winding is due to an alternating current common to, and equally distributed throughout, all of the turns and hence causing uniform flux linkage between neighbouring turns. A convenient expression for the inductance of a single-layer solenoid is "Wheeler's formula" (p. 55 of [33], found to be accurate to better than $\pm$ 0.5 % for coils whose length (or height $\mathcal{H}$) is greater than their diameter $2r$ [80]:

$$L_{DC} = \frac{n^2 r^2}{9r + 10\mathcal{H}} \tag{4.1}$$

where

$L_{DC}$ is the low frequency inductance in microhenrys

$n$ is the number of turns,

$r$ is the coil radius in inches

$\mathcal{H}$ is the coil height (the length if it is orientated horizontally), also in inches

In SI units, the formula becomes (p. 33 of [81])

$$L_{DC} = \frac{\mu_0 \pi n^2 r^2}{\mathcal{H}(1 + 0.9\frac{r}{\mathcal{H}})} \tag{4.2}$$

The apparent self-capacitance of a single-layer solenoidal coil is also based on the assumption of a uniform current distribution in all turns as described by Medhurst [82] who presented empirically derived

tables of numerous self-capacitance measurements. From the results, "Medhurst's formula" is derived:

$$C_s = KD \tag{4.3}$$

where

$C_s$ is the capacitance of a coil in picofarads

$D$ is the coil diameter in centimetres and

$K$ is a constant of proportionality whereby $C_s \propto D$.

Medhurst's results were obtained from measurements at frequencies much lower than the self-resonant frequency of the coil, when mounted horizontally above a ground plane and earthed to it at one end. The results are clearly invalid for vertically mounted resonant helices such as Tesla transformer secondary windings. A detailed examination is presented by [83] and section (4.1) discusses the reasons in detail.

Electromagnetic resonance is a property of a structure or circuit whereby oscillatory energy is stored for a time greater than the period of oscillation of the electromagnetic energy supplied (p. 3948 of [84]). As mentioned in chapter (1), the $Q$ of a circuit or circuit element is a description of the energy stored in it compared with the energy lost by it, per unit time (p. 587 of [39], p. 258 of [41]) :

$$Q = \omega \left[ \frac{J_{stored}}{J_{lost}} \right] \tag{4.4}$$

At the high frequencies present in the secondary coil, an approximate, simple generalised equivalent circuit at a particular parallel resonant mode frequency takes the form shown in figure (4.1),

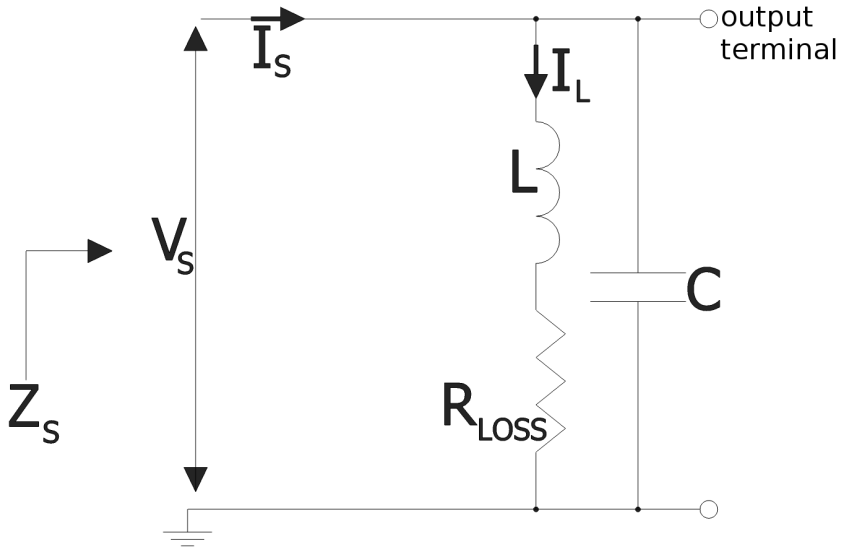


Figure 4.1: Approximate equivalent circuit of unloaded secondary coil

where $R_{loss}$ takes into account conductor $I^2R$ losses, skin effect losses, and dielectric and radiation losses. The quality factor of the secondary circuit $Q_s$ is defined by equation (4.4).

The voltage $V_s$ induced in the secondary coil by a current $I_p$ flowing in the primary circuit of a Tesla transformer at frequency $\omega$ is

$$V_s = -j\omega M I_p \tag{4.5}$$

where $M$ is the primary/secondary winding mutual inductance. It is straightforward to show that at any resonant mode frequency, the secondary circuit impedance $Z_s$ is given by

$$Z_s = R_{loss}\left(1 + Q_s^2\right) \tag{4.6}$$

where the $Q$ factor of the circuit $Q_s$ is

$$Q_s = \frac{1}{R_{loss}}\sqrt{\frac{L}{C}} \tag{4.7}$$

Assuming that $Q_s$ is $\gg 1$ then

$$Z_s \cong R_{loss}Q_s^2 = \frac{L}{CR_{loss}} \tag{4.8}$$

and it is straightforward to show again from figure (4.1) that the current $I_L$ flowing in the unloaded secondary circuit is

$$I_L = I_s Q_s = \frac{I_s}{R_{loss}}\sqrt{\frac{L}{C}} \tag{4.9}$$

and is directly proportional to $Q_S$ for any particular mode frequency. Reductions in $Q$ for a particular mode frequency correspond to reductions in $I_L$ since

$$\Delta I_L = I_s \Delta Q_s \tag{4.10}$$

$Q_m$ is the quality factor of the secondary winding for a particular mode in terms of the secondary winding inductance and an expression for it is (p. 501 of [73], p. 30 of [85])

$$Q_m = \frac{\omega L_{HF}}{R_{loss}} \tag{4.11}$$

where

$\omega$ is $2\pi f_m$ where $m$ is the mode being considered

$L_{HF}$ is the high frequency inductance of the secondary winding at the mode frequency $f_m$ of interest

$R_{loss}$ is the total equivalent loss resistance present in the secondary at a particular mode frequency $f_m$

For fixed values of $L_{HF}$ and $R_{loss}$, $Q_m$ is proportional to $\omega$ and, from equation (4.10), an increase in current would be expected for an increase in $Q_m$. Indeed, Terman [85] observed that in general, $Q$ first increases with frequency because the reactance of a solenoid is proportional to frequency, whereas the RF resistance increases at a slower rate proportional to $\sqrt{f}$. Thus $R_{loss}$ is *not* constant with frequency and equation (4.11) is valid only for small changes in $\omega$.

At radio frequencies, skin effect is apparent and the wire resistance of round conductors becomes (p. 154 of [41]):

$$R_{wire} = \left[\frac{l}{2\pi r_{wire}}\sqrt{\frac{\pi f \mu}{\sigma}}\right] \Omega \tag{4.12}$$

where

$l$ is the length in metres

$r_{wire}$ is the radius in metres

$\mu$ is the magnetic permeability of the conductor in $H/m$

$\sigma$ is the wire conductivity in $S/m$ and

$f$ is the frequency in $Hz$

It is thus clear that, in a resonant secondary winding:

- Since the RF resistance is proportional to $\sqrt{f}$, at higher mode frequencies the $I^2R$ losses increase. Currents at the higher mode frequencies (e.g. $f_3$ and $f_5$) are therefore attenuated in comparison with those of the fundamental ($f_1$) mode frequency.

- A reduction of $Q$ at higher mode frequencies would decrease the current at those frequencies.
- From section (3.2), the frequencies and magnitudes of the responses of a resonant coil corresponding to the $f_3$ mode and above are particularly affected by counter winding, whereas the fundamental is left largely unaltered.

Counter winding a portion of a resonant solenoid thus changes the higher-order mode frequencies and also the higher-order mode current magnitudes. If counter winding causes an *increase* in mode frequency compared with the mode frequency of a standard coil, then a reduction in $Q_s$ at that mode frequency will ensue, along with a corresponding reduction in current at that frequency.

In other words, the output frequency spectrum of a Tesla transformer using a counter-wound secondary coil should contain reduced signal amplitudes at the higher mode frequencies compared with those of a standard winding.

## 4.1 Theoretical modelling

Appendices (B) and (C) provide analyses of both lumped and distributed design approaches. However, by using equations (4.1) and (4.3) alone, the self-resonant frequency of a bare (no toploaded present) solenoid can be approximated for the $f_1$ mode, ignoring any additional capacitance due to field grading structures such as a toroid (see figure (5.1)). De Queiroz [86] has demonstrated methods to compute the exact capacitance for an isolated metal toroid, which can then be used to lower the resonant frequency, calculated via Wheeler and Medhurst's

formulae, to select a secondary resonant frequency which corresponds to the primary coil/capacitor resonant frequency. The choice of toroid size is also a function of breakdown voltage*; a toroid with a larger radius of curvature exhibits a higher corona inception voltage (p. 211ff. and p. 371 of [87]) but also a higher capacitance since its capacitance is proportional to the major diameter. These basic methods are used in this thesis in order to formulate a starting point by which the self-resonant frequency of a secondary winding could be estimated.

Both Medhurst and Wheeler assumed a uniform current distribution for their calculations, whereas transmission line analyses and measurements demonstrate a cosinusoidal $z$ axis distribution of current in a resonant helix. Additional work to identify the self capacitance of a solenoid, at high frequencies, can be found in Grandi et al. [88]. Whilst the fundamental mode for a standard single-layer solenoid coil can be approximated by application of Grandi's/Medhurst's and Wheeler's formulae as per the starting point used for the Tesla transformer described in chapter (5), or via more sophisticated methods [46], the higher-order modes cannot be similarly computed and neither can this approach be applied to any of the experimental counter-wound resonators.

Distributed resonators demonstrate marked resonances at distinct frequencies and a lumped-component equivalent circuit may be used to describe the behaviour at each frequency [89]. A general term for the resonant frequencies of a circuit containing *distributed* $L$ and $C$ can be obtained in which the $m^{th}$ resonant mode frequency $f_m$ is given by (p.

*chapter seven of [18] and chapter four of [87] provide a thorough discussion. A toroid presents a larger capacitance than a sphere, for a given corona inception voltage.

3949 of [84])

$$f_m = \frac{1}{2\pi\sqrt{L_m C_m}} \tag{4.13}$$

where

$L_m$ is the *high frequency* inductance at the $m^{th}$ mode frequency

$C_m$ is the *high frequency* capacitance at the $m^{th}$ mode frequency

The anharmonic nature of the modes can be explained by considering the non-uniform nature of the currents and voltages distributed along the $z$ axis of the coil. At frequencies where the length of the conductor from which the coil is wound is an appreciable percentage of a wavelength at the self-resonant frequencies, the current distribution along the coil winding is no longer constant (p. 198ff. of [41]). This results in non-uniform magnetic flux linkage between turns and so, at the coil's self-resonant frequency, the apparent high frequency inductance (termed $L_{HF}$) is different from Wheeler's low frequency DC inductance $L_{DC}$. The distribution of electric charge along the winding is also non-uniform (p. 274 of [3]), which means that the coil's electric field, and hence its capacitance (termed $C_{HF}$), differs at each mode frequency and does not follow [82] or [88]. As the mode frequencies increase, the current and voltage distributions (modes) change as illustrated in figure (3.4). These differing distributions give rise to different values of inductance and capacitance at each mode frequency and if $\sqrt{L_m C_m}$ varies for each mode, so too does the corresponding resonant frequency. Figure (4.14) illustrates some of the $H$ field patterns modelled in NEC in order to elucidate this mechanism.

Work by numerous authors (e.g. [73] [74] [75]) demonstrates how a conductor, when wound into a helix, forms a slow-wave structure[†]. Sloan [53] investigated the Tesla transformer and noted its transmission-line characteristics (see section (3.1)) in the 1930s. In the 1940s and 1950s, periodic distributions of electric and magnetic fields along the length of a helix were identified and mathematical models constructed to demonstrate the slow wave nature of the structure. Section (2.2) discussed a distributed model of a Tesla transformer and illustrated the superposition of a forward and reverse direction (backward) travelling wave front as a mechanism by which standing waves on a resonant helix may be interpreted. A useful discussion of slow wave structures is given in chapter nine of [41] and chapter three of [90] where the concept of *space* harmonics is introduced. Space harmonics, sometimes referred to as Hartree harmonics, are an infinite series of waves which make up an electric field, where each wave has the same frequency but a different phase from one another (p.56 of [90]). They are related to Fourier series (p. 357 of [41]) and are a description of a propagating EM mode, determined by the geometric, periodic nature of the structure on which such modes travel. The electric field distribution of such modes is given by [41]

$$E(z,t) = \sum_{n=-\infty}^{n=+\infty} E_n e^{j\omega(t-k_n z)} \tag{4.14}$$

where

$E(z,t)$ is the time variation in electric field along the $z$ axis

$E_n$ is the peak electric field for a particular propagation mode $n$

[†]a structure in which the axial propagation of a wavefront is significantly slower than the speed of light in the same medium

$k_n$ is the wave number $\frac{2\pi}{\lambda_n}$ per harmonic mode at that mode frequency (wavelength)

Equation (4.14) describes the amplitude distribution for different modes propagating along the $z$ axis of the helix. As the mode number $n$ increases, the magnitude of the $E(z,t)$ space harmonic rapidly diminishes. Thus low values of $n$ are propagated with low attenuation whereas high order modes are more highly attenuated. This directed the work of this thesis to concentrate on suppression of the lower-order modes, predominantly $f_3$.

Additional analyses that describe the slow-wave behaviour of single-layer solenoids are summarised in [90]. Work by Pierce [91] considered a theoretical sheath helix made by winding a single, infinitesimally thin PEC strand around a cylinder to form an infinitely long helix. The gap between turns is occupied by successive identical individual strands in parallel with the original but insulated from it and from one another, continuing until the gap is filled. The helical sheet formed is similar to the Nagaoka current-sheet (p. 142 of [43]), but because the individual strands in the helix are insulated from one another the only direction for current propagation is along the path described by the helix, with no conduction perpendicular to it. The sheath model further assumes that the circumference of the helix, and the pitch between turns, is much smaller than the wavelength of any alternating current propagating in the helix.

Another model which addresses some of the sheath helix's assumptions is the tape helix [92], constructed from a two-dimensional strip of infinite length and finite width but zero thickness. A

PEC material is again assumed for the strip. Those analyses use terminology which discusses "forbidden" and "accepted" frequency bands, yet later work [93] determines that the helix radiates in those forbidden frequency ranges, and propagates at frequencies in the accepted bands in a $z$ axis direction. Wallington [94] identified from [91] that open periodic structures, such as single-layer solenoidal helices, can be designed such that alternating currents above a certain critical frequency cause the transmission line to radiate EM energy, which results in high transmission loss along the helix. Frequencies below this value are propagated along the line with no EM radiation and hence low transmission loss occurs along the helix.

The sheath and tape models consider infinitely long helices as the basis for analysis. However, a paper by Neureuther et al. [95], referring to earlier work by Klock [96], stated that a truncated helix (along the $z$ axis), standing on a ground plane positioned on the $xy$ plane at $z$=0 as shown in figure (3.2), can be treated as if it were an infinitely long helix.

Wallington [94] noted that the analytical equations from Pierce [91] [97] and Sensiper [92] "are very complex and of limited validity [and] are not really suitable for practical filter design". Vizmuller also analysed these models and concluded that "none of them can be readily applied to a general engineering problem" because they are "burdened with complicated mathematics" (p. 18 of [1]). Additionally, according to [98], "**...** there exists no rigorous solution of Maxwell's equations for the solenoidal helix".

However, Vizmuller investigated the effects of counter winding the uppermost portion of a resonant helix and stated the reason why

the fundamental ($f_1$) mode frequency is unaffected (p. 68ff. of [1]). For a helix of total height $\mathcal{H} = \frac{\lambda}{4}$, counter winding a small upper portion shortens the electrical length of $\mathcal{H}$ and leaves a lower portion, $\mathcal{H}_{lower}$, wound in the normal direction. The length of $\mathcal{H}_{lower}$ is quarter-wave resonant at some higher frequency but the upper counter-wound portion, $\mathcal{H}_{upper}$, adds additional capacitance, which results in a lowering of the overall resonant frequency, whereby $\mathcal{H}_{upper} + \mathcal{H}_{lower}$ again equals $\frac{\lambda}{4}$ at the fundamental $f_1$ mode frequency.

Work by Kandoian and Sichak [75], Sensiper [92], Corum and Corum [98] and Pierce [91] [97] [99] identified expressions for the *velocity factor* ($\mathbb{V}$) of a helix (appendix (C) equation (C.8)). The references show that the helical resonator is a dispersive line, in that $\mathbb{V}$ is not constant for all frequencies and a different propagation velocity exists for differing wavelengths. This is supported by [40] which shows that the phase constant ($\beta$) for a transmission line (see appendix (C)) is not constant with frequency. The wavelength of an RF current flowing in such a dispersive transmission line varies as a function of frequency and hence the electrical dimensions of the resonant solenoid also vary. A resonant solenoid structure which is electrically $\frac{\lambda}{4}$ at $f_1$ is not $\frac{3\lambda}{4}$ at $3f_1$ but at some new frequency $3f_1 + \Delta f$. The dispersive nature of the solenoid transmission line also means that the characteristic impedance presented by the resonant helix is different at different wavelengths (appendix (C) equation (C.9)).

Kraus discussed a $T_0$ transmission mode (in p. 274 of [3] and [100]) which has distributed positive and negative charge collections along the length of a helix. He identified the $T_0$ mode as being the dominant mode of a travelling wave helix with both the circumference of the helix

and the total conductor length comprising the helix needing to be $\ll \lambda$ for the $T_0$ mode to exist. In this case a substantial component of electric field is present along the $z$ axis due to the appreciable separation of charges of opposite sign. Section 7-3 of [3] gives a description of the propagation modes in helices.

The helix propagation mode analyses cited in this section are not trivial, but there is a simple hypothesis which appears feasible. The superposition process on a resonant helical transmission line may be disturbed by the discontinuity introduced by counter winding, such that the interference pattern becomes destructive at higher-order modes whilst leaving the fundamental mode unaffected. An elementary analysis to support this hypothesis is based on a simple and approximate model of the 0% helix compared with one of the counter-wound helices. Figure (4.2) compares *current* distributions in the 0% helix with those in the 33% helix, where in the latter case the top third of the winding turns are counter-wound as illustrated.

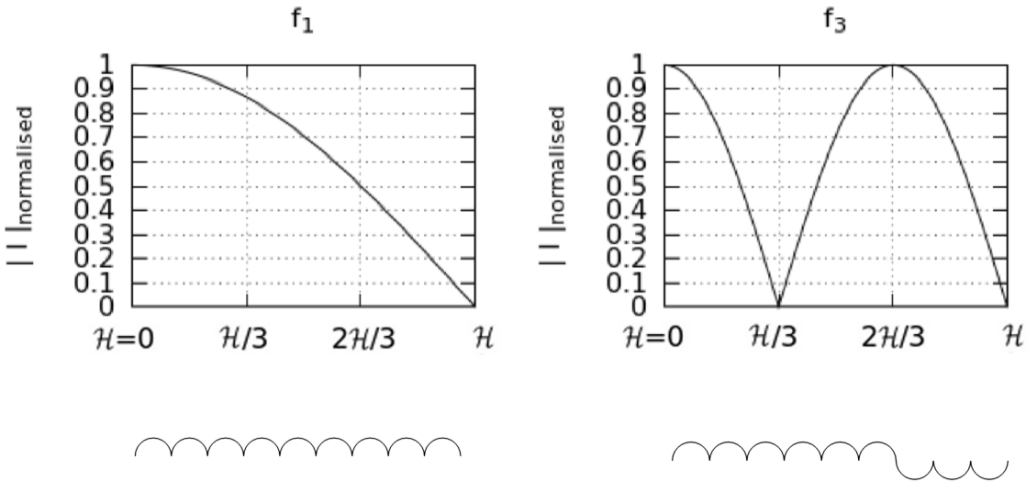


Figure 4.2: Distribution of $f_1$ and $f_3$ mode currents along $\frac{\lambda}{4}$ helical resonators

The peak envelope of the secondary current $|I|$, normalised to unity, is plotted against $\mathcal{H}$ which shows that the $f_1$ mode current exhibits an almost linear reduction of current per turn at locations away from the base ($\mathcal{H} = 0$), towards the top ($\mathcal{H}$). In order to discuss the simple model, assume arbitrarily that the turns are wound in a clockwise sense along the section from the base at $\mathcal{H} = 0$ to the point $\frac{2\mathcal{H}}{3}$ (an *electrical* height of $\frac{\pi}{3}$ radians) and then continue for the remaining third (from $\frac{2\mathcal{H}}{3}$ up to $\mathcal{H}$) in a clockwise sense for the 0% coil, but in a counter-clockwise sense for the 33% coil.

Parallel turns conducting current in the same direction generate magnetic fields around the conductors which aid one another, but when the currents in adjacent conductors flow in opposite directions, the fields around the conductors oppose each other. The mutual inductance between the lower two-thirds and the upper third modifies the total inductance of the winding (p. 65 of [33], [43]):

$$L_{total} = L_{lower} + L_{upper} \pm 2M \tag{4.15}$$

In the 0% resonator, the current in the bottom two thirds (from $\mathcal{H} = 0$ to $\mathcal{H} = \frac{2\mathcal{H}}{3}$) and that in the remaining top third (from $\mathcal{H} = \frac{2\mathcal{H}}{3}$ to $\mathcal{H}$ itself) flows in the same clockwise direction since, for the 0% winding, the turns are all wound in the same direction. The mutual inductance $M$ between the two sections of the coil thus contributes to the total inductance. However, in the 33% coil, the top third of the helix is wound counter clockwise and hence the current flowing in the bottom two-thirds creates a magnetic field opposed to that created by the currents in the top third. The mutual inductance is now subtractive, causing a reduction in the effective overall inductance.

The quasi-static[‡] (low frequency) inductance of a single-layer solenoid is given in terms of the magnetic flux linkage of turns by magnetic field $B$ (p. 159 of [39]):

$$L = \frac{n\psi_m}{I} = \frac{\Lambda}{I} \tag{4.16}$$

where

$n$ is the number of turns

$I$ is the current in the solenoid in A

$\psi_m$ is the total magnetic flux in Wb

$\Lambda$ is the flux linkage, in Wb per turn

Equation (4.16) assumes a uniform current per turn whereas the current in the quarter-wave resonant helix is cosinusoidally distributed along the axis over the range 0 to $\frac{\pi}{2}$. At the fundamental frequency, the total magnetic field due to the circulating current in the lower portion of a 0% winding is the summation of the magnetic field in that portion. The $f_1$ current is distributed with the maximum current occurring at $\mathcal{H}$ = 0 and falling cosinusoidally to zero at position $\mathcal{H}$. The lowest third of the quarter-wave resonator has an electrical height $\mathcal{H}$ equal to $\frac{\pi}{6}$ and has an inductance of $L_{lower}$. The upper portion, the remaining two thirds, has an electrical height of $\frac{\pi}{3}$ and an inductance of $L_{upper}$. The total $z$ axis distributed current for the 0% winding can be described by

$$I_{1(z)_{total}} = \int_0^{\frac{\pi}{6}} \cos(I)\, dz + \int_{\frac{\pi}{6}}^{\frac{\pi}{2}} \cos(I)\, dz \tag{4.17}$$

[‡]having a spatial distribution similar to a time invariant field (p. 1 & p. 71 of [41])

However, at the $f_3$ mode frequency, the current distribution changes and falls from a maximum at $\mathcal{H}$ = 0, to zero at $\mathcal{H}$ equal to $\frac{\pi}{6}$, and then rises to a maximum at $\mathcal{H}$ equal to ($\frac{\pi}{3}$) before again falling to zero at $H$ equals $\frac{\pi}{2}$:

$$I_{3(z)_{total}} = \int_{0}^{\frac{\pi}{6}} \cos(3I)\, dz - \int_{\frac{\pi}{6}}^{\frac{\pi}{2}} \cos(3I)\, dz \tag{4.18}$$

The difference between equation (4.17) and equation (4.18) shows that the inductance for the lower section and the upper section is modified by the different mode current distributions along the helix, which alters the flux linkage between turns (via equation (4.16)). The mutual inductance between the lower and upper portions therefore *changes* at different mode frequencies, because $M$ is proportional to $\sqrt{L_{lower} L_{upper}}$. The mutual inductance between two solenoids sharing a common axis can be found (p. 122ff. of [43]), assuming low frequency inductances $L_{DC}$. The changes in current distribution at different mode frequencies causes changes in the flux linkage between different parts of the winding and hence the high frequency inductance $L_{HF}$, and corresponding resonant mode frequency $f_m$, alter as a function of the current distribution. Similarly, changes in the voltage distribution with mode frequency alter the electric field stored in the vicinity of the coil which alters the capacitance associated with the coil, again causing a change in resonant frequency.

Examination of figure (4.3) shows that the *total* current, and hence total magnetic flux, distributed in the upper portion of the winding from $\frac{2\mathcal{H}}{3}$ to $\mathcal{H}$ is higher for the higher order modes than it is for the $f_1$ mode. The resultant increase in flux linkage leads to an increase in the

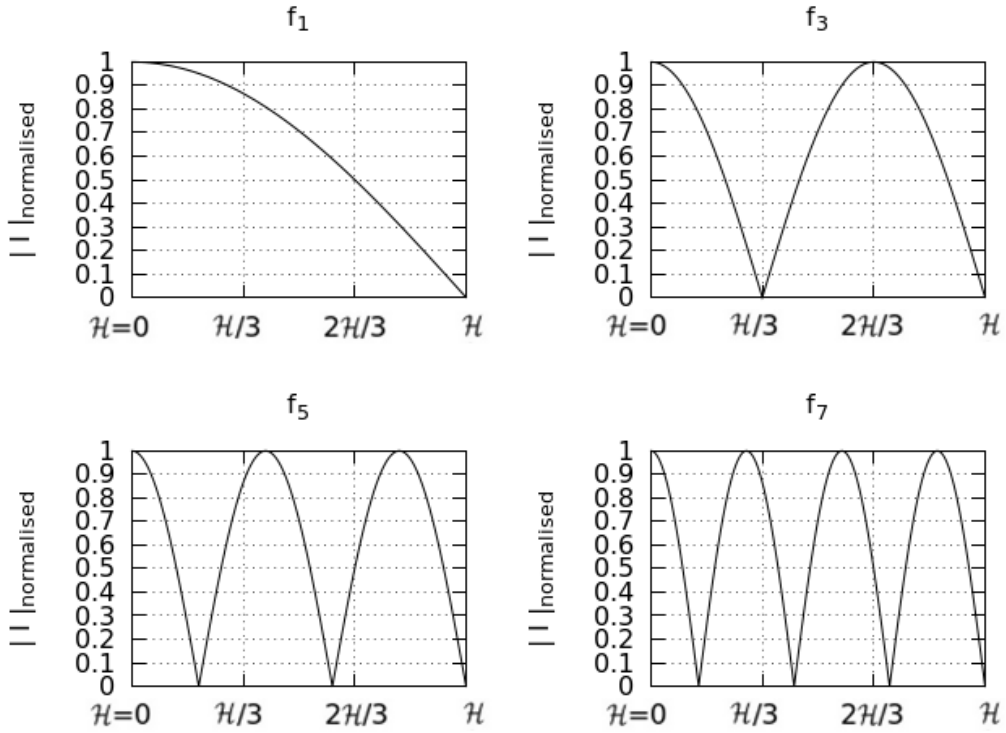


Figure 4.3: Cosinusoidal current distributions for the first four modes in a “0%” winding

high frequency inductance for the upper portion, hence the value of $M$ rises. The magnetic flux of the counter-wound section is in anti-phase to that of the lower section and hence the value of $M$ is subtractive, causing a net reduction in the overall high frequency inductance $L_{HF}$. This increases the resonant frequency of the higher order modes, but has little effect at the fundamental frequency.

## 4.2 SPICE modelling

LTSpice, described in subsection (1.1.4), was used for two tasks. The first was to model the required primary/secondary coupling by simulating the primary/secondary interaction when the primary coil was energised by a step function. The spark gap was simulated as a switch whose on and off resistances could be set and whose switching times and durations could be controlled. The second task was to simulate the frequency spectrum of currents flowing in the secondary winding and a simple distributed model of the 0% secondary coil was implemented in LTSpice, with the value of the total secondary inductance being distributed between ten inductors and the total secondary capacitance similarly distributed between ten capacitors. The following list identifies the SPICE variables used in the model.

- **V_dc** was set to 10 $kV$ to simulate the charging power supply.
- **R1** was set to 5 $k\Omega$ in order to limit the charging current supplied.
- **V_trig** was set to a pulse waveform with rise/fall times set to 50 $ns$, a "mark" width of 100 $\mu s$ and a 200 $\mu s$ wide "space".
- **GAP** was the spark gap, with $R_{on} = 10\ m\Omega$, $R_{off} = 100\ M\Omega$.
- **C_pri** was set to 17.5 $nF$.

- **R_pri** was set to 200 $m\Omega$.
- **L_pri** was set to 70 $\mu H$.
- **k L_pri L_sec** set the coupling coefficient between the primary and secondary.
- **L** set the total secondary winding inductance to 45 $mH$ distributed throughout ten inductors.
- **R_loss** set the total secondary winding loss resistance to 200 $\Omega$ distributed throughout ten inductors.
- **C** set the total secondary winding capacitance to 30 $pF$ distributed throughout ten capacitors.

Figure (4.4) shows the circuit diagram and figure (4.5) shows the SPICE netlist for that circuit.

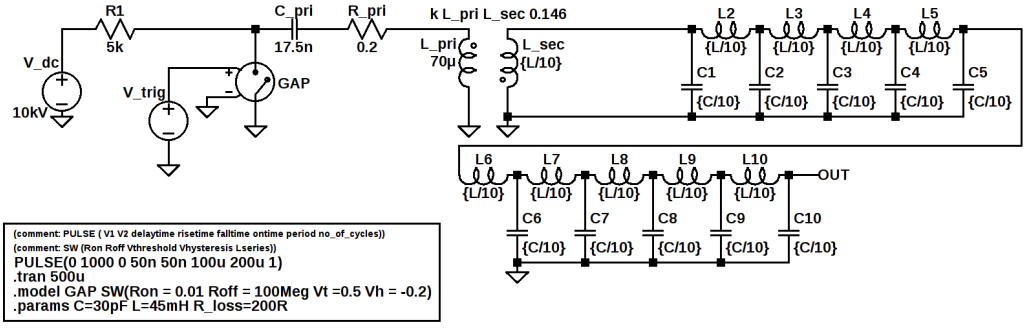


Figure 4.4: SPICE circuit model, generated using LTspice

```
* V_switch_distributed_sec2.asc
S1 0 N002 N010 0 GAP
V_trig N010 0 PULSE(0 1000 0 50n 50n 100u 200u 1)
V_dc N001 0 10kV
R1 N002 N001 5k
C_pri N002 N003 17.5n
L_pri 0 N004 70u
L_sec N005 0 {L/10}
R_pri N003 N004 0.2
C1 N005 0 {C/10}
C2 N006 0 {C/10}
C3 N007 0 {C/10}
C4 N008 0 {C/10}
C5 N009 0 {C/10}
C6 N011 0 {C/10}
C7 N012 0 {C/10}
C8 N013 0 {C/10}
C9 N014 0 {C/10}
C10 OUT 0 {C/10}
L2 N006 N005 {L/10} Rser={R_loss/10}
L3 N007 N006 {L/10} Rser={R_loss/10}
L4 N008 N007 {L/10} Rser={R_loss/10}
L5 N009 N008 {L/10} Rser={R_loss/10}
L6 N011 N009 {L/10} Rser={R_loss/10}
L7 N012 N011 {L/10} Rser={R_loss/10}
L8 N013 N012 {L/10} Rser={R_loss/10}
L9 N014 N013 {L/10} Rser={R_loss/10}
L10 OUT N014 {L/10} Rser={R_loss/10}
.model GAP SW(Ron = 0.01 Roff = 100Meg Vt =0.5 Vh = -0.2)
.tran 500u k L_pri L_sec 0.146
.params C=30pF L=45mH R_loss=200R
* (comment: PULSE ( V1 V2 delaytime risetime falltime ontime period no_of_cycles))
* (comment: SW (Ron Roff Vthreshold Vhysteresis Lseries))
.backanno
.end
```

Figure 4.5: SPICE netlist for figure (4.4)

Figure (4.6) shows that at approximately 95 $\mu s$ the "notch" point occurred in the simulated coupled waveform i.e. the point in time at which complete energy transfer has been achieved.

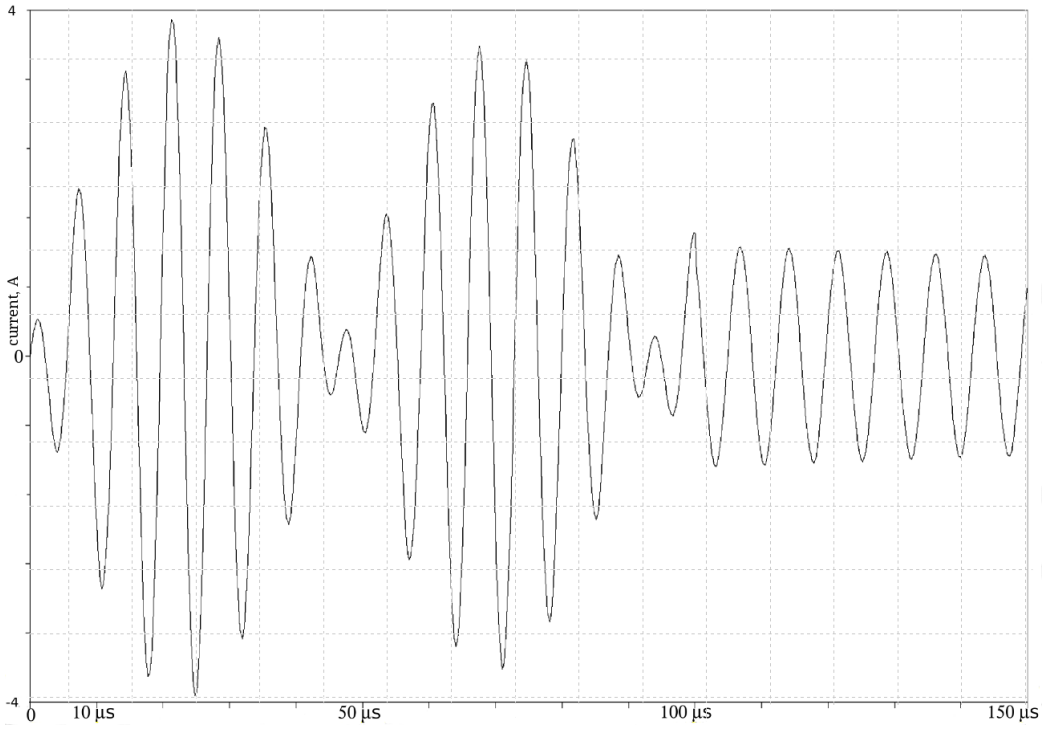


Figure 4.6: primary:secondary energy transfer

Table (B.1) in appendix (B) shows that $k$ = 0.146 is one value for complete energy transfer, requiring 11 cycles to complete. However, figure (4.6) shows that an earlier "notch" is predicted at approximately 50 $\mu s$. Had the experimental spark gap been more effectively quenched, this earlier notch time could have been met. One method of achieving improved quenching could be via faster air flow.

Figure (4.7) shows the $\frac{\pi}{2}$ separation in phase between the current flowing at the base of the winding and the voltage at the top of the winding.

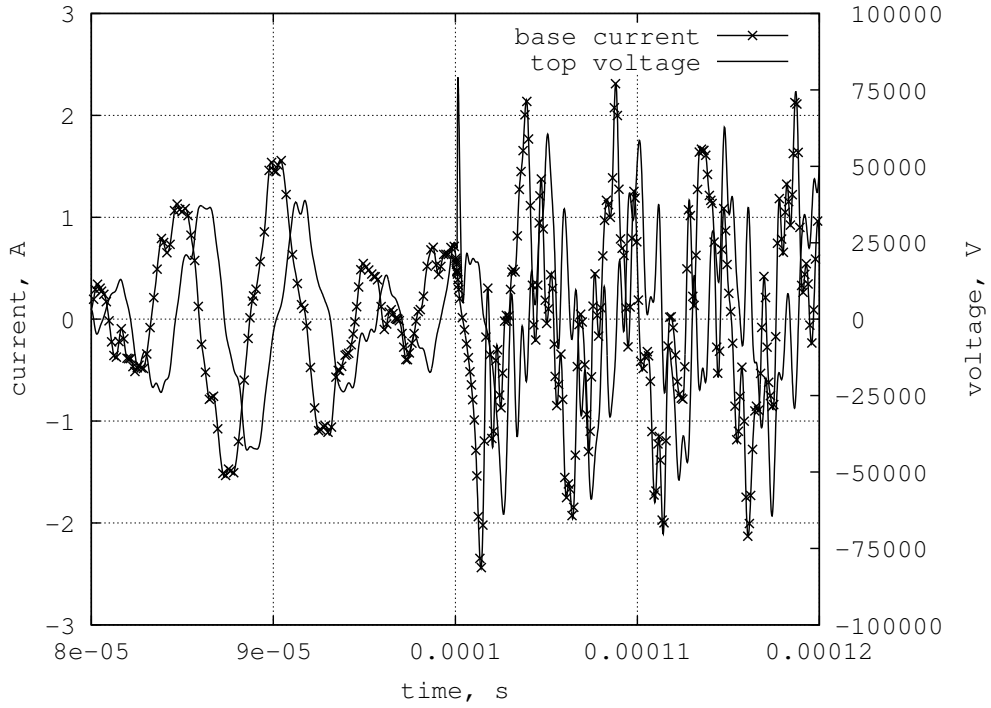


Figure 4.7: Secondary base current waveform and top load voltage showing $90^o$ phase shift

A fast Fourier transform (FFT) plot, shown in figure (4.8), was generated from the time domain waveforms in order to show the secondary coil's current spectra. The fundamental ($f_1$) is labelled and visible near the origin, and the $f_3$ and $f_5$ modes are labelled.

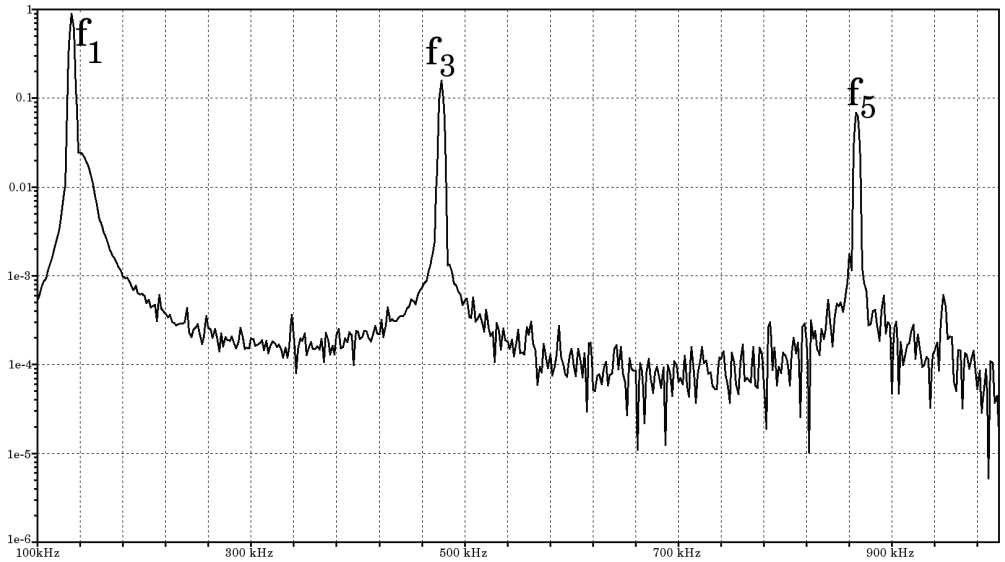


Figure 4.8: LTspice spectrum of the lumped-circuit model:
$f_1$ ≈140 $kHz$, $f_3$ ≈480 $kHz$, $f_5$ ≈870 $kHz$

It is interesting to note that comparing the modelled and measured mode frequency results, given in table (4.1), shows decreasing SPICE model accuracy at higher mode frequencies.

| mode | LTSpice simulation, $kHz$ | measured, $kHz$ | % error |
|---|---|---|---|
| $f_1$ | 137 | 136 | 0.7 |
| $f_3$ | 478 | 485 | 1.4 |
| $f_5$ | 870 | 764 | 14 |

Table 4.1: LTSpice simulation vs measured mode frequencies

This LTSpice modelling successfully enabled the coupling coefficient and spark gap dwell time interaction to be explored. SPICE modelling of the distributed secondary indicated that a number of mode frequencies would be present when measuring the current spectrum of an experimental Tesla transformer built to a similar specification.

## 4.3 TSSP modelling

The Tesla Secondary Simulation Project [2] is an online collaboration which claims to maintain (*sic*) a precise software model of single-layer solenoidal secondary windings. In this thesis, a modified form of TSSP software was utilised to model the effects of counter-wound turns on the various mode frequencies predicted by TSSP.

As part of the TSSP project, a suite of computer programs was developed which could be compiled to run under Linux. The programs allowed a simulation to be run which modelled the dimensions of the environment surrounding a solenoid (for example, laboratory ceiling height) and then predicted the $f_1$ (fundamental) self-resonant frequency and the first few overtone frequencies $f_3$, $f_5$ etc. A modified version of part of the set of TSSP programs was used to describe the coil geometry in terms of height, diameter, number of turns and, as a result of programming code modification, an expression for the percentage of reversed turns was added (see figure (4.9)). Thus a mechanism was produced by which the TSSP programs could predict the resonant frequencies of different modes in a simulated standard 0% coil, and one in which some turns had been counter-wound. By running aspects of TSSP in a Bash-scripted[§] loop, it was possible to generate the graph shown in figure (4.10).

The graph demonstrates, for example, that counter winding approximately 30% of the turns caused the fundamental resonant frequency to change by less than 5%. The $f_3$ mode frequency increased by more than 12% and the $f_5$ mode frequency decreased by 3%.

[§]"Bash" is a form of interpreted programming language, intrinsic to Linux, which can be used as a simple yet powerful utility to automate numerous computing tasks

```
BEGIN
model {gran 2}
world {ground_radius 3.4/2 wall_radius 3.4/2 roof_height 2.4}
secondary {radius 113.616e-3/2 height _HEIGHT_ length 0.563 turns
1618 conductor 0.35e-3/2 revt 1618 * (1 - _REWIND_) }
END
```

Figure 4.9: TSSP code for full-size resonator

| coil rewind % | $\Delta f_1$% | $\Delta f_3$% | $\Delta f_5$% |
|---|---|---|---|
| 29 | +4.1 | **+12.3** | -2.0 |
| 54 | +9.7 | -1.4 | **+10.8** |
| 73 | **+12.1** | 1.7 | -2.6 |

Table 4.2: Mode frequency changes modelled by TSSP

Comparison with real measurements showed that TSSP modelled $f_1$, $f_3$ and $f_5$ with reasonable accuracy but with reduced accuracy at higher mode frequencies.

Examination of the simulation data of figure (4.10) showed specific counter winding percentages which gave the largest increase in frequency per resonator mode, as shown in table (4.2) where the pertinent increases are highlighted in bold. Table (4.2) shows that when the top 29% of the coil was counter-wound, the $f_1$ mode frequency increased by only 4.1% whilst the $f_3$ mode frequency increased by 12.3% and $f_5$ was hardly altered. The table also records other significant shifts in $f_3$ or $f_5$ mode frequency, but at the expense of significant shifts in the $f_1$ frequency.

Overall the results suggested that a coil with 29% of its turns counter-wound would demonstrate the largest change in frequency of the unwanted modes whilst imparting the smallest change in frequency to the $f_1$ mode. Based on this modelling, it was decided to manufacture and evaluate a range of experimental coils which were

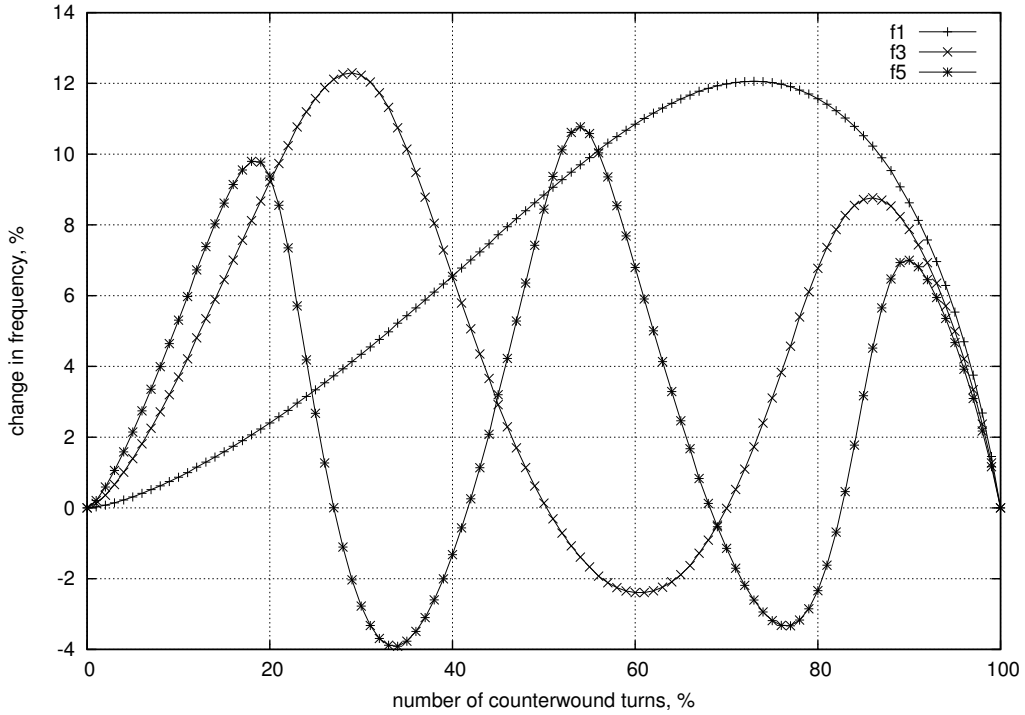


Figure 4.10: TSSP modelling of changes in resonator mode frequency with winding reversal (uppermost turns)

made with counter-wound portions of 10% through to 50%.

## 4.4 NEC modelling

NEC modelling was deemed to be useful for two main reasons. The first was that the effects of counter-wound turns could be modelled, which was not the case for SPICE models which cannot account for differences in winding direction. The second was because NEC allows simple visualisation of the $E$ and $H$ field distributions in the vicinity of the secondary coil, both standard and counter-wound, when the coil was energised at the various mode frequencies. The mode frequencies for the various models could be identified within the model via frequency sweeps.

A full-size model of the bare secondary coil outlined later in table (5.1) was written using nec2c [5]. The NEC input (in a form known as a "card") is described in figure (4.11). The conductor was set to PEC because NEC was used only to generate field distributions rather than $Q$ factor results i.e. the results were not dependent on real conductivity values for the winding.

Unfortunately, computer[¶] run times in excess of 14 days were required for the resonator input impedance solution alone to be computed and written out to a file. As a result it was only practical to model the $f_1$ frequency response of the various resonators. To plot each individual $E$ and $H$ field for the various modes in the full scale 0% resonator, it was estimated that many weeks would be required per plot. This was deemed to be impractical.

[¶]a 24 CPU computer with 128GB of RAM

```
CM —— 0% 1600 turns
CE
GH 1 31700 3.55205E-04 0.563 5.7E-02 5.7E-02 5.7E-02 5.7E-02 1.75E-04
GM 0 0 0.0E+00 0.0E+00 0.0E+00 0.0E+00 0.0E+00 5.E-01 0.0E+00
GW 2 5 0.0E+00 0.0E+00 0.0E+00 0.0E+00 0.0E+00 5.0E-01 1.75E-04
GW 3 5 0.0E+00 0.E+00 5.0E-01 5.7E-02 0.E+00 5.0E-01 1.75E-04
GE 1 0 0.0E+00 0.0E+00 0.0E+00 0.0E+00 0.0E+00 0.0E+00 0.0E+00
GN 1 0 0 0 0.0E+00 0.0E+00 0.0E+00 0.0E+00 0.0E+00 0.0E+00
FR 0 101 0 0 2.0E-01 1.0E-03 3.0E-01 0.0E+00 0.0E+00 0.0E+00
EX 0 2 2 0 1.0E+00 0.0E+00 0.0E+00 0.0E+00 0.0E+00 0.0E+00
XQ 0 0 0 0 0.0E+00 0.0E+00 0.0E+00 0.0E+00 0.0E+00 0.0E+00
EN 0 0 0 0 0.0E+00 0.0E+00 0.0E+00 0.0E+00 0.0E+00 0.0E+00
```

Figure 4.11: NEC code for full size resonator model

To make best use of the available computer time, a less computationally intensive NEC simulation model was written to be similar to the 0% simulation model listed in figure (4.11), but scaled from the full-sized model to a higher frequency model which had the same 563 $mm$ winding height and 114 $mm$ diameter but rather than containing 1600 turns, contained 56.3 turns i.e. 1 turn spaced every 10 $mm$. At the same time, a real coil was wound to match the specification of the 0% simulation model and figure (4.12) shows the finished physical coil prior to electrical measurement. The aim was to measure the 0% resonant mode frequencies for the constructed scale model and compare these to NEC simulations. The comparison, if similar, would lead to comments on the veracity of the scaled simulation model, such that modelled $E$ and $H$ field distribution and current flow in the resonator could all be assessed.

The “xnec2c” software was used to run the NEC simulation file and

Figure 4.12: Photograph of 56.3 turn constructed model coil

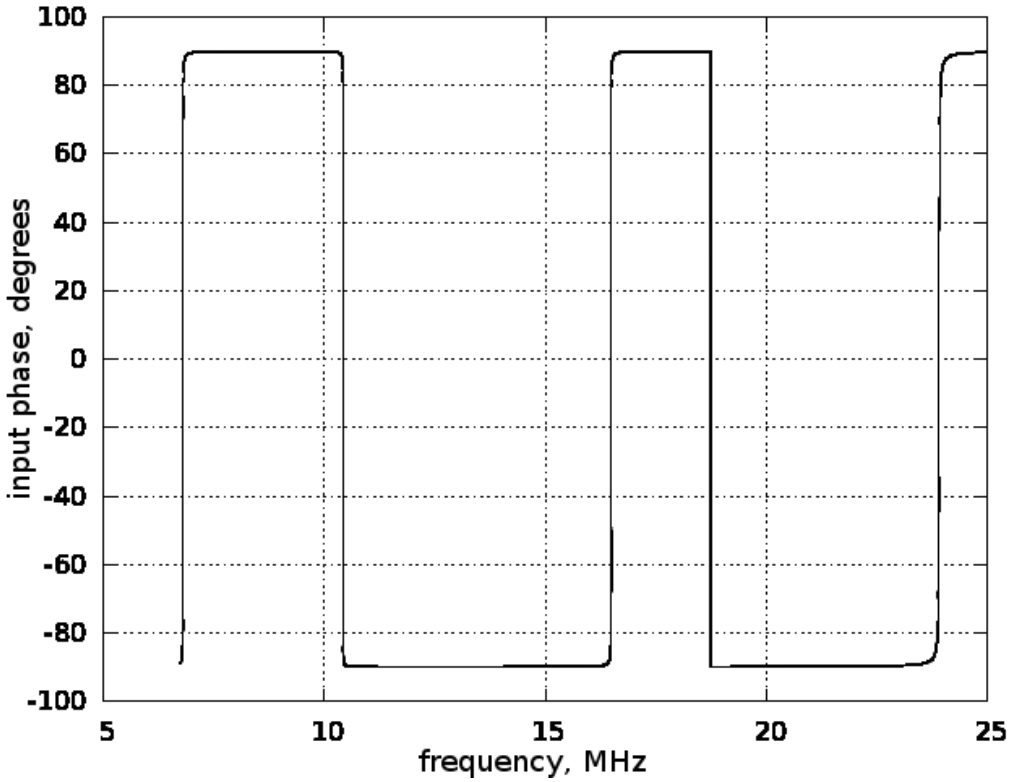


Figure 4.13: The first three resonant modes for n = 56.3, 0% resonator

explore the resonant modes. The results for the 0% model with n = 56.3 turns are shown in figure (4.13). It can be observed that various modes occur at approximately 7 $MHz$, 16 $MHz$, 24 $MHz$ where the phase of the input impedance crosses $0°$, which is coincident with the real part of the input impedance $Z$ reaching a local minimum.

Further explorations using finer resolution frequency sweeps were made in order to more accurately determine the theoretical $f_1$, $f_3$ and $f_5$ mode frequencies. Comparison measurements were taken from the 56.3 turn coil, with the first three resonant modes detected using an Advantest U6341 spectrum analyser/tracking generator. The results recorded in table (4.3) show that, overall, the mean error in the model predicted an increase of approximately 7% i.e. a 7% error when

| 0% resonator mode | $f_1$ | $f_3$ | $f_5$ |
|---|---|---|---|
| NEC modelled resonant mode frequency, $MHz$ | 6.788 | 16.756 | 24.417 |
| measured resonant mode frequency, $MHz$ | 6.397 | 15.597 | 22.621 |
| difference, $MHz$ | 0.391 | 1.159 | 1.796 |
| % error | +6.1 | +7.4 | +7.9 |

Table 4.3: n=56.3 0% resonator modes modelled in NEC & compared with measured results

comparing computer simulation with laboratory measurement.

Given that the mean error between the measured and modelled mode frequencies for the 0% resonator was reasonably small at 7%, it was decided that continued modelling results would be valid. Further NEC modelling was implemented to illustrate the current and voltage distributions along the windings, and distribution of the $E$ and $H$ fields around the windings at the various mode frequencies, for the 0% coil and for coils where n=56.3 turns but with the upper 10%, 33% etc. counter-wound. Interpretation of numerous[‖] NEC field plots (see figure (4.14) for examples) assisted in elucidation and development of the hypothesis presented in section (4.1). The associated $E$ and $H$ fields surrounding the windings at each mode frequency were mapped by resolving the vector representing each field point into its Cartesian components in a plane $(x, z)$ passing through the axis of the coil (i.e. at $y = 0$). Each $H$ field was summed to show the total field in each case and the resolved $(x, y, z)$ components were plotted. Manipulation via GIMP, a free tool found in most Linux distributions for manipulating the appearance of graphic files, rendered the field plots suitable for paper printing.

[‖]>100 current and voltage distributions and $E$ and $H$ field plots were created for the 56.3 turn models

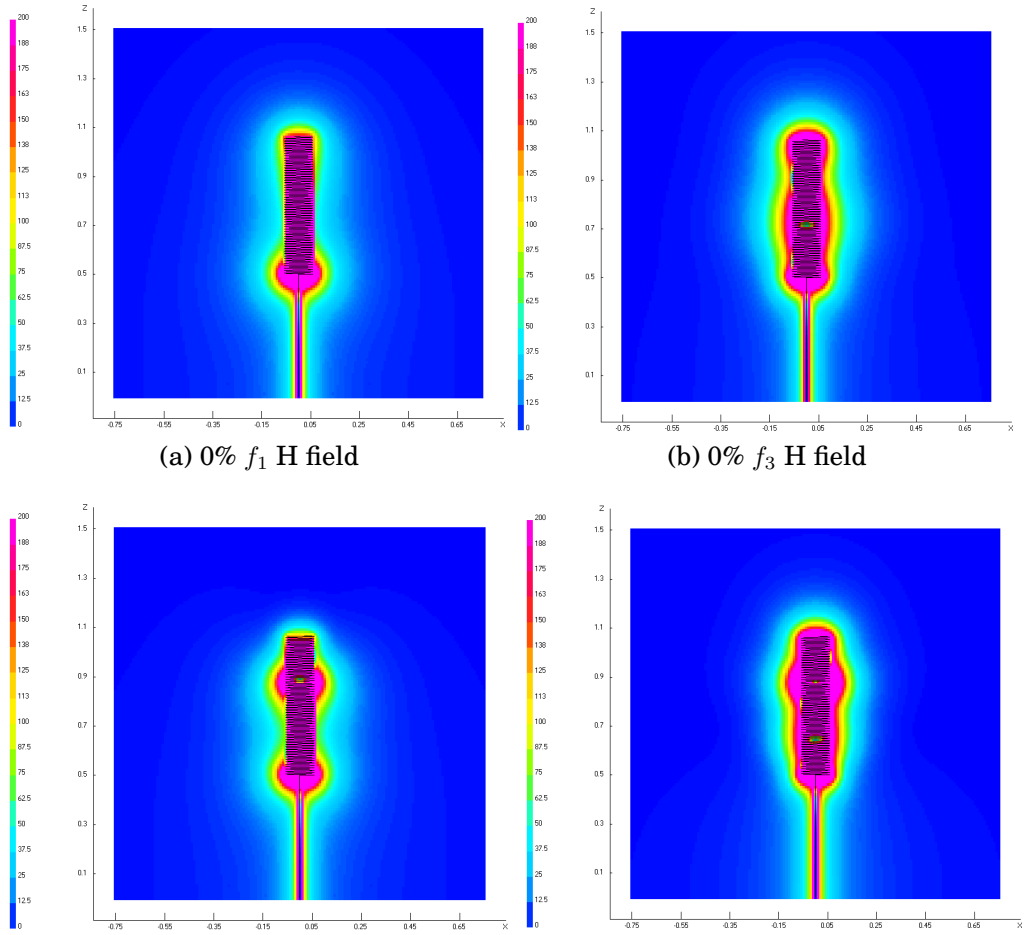

(a) 0% $f_1$ H field

(b) 0% $f_3$ H field

(c) 33% $f_1$ H field

(d) 33% $f_3$ H field

Figure 4.14: Some example H field distributions ($x$ axis scale is $^{-}0.75$ $m$ to $^{+}0.75$ $m$, $y$ axis scale is 0 to 1.5 $m$ and field strength colour scale is 0 to 200 $A/m$)

# Chapter 5

# Design, testing and measurement of an experimental Tesla transformer

A simple Tesla transformer with a secondary wound as a cylindrical solenoid was designed, constructed and used as a test-bed. The design goal for this Tesla transformer was to achieve a repeatable high output voltage, employing simple components and convenient air insulation at standard atmospheric pressure, acknowledging that this would be at the expense of power transfer efficiency (see section (2.3)). The transformer was designed to be a reliable reference generator, in which the responses of a conventionally-wound secondary coil and a number of experimental counter-wound secondary coils could be tested and compared with one another.

Some aspects of the Tesla transformer's design were constrained

by the components available. For example, the primary spark gap was made to a novel segmented design (see figure (5.2)), inspired by a type of pulse generator discussed in Frungel (vol. III p. 161ff of [101]). The design consists of eight highly parallel copper rods of 25 $mm$ diameter and 75 $mm$ length, pitched around a circumference of 75 $mm$ diameter but separated from one another by a fixed and equal distance, and mounted between two insulating support disks of 125 $mm$ diameter. Selection of adjacent segments connects one or more gaps in series, thus allowing simple and repeatable gap adjustment. Forced-air cooling/quenching was implemented in an attempt to shorten the "on" time of approximately 90 - 100 $\mu s$. Those two constraints governed the choice of coupling coefficient for this Tesla transformer design. Firstly the relatively slow performance of the gap meant that the transformer coupling coefficient was inevitably low. Secondly it should be noted from subsection (2.3.2) that high coupling, employing atmospheric pressure air insulation only, is not possible. The design requirement was therefore met by a geometry giving rise to a coupling coefficient $k$ of 0.146, calculated from appendix (B) and achieved by adjusting the height of the secondary coil base relative to the plane of the Archimedean spiral primary coil.

Using formulae described in appendix (C), the secondary coil/topload combination was designed to resonate at 136 $kHz$, a value chosen to coincide with a UK amateur radio frequency allocation* in an attempt to mitigate any EMI. The frequency chosen also suited available materials and minimised switching losses. The secondary winding was directly connected to a conductive toroid "topload" which

*ITU region 1, of which the UK forms part, allocates 135.7–137.8 $kHz$ for amateur radio use

had a major diameter of 530 $mm$ and a minor diameter of 75 $mm$. Field grading toroids (figure (5.1)) are often made by spinning a metal sheet on a lathe and forming against a mandrel to shape the flat sheet into a half-toroid. The resultant upper and lower halves are then precision welded together, and the welded joint or seam is ground flush prior to polishing to provide a very uniform surface.

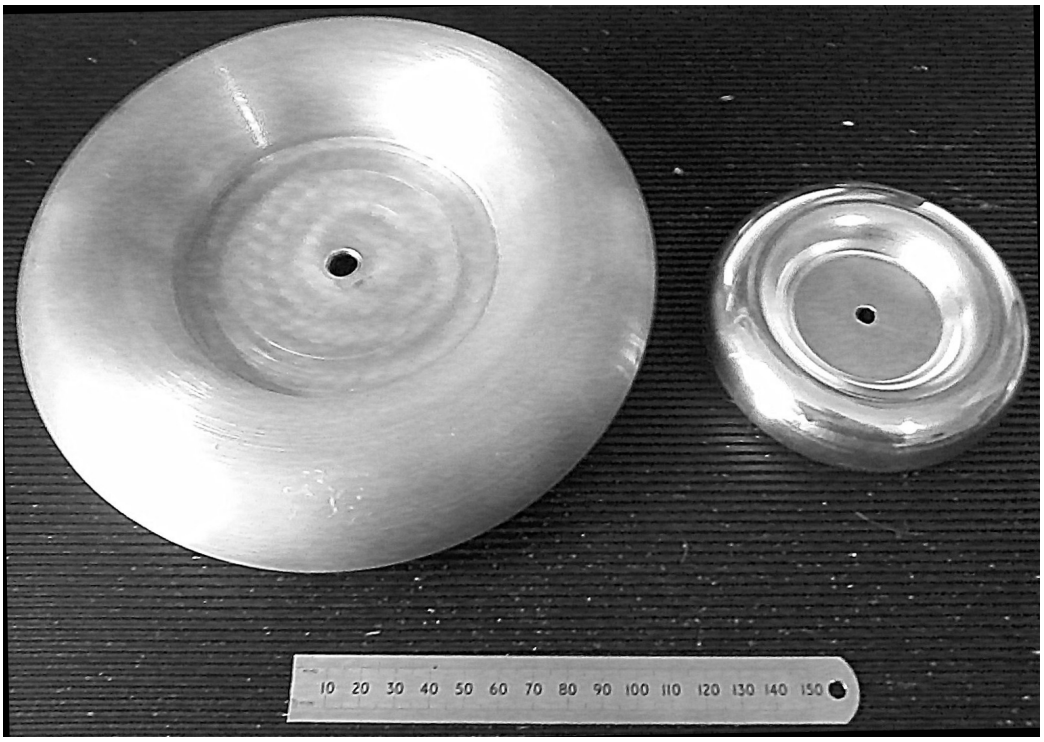


Figure 5.1: Two field grading toroids of different capacitances

The design of the spark gap and the type of primary capacitor were selected to allow the transformer to be operated both in a single-shot mode when used in conjunction with a low current power supply, or in a repetitive-shot mode when used with a higher current power supply. The transformer used as a bench mark a standard conventionally wound secondary coil with its topload in place, and the response of

that coil when energised from the primary circuit was measured via a range of transducers and instrumentation. This reference benchmark could then be used in comparison with the various experimental (part counter-wound) secondary windings with the toploaded in place i.e. the prototype secondaries could be substituted for the conventional secondary and their performance assessed and compared with both that of the conventional secondary and with modelled simulation results.

A low current (200 $\mu A$) 10 $kV$ dc-to-dc converting power supply [102] was used to trickle charge the primary capacitors, which were then fired at low repetition rates. These operating conditions enabled the primary spark gap to fire regularly, once every few seconds, at a reliable and repeatable firing voltage. The power supply enabled single-shot measurements to be easily implemented and the secondary coil mode frequencies and currents (with and without the toploaded) were measured and compared with the previous $Q$ measurements of the secondary coils when isolated.

The measured transformer parameters are listed in table (5.1).

A primary circuit was designed whereby the available pulse power capacitor was tuned by an external inductance to resonate the primary circuit at the chosen frequency. An estimate of the mutual coupling $M$ between primary and secondary coils (see section (4.2) and appendix (B)) enabled the coupling coefficient to be determined, which in turn placed constraints on the spark gap performance. Figure (5.3) shows the primary winding around the base of one of the experimental secondaries, with the spark gap and power supply visible to the left. The ability of a spark gap to switch rapidly from the conducting to


Figure 5.2: Novel spark gap design

| parameter | calculated value | measured value |
|---|---|---|
| Primary coil inductance $L_P$ | 70$\mu H$ | 70$\mu H$ |
| Primary capacitance $C_p$ | 17.5 $nF$ | 17.5 $nF$ |
| Primary capacitor stored energy | 875 $mJ$ | 875 $mJ$ |
| Primary resistance (inc. spark gap) | 200 $m\Omega$ | <500 $m\Omega$ |
| Primary resonant frequency $f_p$ | 145 $kHz$ | 144 $kHz$ |
| coupling coefficient $k_c$ | 0.146 | $\approx$ 0.145 |
| Secondary diameter $d$ | 114 $mm$ | 114 $mm$ |
| Secondary height $\mathcal{H}$ | 563 $mm$ | 563 $mm$ |
| Number of secondary turns $n$ | 1600 | $\approx$ 1600 |
| Secondary coil inductance $L_{dc}$ | 45 $mH$ | 45 $mH$ |
| Secondary coil DC resistance $R_{dc}$ | - | 111 $\Omega$ |
| Secondary coil RF resistance $R_{ac}$ | - | 200 $\Omega$ |
| Secondary coil capacitance $C_{sec}$ | 10 $pF$ | 9.4 $pF$ |
| Topload capacitance $C_{top}$ | 21 $pF$ | 20 $pF$ |
| Secondary (loaded) resonant frequency $f_s$ | 136 $kHz$ | 137 $kHz$ |

Table 5.1: Experimental Tesla transformer parameters

the insulating state is a function of its complexity (it may involve compressed gases, unusual gases such as $SF_6$, or even flammable gases such as hydrogen (p. 335 of [61])) and hence a relatively simple gap design cannot compete with more sophisticated designs [63].

A simple motorised coil-winding lathe was developed and a series of solenoid coils were produced (see figure (5.4)). In each case, identical acrylonitrile butadiene styrene (ABS) plastic formers were employed, constructed from 1 $mm$ wall thickness tube of 114 $mm$ outer diameter and 570 $mm$ in length, upon which an identical length of enamelled copper wire was wound such that each coil was made to the same dimensions with the same number of turns ($n$) occupying the same length. One coil was a conventional single-layer air-cored solenoid comprising 1600 turns and the others were basically similar but

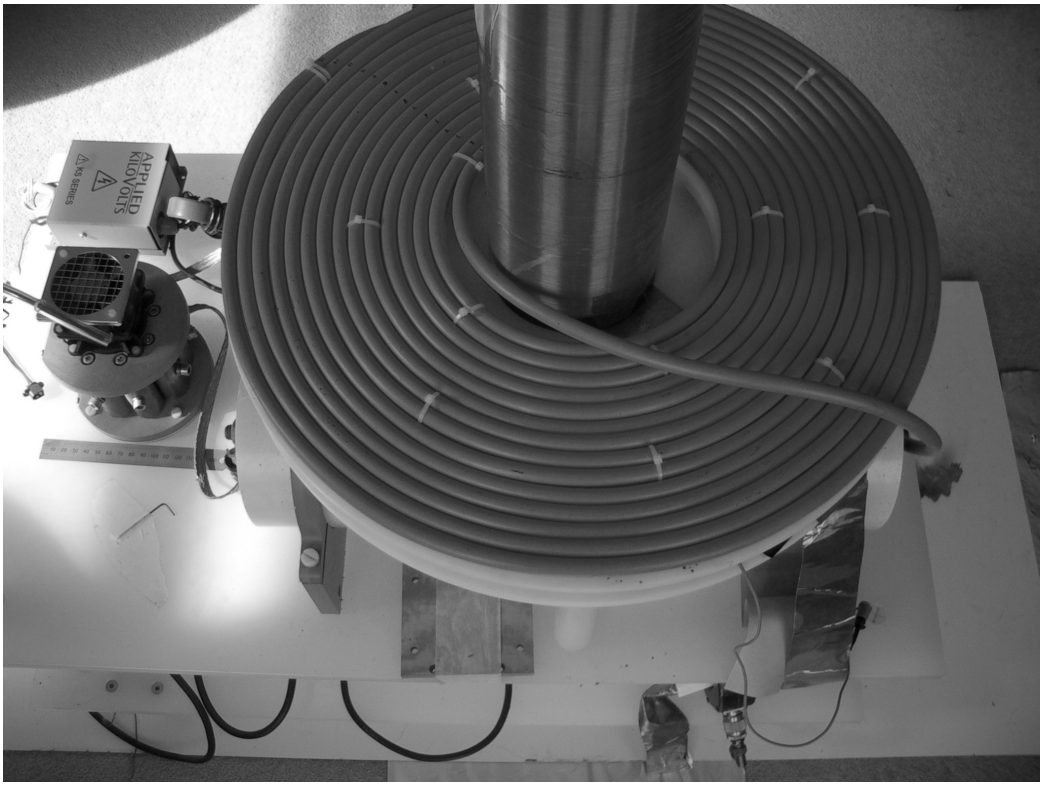


Figure 5.3: Detail of Tesla transformer used in experiments, showing primary and a secondary coil

Figure 5.4: A set of experimental coils

with the top 10%, 22.5%, 33% and 50% of the turns counter-wound. These sample dimensions were chosen to suit the experimental Tesla transformer benchmark which was described earlier. The proportion of turns comprising the counter-wound portion were selected across a limited range of values suggested by TSSP modelling (see section (4.3)) and which were considered to be easy to construct and measure.

In tandem with construction of this benchmark Tesla transformer, a range of instrumentation transducers were obtained and, where necessary, designed and constructed for use in conjunction with

standard laboratory test and measurement equipment[†].

## 5.1 $Q$ factor measurements

A number of methods [73] [103] [104] [105] are available by which $Q$ factor can be measured and the differences between loaded and unloaded $Q$ are discussed in the references. Loaded $Q$ is a term usually applied to the apparent $Q$ of an in-circuit resonant component or resonant network. The $Q$ is lowered, typically by loading from the signal generator used to provide the test current, or by connecting an electronic circuit to the device under test [103].

In order to find the true unloaded $Q$, it is necessary to remove from the experimental Tesla transformer secondary windings all external influences which might diminish the true $Q$. It is not possible to prevent coupling from the Tesla transformer secondary winding into its surroundings, or to prevent losses due to EM radiation propagating away into the far field. It is thus impossible to determine accurately the true unloaded $Q$, but there is value in using techniques to reduce the influence of loading [106] and those techniques were employed in the measurements made during this work.

### 5.1.1 $Q$ measurements via the 3dB method

At resonance, the complex input impedance of a circuit is real, since the imaginary components of the impedance cancel as the magnetic

[†]Tektronix and Rigol 1GS/s digital oscilloscopes, an Advantest 100 $kHz$ - 3 $GHz$ spectrum analyser/tracking generator and Hewlett-Packard and Rhode-Schwarz vector network analysers (VNAs) covering 100 $kHz$ - 3 $GHz$ were obtained along with other standard laboratory equipment such as signal generators and frequency counters etc.

field and electric field energies are equal. At both a specific frequency above and below the resonant frequency, the resistive (real) part of the complex impedance equals the magnitude of the reactive (imaginary) part:

$$R = \pm|jX| \tag{5.1}$$

which shows that the inductive or capacitive reactance is equal in magnitude to the resistive part of the coil's impedance, at some frequency either side of the resonant frequency. In both cases, half of the power supplied to the resonator is dissipated in the resistive part and half is stored in a continuous exchange between the electric and magnetic fields which comprise the reactive part. If the complex impedance of the coil is measured by a VNA and displayed on a Smith chart [38] [39] [105] [107], the input impedance at the resonant frequency ($f_0$) can be measured and the fundamental and overtone frequencies at which the inductive reactance and the capacitive reactance are equal in magnitude to one another can be determined. This enables the half-power points to be found for the fundamental and the higher mode resonances. Scalar impedance (impedance magnitude with no complex component) can be measured as a function of frequency, by using a spectrum analyser and tracking generator since the lower ($f_l$) and upper frequencies ($f_u$), corresponding to a halving of input power, can be determined [108]. Determining $Q$ in this way is often known as the "3dB" method and is a simple way of estimating the circuit quality factor, but it can only show the *loaded* $Q$ for a device under test due to the influence of the signal generator discussed in section (5.1).

Then $Q$ obtained this way is given by ([3], [109])

$$Q = \frac{f_0}{f_u - f_l} \tag{5.2}$$

In order to make loaded $Q$ measurements, the fundamental resonant frequency and the $f_3$ and $f_5$ modes were calculated approximately from the self-inductance (equation (4.2)) and self-capacitance (equation (4.3)) of a bare coil, and confirmed by measurement with the coil positioned as shown in figure (5.5). The base of the coil to be measured was set at 0.5 $m$ to match the height when used later in the experimental Tesla transformer. A series of frequency domain measurements were made on each of the individual experimental coils in a constant laboratory environment by energising them with a constant amplitude RF current, swept in frequency from below the fundamental resonant frequency to above the $f_5$ mode.

A typical spectrum analyser measurement, from which the loaded $Q$ can be calculated by the 3dB method, is shown in figure (5.6). Table (5.2) records the results of the measurements performed, using "$Q_l$" to denote that the $Q$ recorded is the loaded $Q$ since the resonator experienced external influence when being measured. The data from table (5.2) is expressed graphically in figure (5.7).

It is interesting to note an empirical formula [75] that gives the resonant frequency of a helical resonator as:

$$f_1 = \frac{29.85 \left(\frac{\mathcal{H}}{d}\right)^{\frac{1}{5}}}{nd} \tag{5.3}$$

where

$f_1$ is the fundamental self-resonant frequency in $MHz$

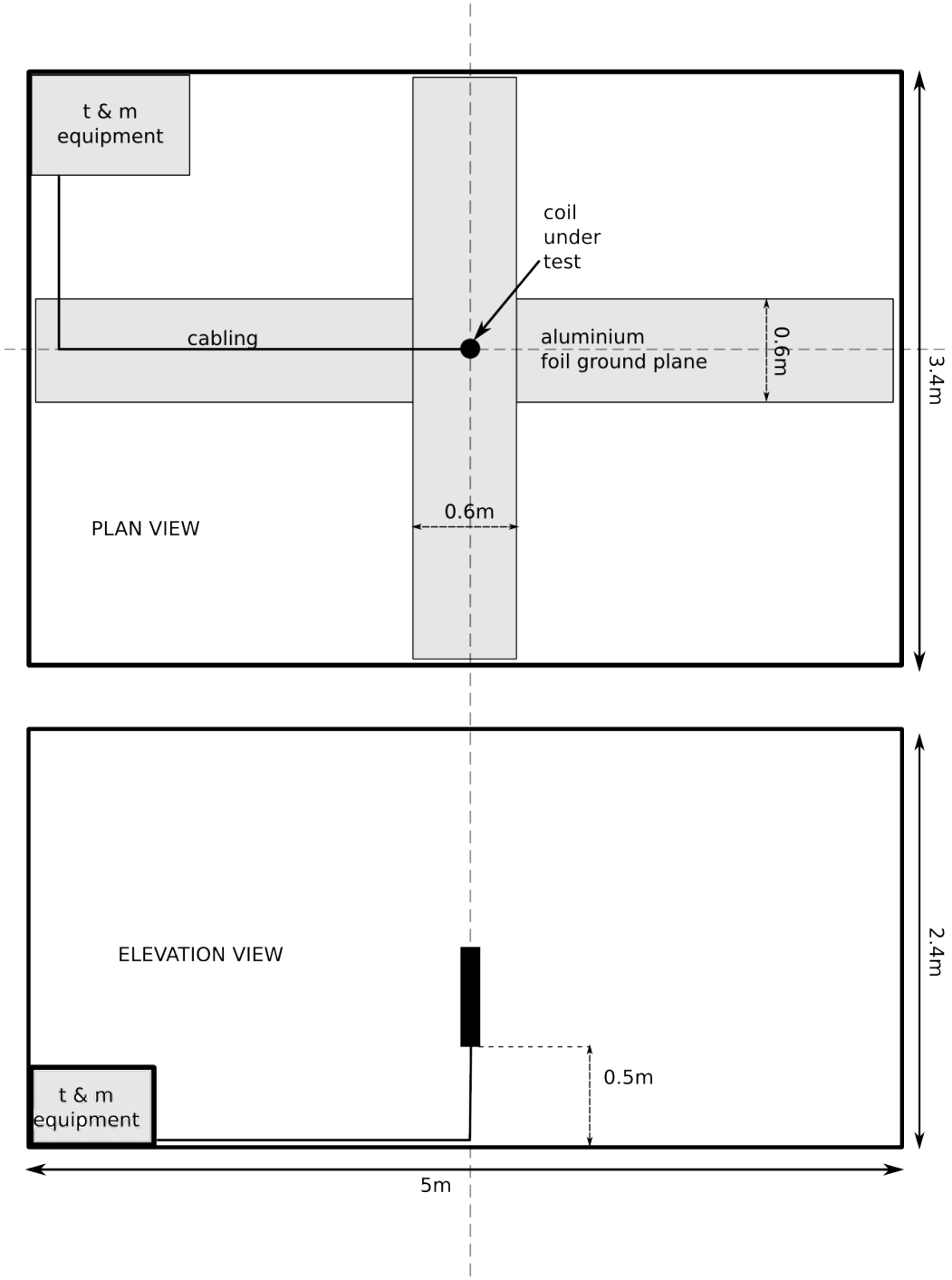


Figure 5.5: Diagram of test area

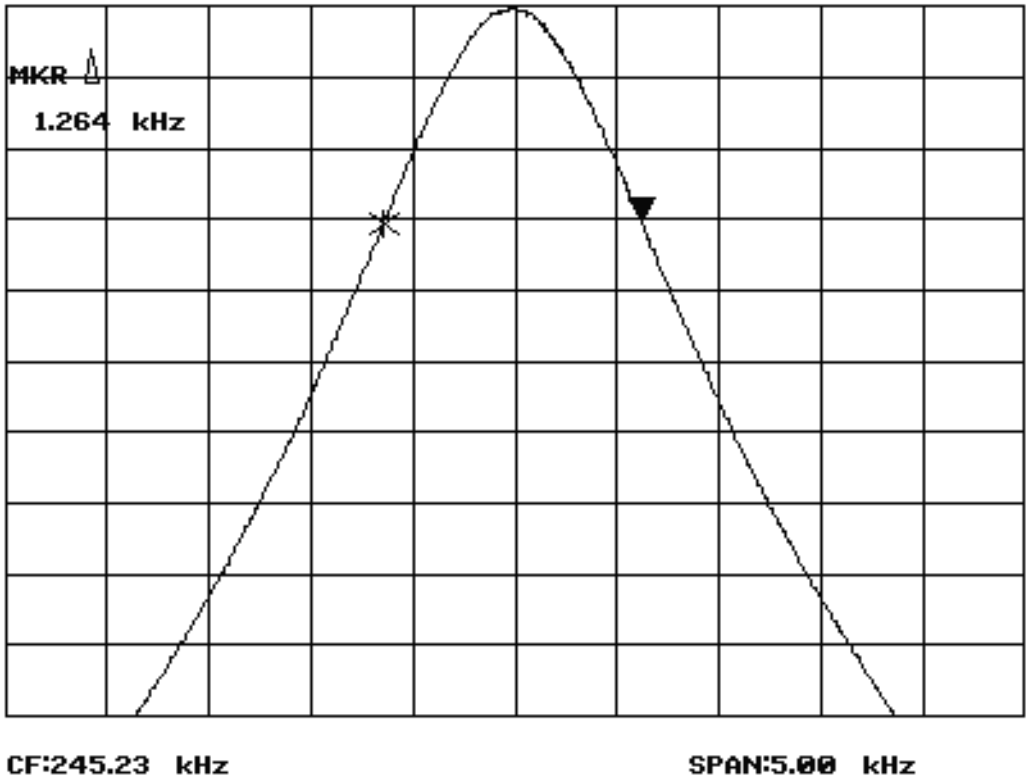


Figure 5.6: Typical spectrum analyser display of a swept-frequency measurement from which $Q$ can be derived via the 3dB method

| coil | $f_o$, $kHz$ | $Q_l$ |
|---|---|---|
| $0\% f_1$ | 233 | 199 |
| $0\% f_3$ | 566 | 255 |
| $0\% f_5$ | 811 | 194 |
| $10\% f_1$ | 259 | 202 |
| $10\% f_3$ | 648 | 234 |
| $10\% f_5$ | 942 | 172 |
| $22.5\% f_1$ | 248 | 203 |
| $22.5\% f_3$ | 649 | 220 |
| $22.5\% f_5$ | 883 | 187 |
| $33\% f_1$ | 258 | 201 |
| $33\% f_3$ | 659 | 225 |
| $33\% f_5$ | 821 | 231 |
| $50\% f_1$ | 281 | 191 |
| $50\% f_3$ | 622 | 272 |
| $50\% f_5$ | 972 | 158 |

Table 5.2: Loaded $Q$ measurements of **bare** coils, via 3dB method

$\mathcal{H}$ is the coil height in metres

$d$ is the coil diameter in metres

$n$ is the number of turns

For the experimental 0% resonator described in table (5.1), equation (5.3) yields $f_1$ as 225 $kHz$ which is within 3.4% of the measured $f_1$ value of 233 $kHz$ shown in table (5.2). Examination of equation (5.3) shows that the $\frac{\mathcal{H}}{d}$ ratio only weakly determines the self-resonant frequency whereas the the number of turns and the diameter of the coil both have a strong influence.

### 5.1.2 $Q$ measurements via the Smith chart method

The Smith chart provides versatile yet easy graphical representation and manipulation of complex impedances and admittances via

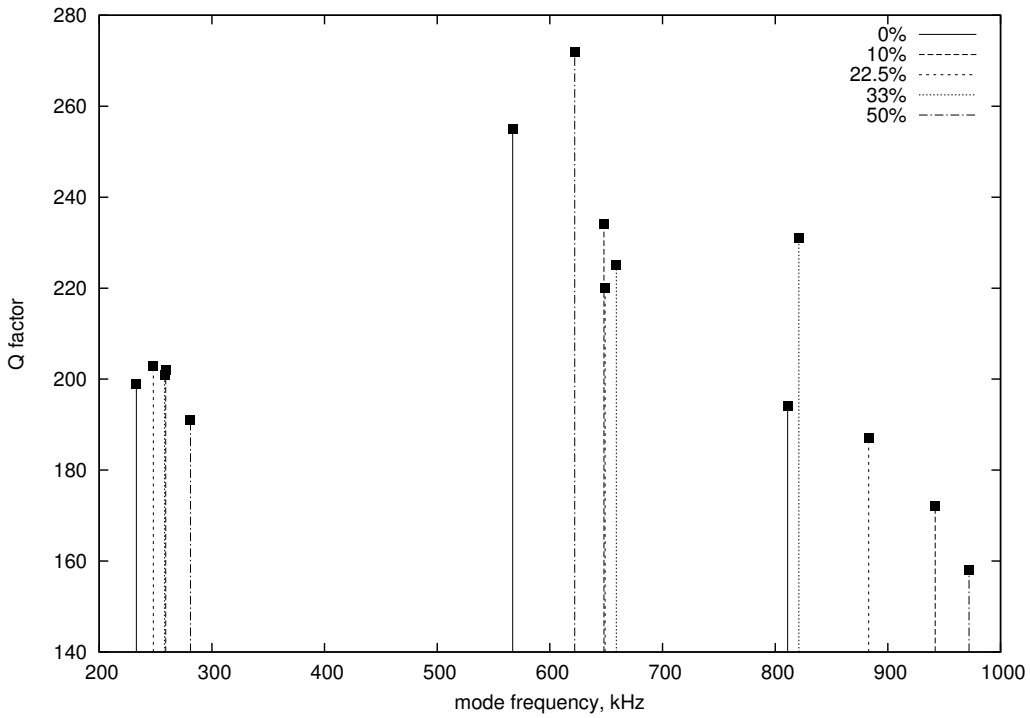


Figure 5.7: Loaded $Q$ measurements of bare coils, via 3dB method, from table (5.2): $f_1$ modes around 250 $kHz$, $f_3$ modes around 600 $kHz$ and $f_5$ modes above 800 $kHz$

scattering parameters [110]. It is extensively employed by RF/microwave physicists and engineers and finds everyday use in the design of antennas, impedance transforming circuits (i.e. matching networks), filters, amplifiers and oscillators.

When a VNA is used to display a Smith chart, the input impedance of a resonant winding describes a circular trajectory on the complex plane when the RF current from the VNA source generator is swept across the resonator's bandwidth. The resulting "$Q$-circle" allows a number of salient points to be defined[‡] ([103] [111] [112]) as illustrated in figure (5.8). However, the unloaded $Q$ obtained by this method removes only the influence of the external RF generator loading impedance and cannot account for losses due to external coupling into the environment (see subsection (5.1.1)).

A VNA enabled a range of $S_{11}$ measurements to be made on the full-size (1600 turn) and scaled (56.3 turn) coils, again positioned as shown in (5.5). The measurement data were recorded in the form of s1p datasets i.e. single port s-parameters. The datasets were then used to determine the unloaded and loaded $Q$ factors of the experimental coils, using the experimental setup of figure (5.5). This shows that the coils were located at a fixed height above a cross-shaped aluminium foil ground plane. Raw s-parameter datasets were manipulated in Awk[§] to present the data in a form suitable for QUCS or RFSim99 (see subsections (1.1.6) and (1.1.7)). Figure (5.9) shows a typical RFSim99 Smith chart display suitable for analysis.

[‡]personal email communications with Dr Fritz Caspers, CERN, June/July 2012

[§]a standard Linux command-line language, suited to numerical data extraction and manipulation, see http://www.gnu.org/software/gawk/manual/gawk.html

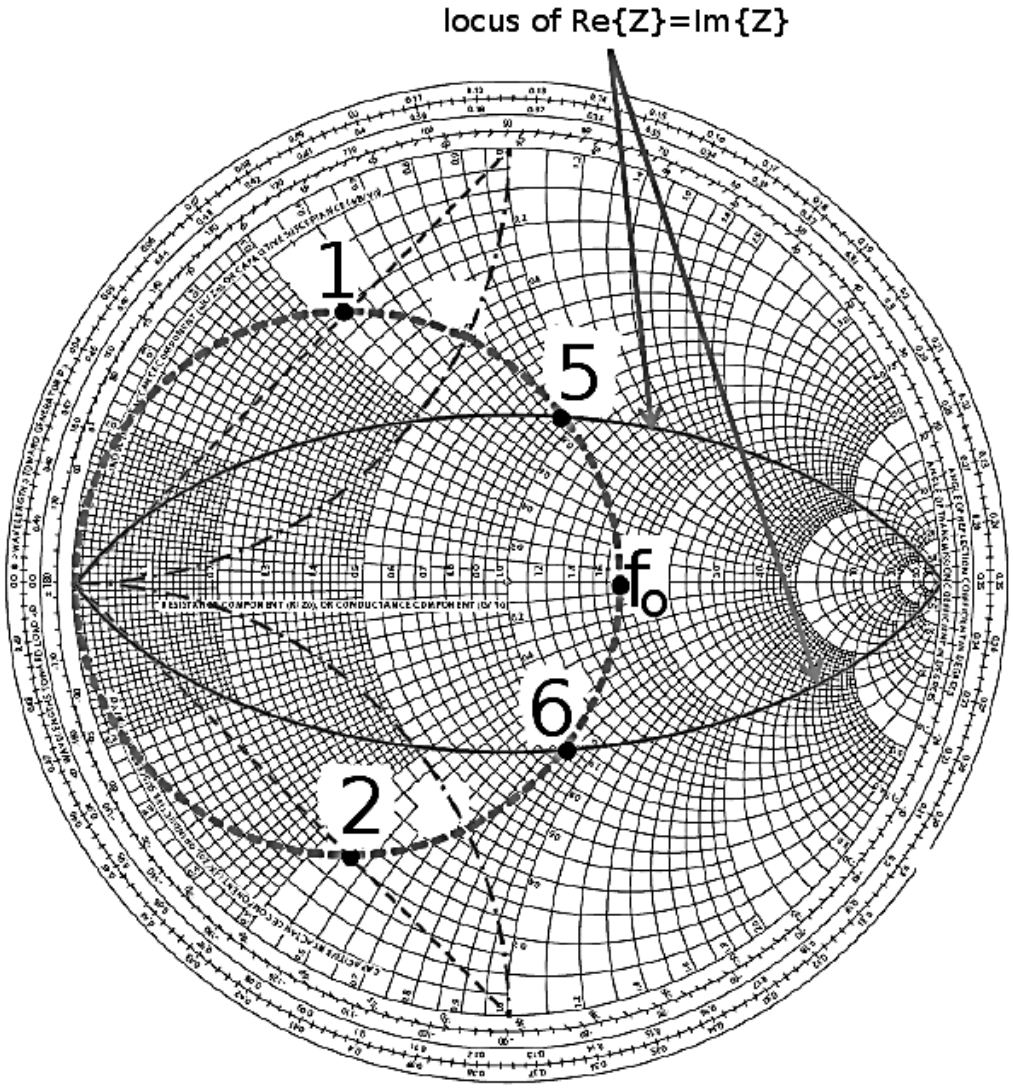


Figure 5.8: Resonator $Q$ measurements via Smith chart. $f_0$ is the coil resonant frequency at $|X| = 0$, $Q_u$ is the unloaded $Q$ which can be determined from Re{Z} = Im{Z} at frequency points **5** and **6** and $Q_l$ is the loaded $Q$ which can be determined from $|Im\{S_{11}\}|_{max}$ at frequency points **1** and **2** (adapted from [111])

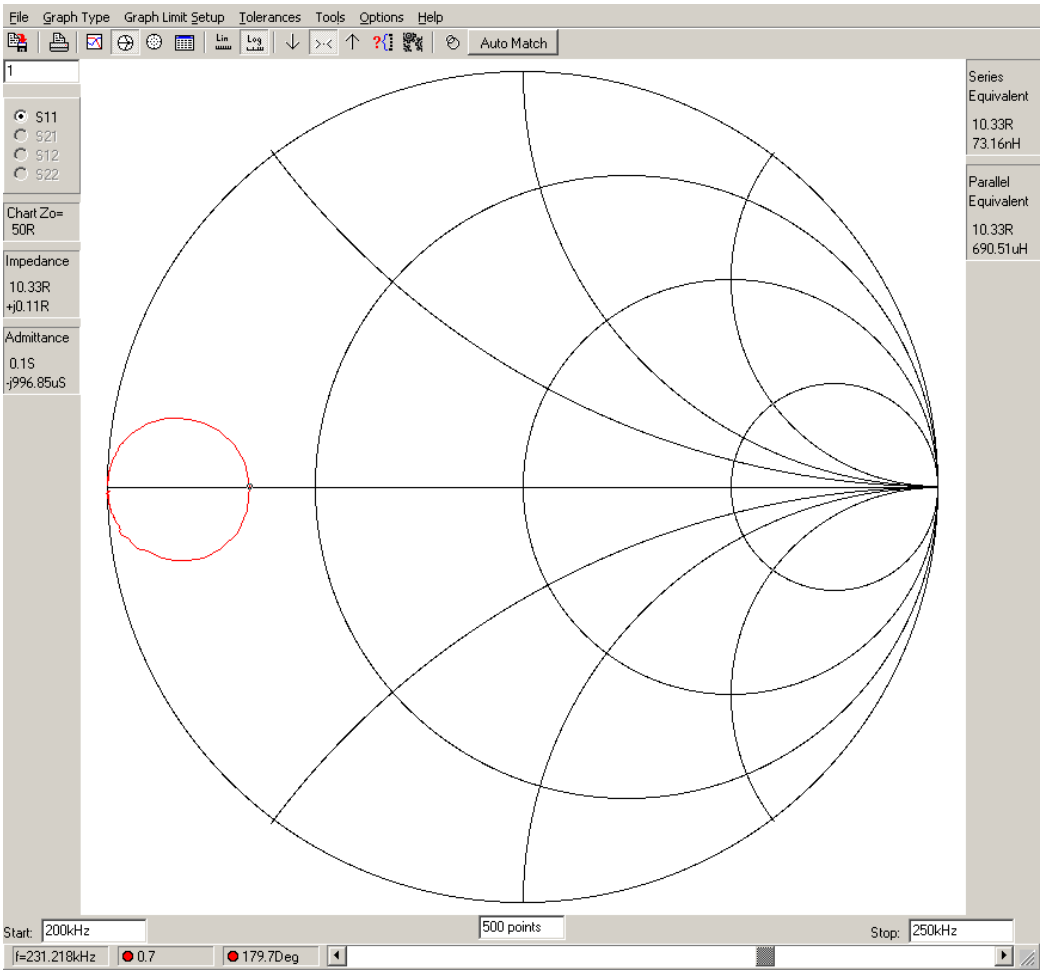


Figure 5.9: Input impedance (red) of a secondary coil, displayed in RFSim99

### 5.1.3 $Q$ factor measurements of bare and toploaded coils

As discussed in chapter (2), to apply voltage grading to a Tesla transformer requires a high-voltage terminal with a large radius of curvature to be attached to the high-voltage end of the secondary winding. This introduces additional capacitance to the secondary system and thus lowers the self-resonant frequency. The $Q$ of the coils was again measured and the input impedance for each coil at each mode frequency was determined. The unloaded $Q$ factors ($Q_u$) and input impedances ($Z_{in}$) for the bare and the toploaded coils are summarised in table (5.3). Note that "toploaded" signifies that the coil has been terminated at its upper end with the aluminium toroid discussed earlier in the chapter.

### 5.1.4 Analysis of $Q$ measurement results

The mean difference between the measured values for unloaded $Q$ (via the 3dB method) and loaded $Q$ (via the Smith chart method) was 4.4% with a standard deviation of 2.6%, due largely to in-band interference caused by AM broadcast stations. This made accurate Smith chart assessments difficult in approximately 20% of the measurements taken. The mean difference between the resonant frequencies obtained via the 3dB $Q_l$ method and the resonant frequencies obtained via the Smith chart $Q_l$ method was 0.23% with the largest difference being 0.64%. The results were within three standard deviations of the statistical population mean ($3\sigma$).

| coil | "bare" $Q_u$ | "bare" $Z_{in}$, $\Omega$ @ $f_o$ | "toploaded" $Q_u$ | "toploaded" $Z_{in}$, $\Omega$ @ $f_o$ |
|---|---|---|---|---|
| 0% $f_1$ | 184.6 | 10.2+j0 @ 231.2 $kHz$ | 199.6 | 8.2+j0 @ 222.2 $kHz$ |
| 0% $f_3$ | 244.9 | 3.9+j0 @ 561 $kHz$ | 260.8 | 3.7+j0 @ 536.1 $kHz$ |
| 0%$f_5$ | 199.3 | 1.6+j0 @ 807.4 $kHz$ | 205.6 | 1.6+j0 @ 803.5 $kHz$ |
| 10%$f_1$ | 194.6 | 12.1+j0 @ 257.8 $kHz$ | 189.4 | 11+j0 @ 223 $kHz$ |
| 10%$f_3$ | 233.3 | 4.3+j0 @ 643.5 $kHz$ | 226.5 | 4.4+j0 @ 611.6 $kHz$ |
| 10%$f_5$ | 174.9 | 1.7+j0 @ 938.5 $kHz$ | 163.2 | 1.6+j0 @ 916.6 $kHz$ |
| 22.5%$f_1$ | 193.5 | 11+j0 @ 245.3 $kHz$ | 185.8 | 10+j0 @ 238.8 $kHz$ |
| 22.5%$f_3$ | 202.3 | 4+j0 @ 642.5 $kHz$ | 217.2 | 3.9+j0 @ 600.5 $kHz$ |
| 22.5%$f_5$ | 195.6 | 0.8+j0 @ 877.6 $kHz$ | 225.5 | 1.4+j0 @ 805 $kHz$ |
| 33%$f_1$ | 203.5 | 12+j0 @ 256.5 $kHz$ | 185.0 | 10.6+j0 @ 221.9 $kHz$ |
| 33%$f_3$ | 225.3 | 2.5+j0 @ 655.5 $kHz$ | 249.4 | 2.9+j0 @ 583.8 $kHz$ |
| 33%$f_5$ | 240.5 | 2.1+j0 @ 818.6 $kHz$ | 230.7 | 2.8+j0 @ 798.4 $kHz$ |
| 50%$f_1$ | 178.9 | 12.6+j0 @ 278.7 $kHz$ | 178.2 | 11.6+j0 238.1 $kHz$ |
| 50%$f_3$ | 210.5 | 2.7+j0 @ 620.1 $kHz$ | 269.2 | 4.2+j0 @ 555.3 $kHz$ |
| 50%$f_5$ | 160.2 | 2.3+j0 @ 967.2 $kHz$ | 149.6 | 1.9+j0 @ 948.3 $kHz$ |

Table 5.3: Summary of Smith chart measurements of resonant frequencies, unloaded $Q$ and $Z_{in}$ for bare and toploaded coils

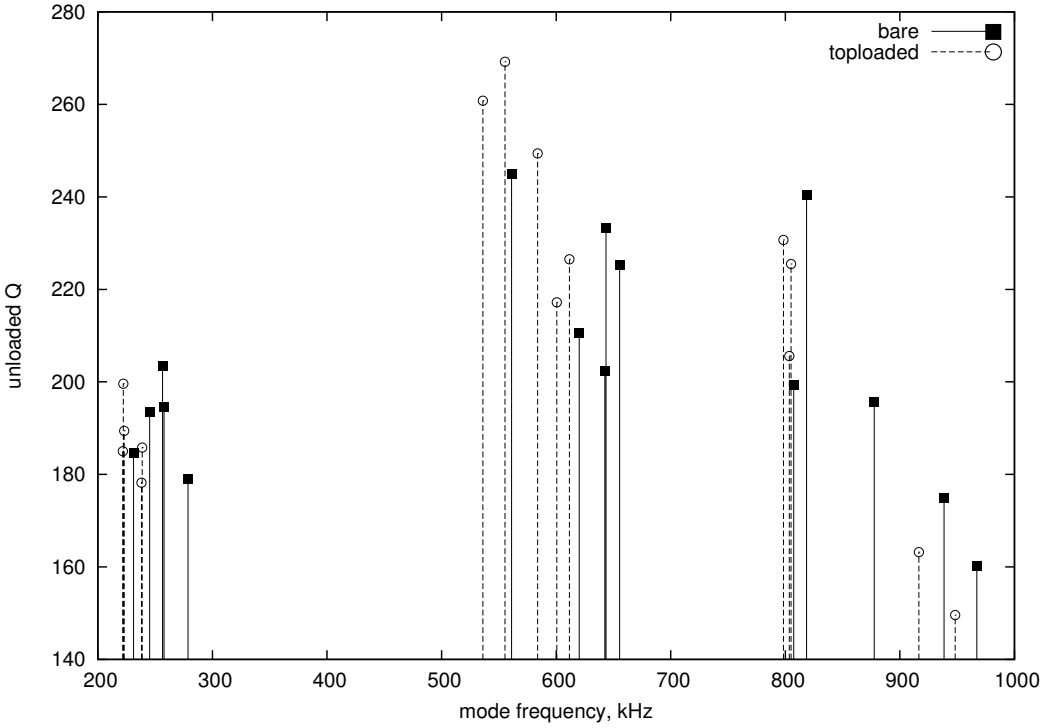


Figure 5.10: Smith chart derived unloaded $Q$ for all coils and modes

| mode | $f_1$ | | $f_3$ | | $f_5$ | |
|---|---|---|---|---|---|---|
| coil | $kHz$ | $Q_l$ | $\Delta kHz$ (%) | $\Delta Q_l$ (%) | $\Delta kHz$ (%) | $\Delta Q_l$ (%) |
| 0% | 233 | 199 | 567 | 255 | 811 | 194 |
| 10% | +11.2 | +1.5 | +14.2 | **-8.2** | +16.2 | -11.4 |
| 22.5% | +6.4 | +2.0 | +14.5 | **-13.7** | +8.9 | -3.6 |
| 33% | +10.7 | +1.1 | +16.2 | **-11.8** | +1.2 | +19 |
| 50% | +20.6 | -4.0 | +9.7 | +6.7 | +19.9 | -18.6 |

Table 5.4: Coil responses as % changes compared with 0% (reference) coil, with significant $Q_l$ reductions for the $f_3$ mode emphasised in bold

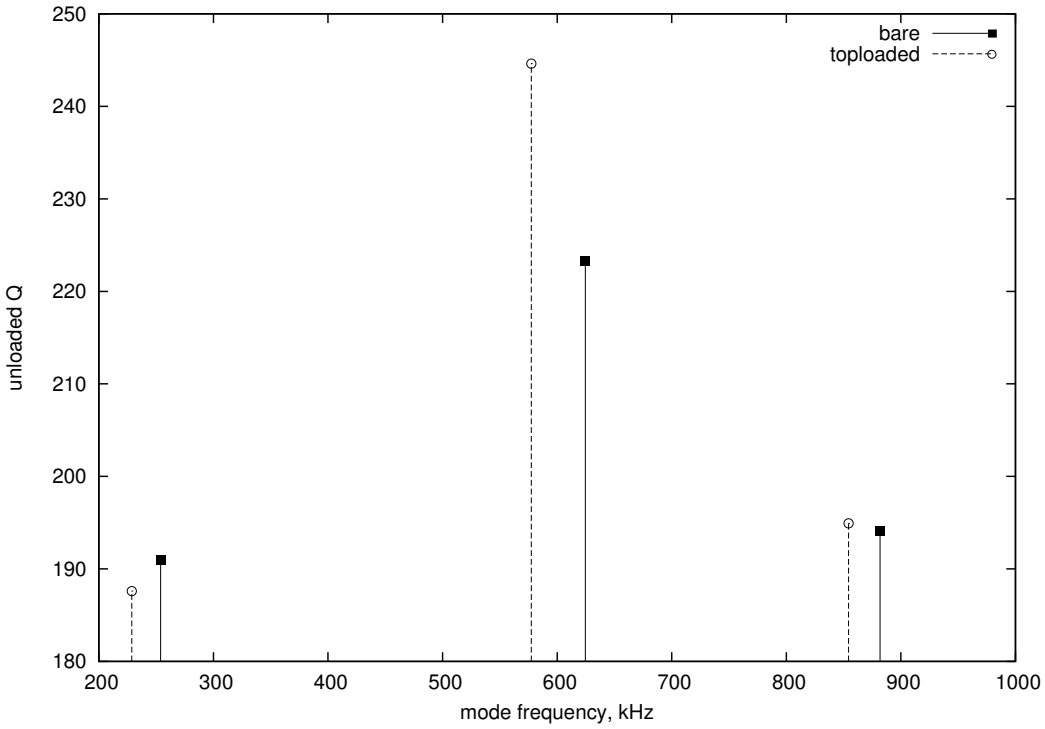


Figure 5.11: Mean unloaded $Q$ plotted for bare and toploaded coils

## 5.2 Spectrum measurements

The experimental Tesla transformer described previously was positioned in the test location (figure (5.5)) and operated in turn with each of the experimental secondary coils, such that the secondary coils were again centrally located and positioned 0.5 $m$ above the ground plane as for previous $Q$ measurements. The coil under test was toploaded by the toroid described in chapter (5) which had a capacitance of 20 $pF$. Initially, an electric field probe (a dipole antenna whose dimensions were very small compared with the wavelengths being measured) was positioned 3 $m$ from the Tesla transformer. At this range no detuning of the secondary was observed, which showed that any capacitive loading, due to the proximity of the electric field probe, was small. The secondary coil $E$ field, in which the antenna was immersed, was sampled and the voltage waveform recorded. Results showed a decaying sinusoidal response, and FFT analysis in Octave identified spectral components at the $f_1$, $f_3$ etc. mode frequencies. Significant EMI meant the recordings exhibited low signal to noise ratio and hence were of poor quality.

The instrumentation configuration was altered to mitigate the problems caused by EMI. Instead of sampling the secondary coil $E$ field, the secondary coil current was measured using a Singer 91550-1 100 $MHz$ bandwidth current transformer (see figure (5.12)) and a digital oscilloscope capable of measuring upto 100 $MHz$ at 1 GS/s acquisition. The vertical gain accuracy of the digital oscilloscope utilised is quoted as being better than 3% and the timebase accuracy is quoted as being better than 0.01%. The captured data were subsequently processed in Octave to generate an FFT spectrograph

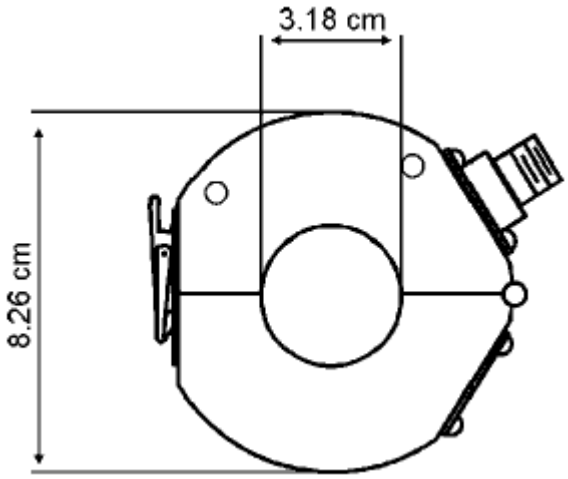


Figure 5.12: Illustration of Singer 91550-1 current transformer

that resolved the frequency components in the waveform and it is estimated that the amplitude accuracy of the measured spectrum responses was better than $\pm 1\ dB$. Figure (5.13) demonstrates the spectrum of currents flowing in the grounded end of the "0%" reference coil and it is easy to identify the components at the first three mode frequencies $f_1$, $f_3$ and $f_5$. Higher mode frequencies could not be resolved due to the high noise floor of the measurement system and the low sensitivity of the instrumentation.

The experimental coils were toploaded by an aluminium toroid and figure (5.13) shows the response of a standard 0% winding. The fundamental mode $f_1$ can be clearly observed at approximately 140 $kHz$, with the $f_3$ mode at just below 490 $kHz$. The $f_5$ mode is at approximately 780 $kHz$ and the $f_7$ mode is indistinct.

Examining the response of the 10% experimental winding shown in figure (5.14) shows that its $f_1$ mode experienced a small change in amplitude and frequency compared with the 0% resonator of figure (5.13) and the amplitude of the $f_3$ mode was significantly reduced.

For each of the experimental coils, investigation of the measured data in numerical form allowed the suppression of the $f_3$ mode to be accurately calculated and table (5.5) shows that a significant 15dB suppression of the $f_3$ mode was evident for the 10% resonator. These measurements demonstrated that the "counter winding" design principle was applicable to Tesla transformers and that the 10% winding demonstrated the greatest suppression compared with the other experimental winding configurations.

All the $Q$ measurements described in section (5.1) were implemented with the output terminal of the Tesla transformer, either the bare coil end or the toroid "topload", left unconnected. The spectrum measurements discussed in section (5.2) were made under conditions whereby a high voltage corona was formed (p. 6 of [20], p. 371 of [87], vol. IV of [101]), due to the high RF voltage generated. This acted as a load ($Z_{load}$) connected to the Tesla transformer output terminal.

The oscillatory nature of the currents and voltages flowing in the Tesla transformer secondary circuit is affected by $Z_{load}$ (p. 329 of [32], p. 910ff. of [113]). Transmission line loss is affected by conductance ($G$) connected across the line (p. 247ff. of [41], and appendix (C)). The $Q$ of a "lossy" resonant transmission line is inversely proportional to $G$ (p. 257ff. of [41]). Thus a decrease in $Z_{load}$ connected to the Tesla transformer secondary causes an increase in $G$ which increases the attenuation and reduces the $Q$. If $Z_{load}$ is invariant, the reduction in $Q$ at the fundamental and overtone frequencies will be equal for each mode but if the value of $Z_{load}$ varies with frequency then the response of the coil is more complex.

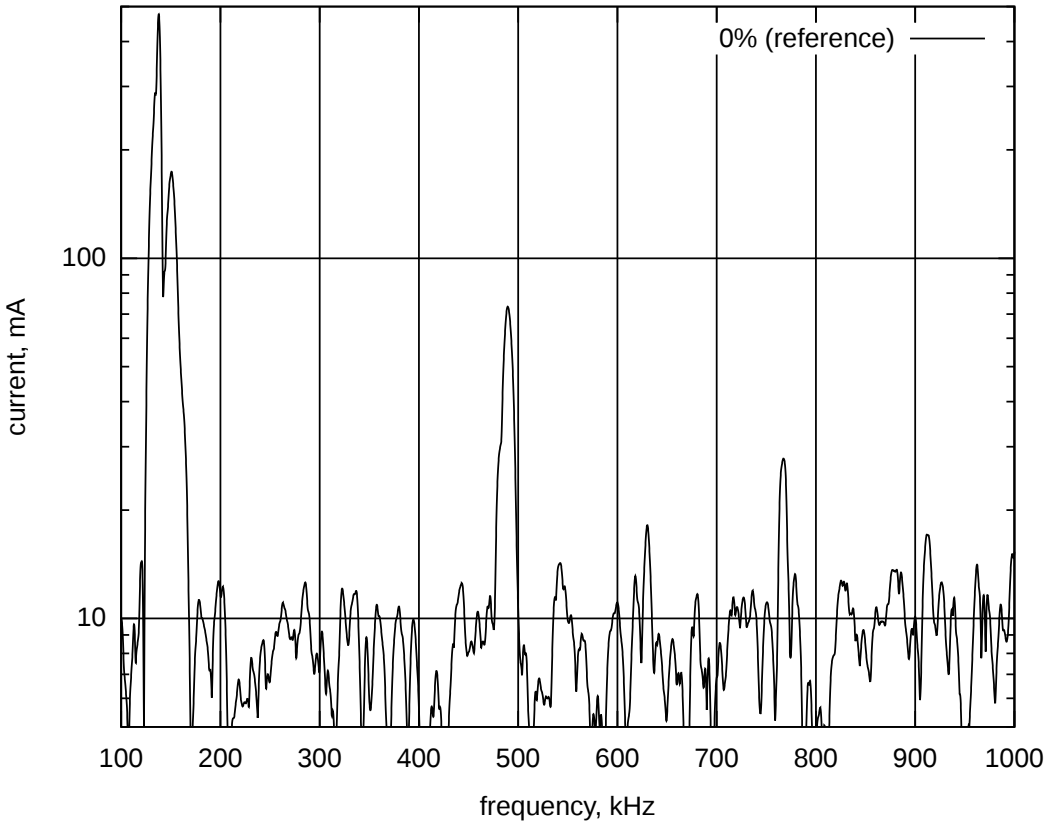


Figure 5.13: 0% toploaded resonator spectrum with $f_1$, $f_3$ and $f_5$ responses clearly visible

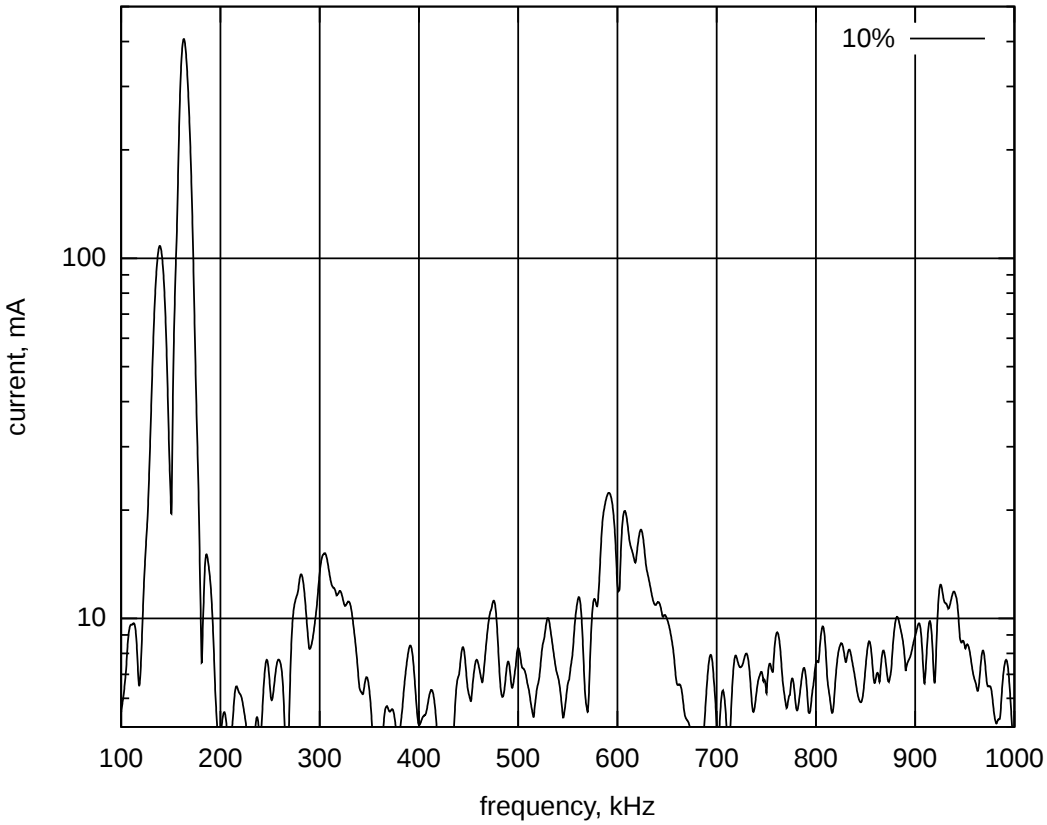


Figure 5.14: 10% toploaded resonator spectrum, demonstrating suppressed $f_3$ and $f_5$ responses

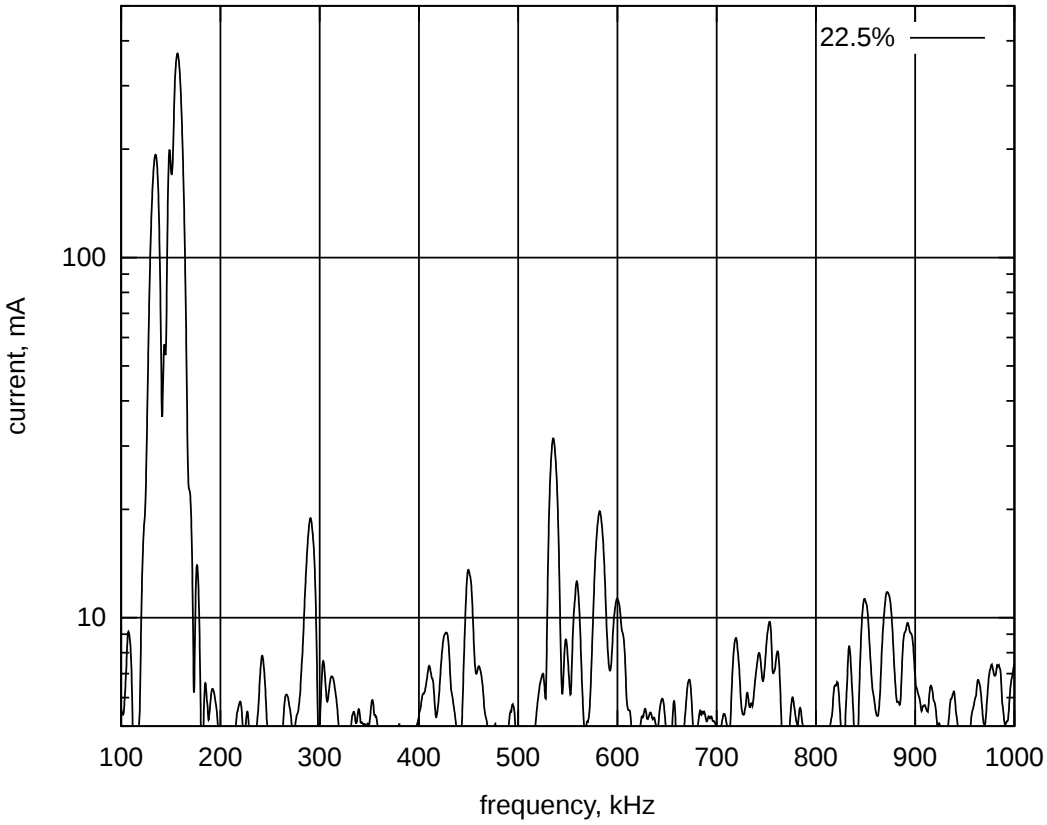


Figure 5.15: 22.5% toploaded resonator spectrum

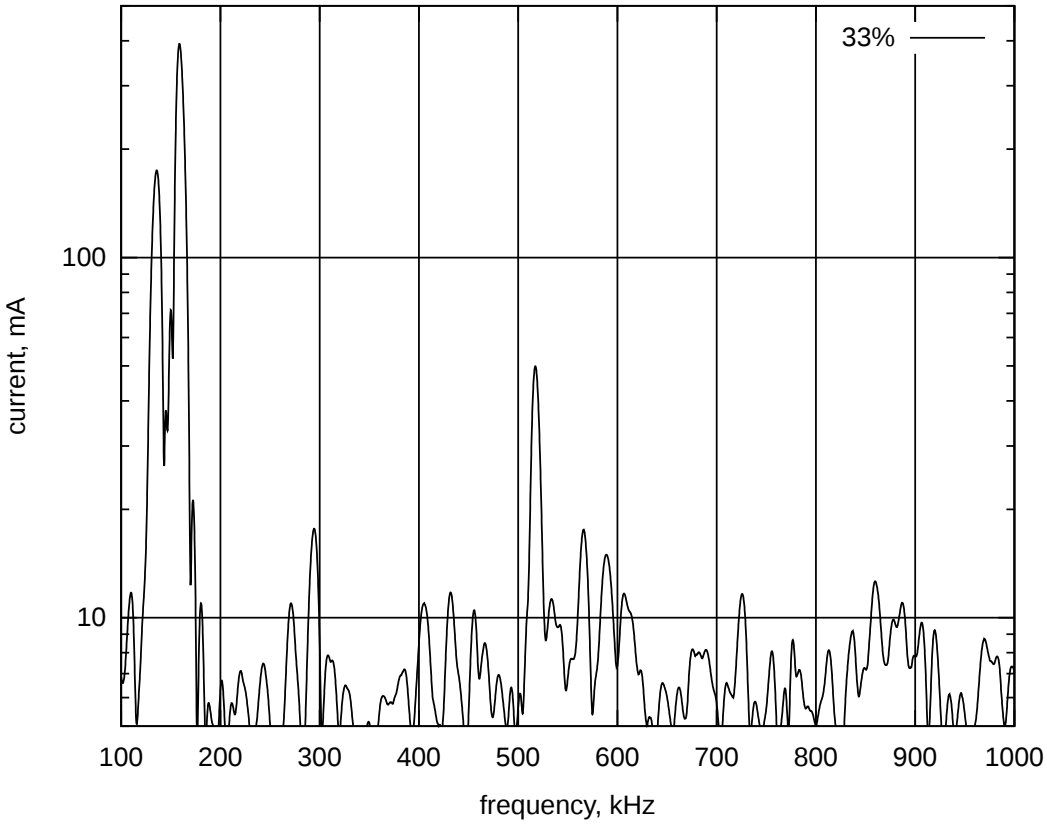


Figure 5.16: 33% toploaded resonator spectrum

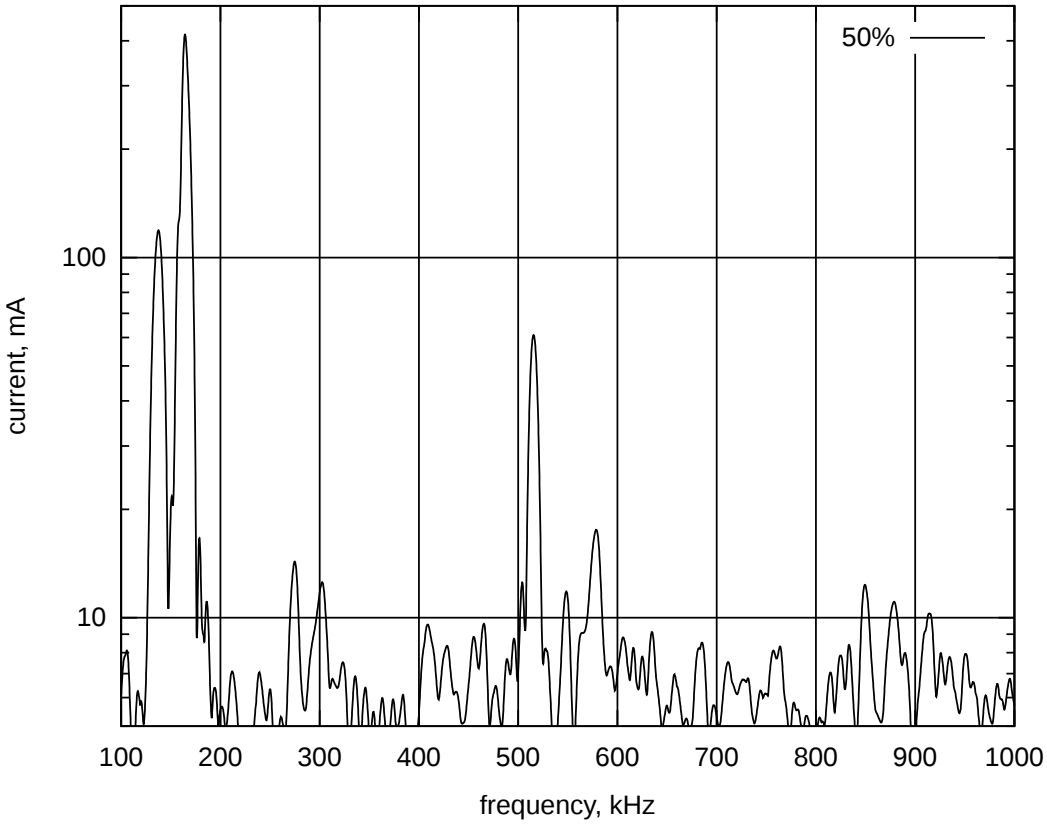


Figure 5.17: 50% toploaded resonator spectrum

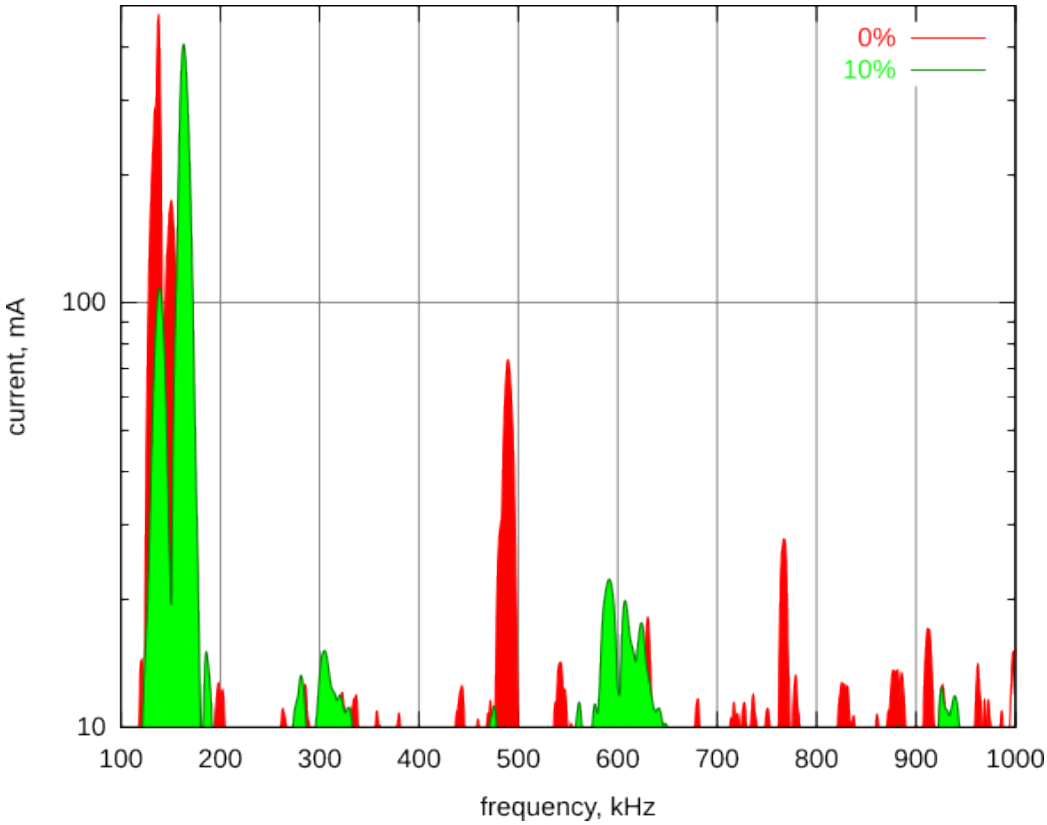


Figure 5.18: Spectra of the 0% (reference) toploaded resonator compared with the 10% toploaded resonator

| resonator | 0% (reference) | 10% | 22% | 33% | 50% |
|---|---|---|---|---|---|
| $f_3$ mode suppression | 0 $dB$ | **15** $dB$ | 0.8 $dB$ | 1.6 $dB$ | 0.2 $dB$ |

Table 5.5: $f_3$ mode suppression

# Chapter 6

# Secondary coil loss

According to Zverev (p. 499 of [73]) the single-layer solenoid can realise a maximum $Q$ of approximately 200. This value is low compared with the author's experience and with the results of a collective study into helical resonators used for Tesla transformer secondary coils [2]. There are a number of familiar loss mechanisms responsible for lowering $Q$, the predominant one being skin effect (see chapter (4)). Other losses may occur due to proximity effect, dielectric losses, induction field loss and EM radiation loss, which are discussed in detail in appendix (D).

The secondary winding conductor resistance has a direct effect on $I^2R$ losses and hence on $Q$, and chapter (4) shows the effect of altering the frequency at which an alternating current flows (skin effect), or changing the conductivity or diameter of the conductor from which the coil is wound.

Changes in $Q$ with frequency can be compared by overlaying figure (6.1), which shows $Q$ versus frequency for a solenoid, with figure (5.7) which is a plot of measured coil $Q$ vs mode frequency for the standard

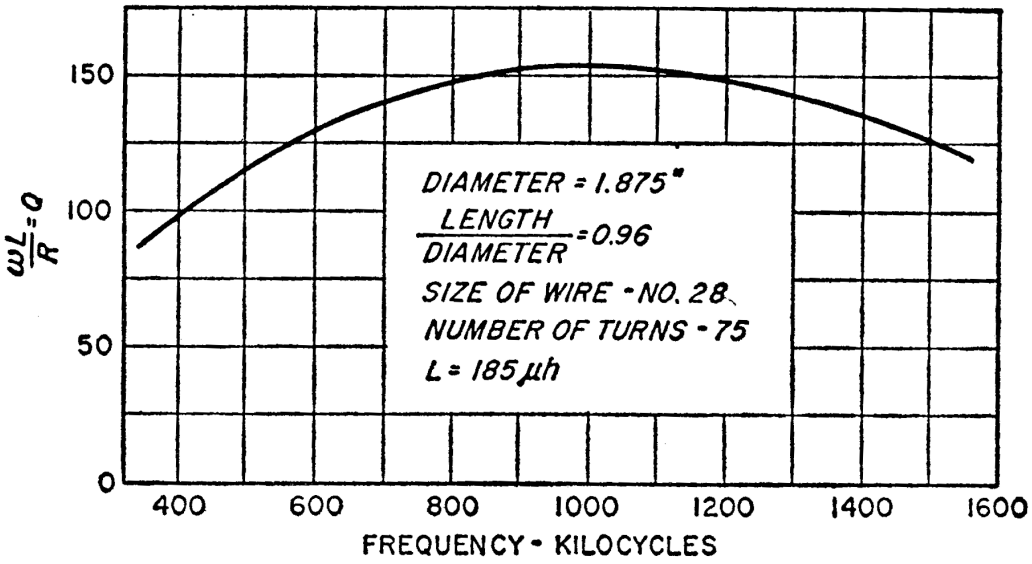


Figure 6.1: Variation of $Q$ with frequency for an air-cored coil (from p. 32 of [85])



(0%) and the various experimental secondary windings. Figure (6.2) shows the result and it can be seen that the changes in $Q$ with frequency are similar.

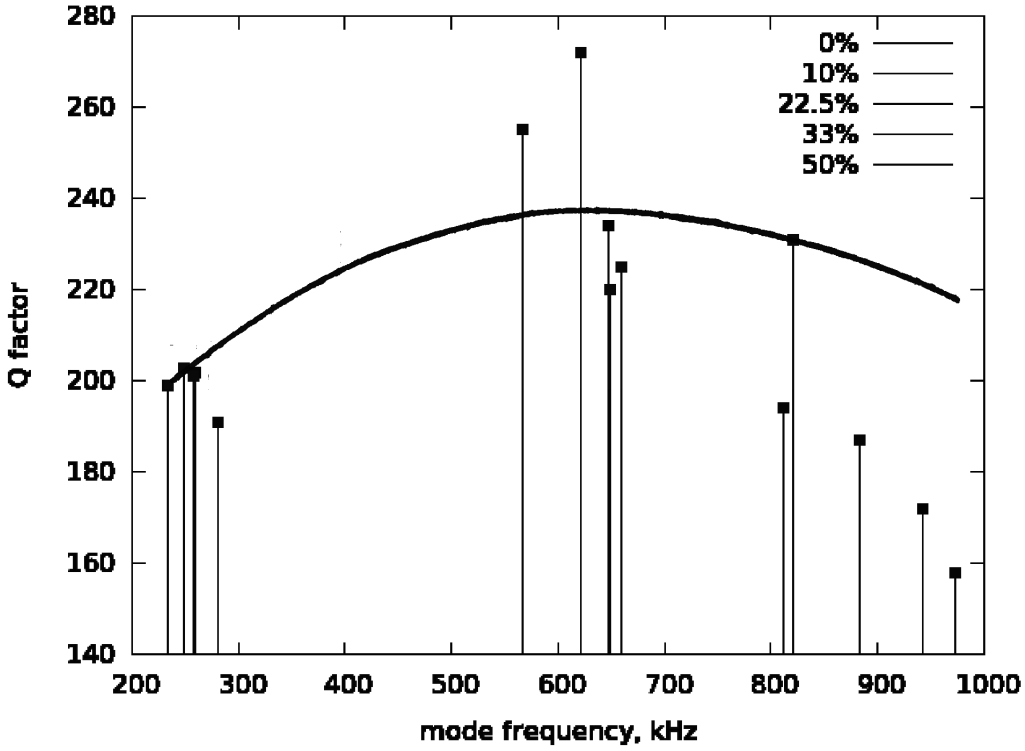


Figure 6.2: Comparison of measurements with graph from [85]

# Chapter 7

# Conclusions and recommendations

The aim of this thesis was to establish whether helical filter design techniques could be applied to Tesla transformers to improve the spectral purity of the transformer output.

A number of assertions were stated in chapter (1) in developing this thesis and these were subsequently established to be valid. The response of a Tesla transformer secondary winding was analysed at its fundamental resonant frequency and the first few overtones. A series of experimental coils were constructed by counter winding the top portions of single-layer solenoid coils and the various mode frequencies and their associated $Q$ factors were measured. The winding configurations were derived from work by Vizmuller for improving the design of helical filters. Modelling was employed to illustrate the effects when differing portions of the secondary coil were counter-wound. A Tesla transformer was designed and constructed as

a benchmark with which the frequency response of different winding designs, and particularly differences in fundamental and overtone frequency response, could be investigated and demonstrated. The various multi-order oscillatory voltages and currents flowing in the experimental secondary coils were measured, under loaded conditions, at the fundamental and overtone frequencies.

Suppression of a Tesla transformer's higher-order frequencies was achieved, particularly the $f_3$ response, whilst causing little change to the fundamental $f_1$ response. Changes in the $f_5$ and $f_7$ responses were observed but these were insignificant compared with the reduction in amplitude of the $f_3$ response. This demonstrates that the aims of the thesis were met:

- An established helical filter design technique consists of counter winding a portion of turns of the resonant helix.
- The technique is employed to suppress higher order responses in radio frequency helical filters.
- An experimental Tesla transformer was constructed with a range of secondary windings comprising differing counter-wound portions.
- Measurements demonstrated that the fundamental frequency was largely unaffected but that the higher order responses, particularly the $f_3$ response, were diminished.

## 7.1 Thesis contribution

It has been demonstrated that $Q$ at the fundamental frequency can be left unchanged but reduced at overtone frequencies, resulting in the current and voltage output waveforms showing a reduction in the corresponding overtone frequency content for a two-coil Tesla transformer.

A new method has been presented which enables the output power frequency spectrum of a Tesla transformer to be modified. A conference paper was presented in 2011 [114] and a further paper, based on the work in this thesis, has been published by the Institute of Electrical and Electronics Engineers (IEEE) [115]. An Electronics Letter [116] and further conference papers [117] [118] are in preparation. This technique can be employed to reduce unintentional radio frequency interference (RFI) or EMI. Pulsed power research by government and industry sectors may include defence technology areas such as EW jammers. Battlefield deployment of jamming technology mandates spectrum control and management, so the ability to control the harmonic purity of signal transmitted from such systems becomes essential.

## 7.2 Recommendations for further research

The benchmark Tesla transformer discussed in chapter (5) was designed to resonate in the 135.7 $kHz$ – 137.8 $kHz$ band as a means of minimising EMI and RFI (the frequency band is coordinated by the ITU, nationally and internationally, for radio amateur use). This resulted in the designed self-resonant frequency of the reference

and experimental secondary windings being constructed with coils of numerous (1600) turns wound with thin (0.35mm diameter) wire. This ultimately presented practical construction difficulties and, in hindsight, a different approach involving fewer turns of larger diameter wire would have been easier to wind and count during construction. Such a design would have resulted in an increase in the resonant frequency of the secondary winding and an increase in the various overtone mode frequencies. This may have moved the frequencies of interest to a different part of the radio spectrum less prone to EMI (received interference from AM broadcast transmissions spoiled numerous measurements during this thesis). A further difficulty encountered was one of instrumentation, in that the Agilent 8753B VNA employed was incapable of measuring at frequencies lower than 300 $kHz$ and a second instrument (Rhode-Schwarz FSH-8) was needed to complete the work at the lower frequencies.

The switch used in the test-bed was suited to the task. However, a better solution may have been to use a different, lower-voltage power supply, perhaps derived from full-wave rectified domestic mains as per the OLTCs discussed in subsection (2.3.3). In conjunction with semiconductor switches, easier control of the on and off durations may then be achievable, which in turn may enable a wider range of coupling coefficients to be considered. In addition, alternative and potentially more convenient methods of $Q$ measurements may have become feasible, as discussed via the TSSP (see section (4.3) and reference [2]). However, such an approach would have had no effect on the ability to discern whether the thesis aims were or were not met.

To establish the principle, the measurement and modelling effort

concentrated on a small subset of the total number of counter winding possibilities and only the effects of counter winding the top portions of the experimental coils were considered. An alternative would be to invert the coils so that the counter-wound portion became the bottom portion, and comparison with figure (4.10) could add insight. The notion of an entirely distributed counter-wound pattern could also be considered. For example, implementation of a 33% counter-wound coil would require every third turn to be counter-wound. Alternative winding patterns could be tested, for example a "33%" coil could be formed by using three counter-wound sections, each consisting of 11% of the total number of turns, with one section towards or at the base, one towards or in the centre and one towards or at the top of the coil. Another option may be to mount two windings coaxial to one another, one of slightly smaller diameter, and to connect them in parallel. A small difference in diameter will cause a small difference in inductance or electrical length, which could be compensated for by slightly altering the winding pitch. Small differences in coil geometry would merely give rise to small differential voltages between the two coaxial coils, such that insulation coordination would perhaps not be insurmountable. It may then be practicable to experiment with differing counter windings on the inner and outer coils. Clearly many permutations exist by which the proportion of counter-wound turns could be achieved.

Vizmuller's original work investigated the effect of the counter winding of coils enclosed within cavities and this thesis has demonstrated that the same counter winding approach is valid for "open" Tesla transformers. The analytical references discussed in section (4.1) establish that the helix radiates in certain forbidden

frequency bands and propagates in certain accepted bands. If the Tesla transformer was contained within a cavity, as in some of the "enclosed" examples of section (2.3), the opportunity may exist to counter wind the secondary coil, specifically to modify the anharmonic responses, and correspondingly make the cavity reflective only at the fundamental frequency and absorptive at all other unwanted anharmonic frequencies. A technique for doing so may be derived from an area of active study in electromagnetic physics, namely that of metamaterials [107] which are defined as periodic structures possessing unusual electromagnetic properties. One class of metamaterial is known as a frequency selective surface (FSS) (p. 600 of [3]), and it may be feasible to design an FSS structure into the wall of a cavity-mounted Tesla transformer. The FSS could be made to be reflective at the fundamental designed frequency, but transmissive at anharmonic frequencies and to present a matched terminating impedance to the unwanted mode fields. This may aid in further suppression of unwanted modes and thereby a reduction of their contribution to the Tesla transformer output frequency spectrum. It may also be feasible to apply the technique to helical filters used in radio communications.

The Tesla transformer output power spectrum was measured under operating conditions which caused a high voltage corona discharge and sparks to be generated around and from the conducting toroid, representing a load into which power was dissipated. Further work could investigate the use of other loads and the effects of differing load impedances (p. 215ff. of [40]) associated with the Tesla transformer applications discussed in section (2.4).

# Appendices

A: numerical electromagnetic modelling methods

B: lumped component analysis

C: distributed analysis

D: resonator loss mechanisms

# Appendix A

# Numerical electromagnetic modelling methods

Several numerical techniques have been developed [119] to enable computer-based modelling of electromagnetic problems. This thesis makes use of the MoM process (subsection (1.1.1)) but other methods exist which in some circumstances might have advantages over MoM in analyses such as the radiation of EM waves from a structure, or EM wave reflection/refraction from objects within the EM field. Selection of the most appropriate modelling technique used in this thesis was based on careful analysis of the different EM mechanisms present in the problem to be analysed (for example propagation in a transmission line, or radiation in free space). Direct computation of the $E$ and $H$ fields via Maxwell's equations is impractical unless the originating structure is simple (e.g. a short dipole). Most real-world problems are too complex to employ direct numerical computation, so an iterative approach is usually adopted.

Numerical techniques tend to use either the time domain version

of Maxwell's equations or the frequency domain version (differential or integral versions, respectively) [119]. A variety of computer software packages exist for this purpose, varying in complexity and cost. In terms of electromagnetic modelling, numerical analysis methods use a range of techniques:

- Method of Moments (MoM)
- Finite Difference Time Domain ( FDTD)
- Finite Element Method (FEM)
- Transmission Line Matrix (TLM)

## A.1 Method of moments

The Method of Moments (MoM) uses a boundary element solution technique in which computation is used to numerically solve electric field volume integrals. The code generates full wave frequency-domain solutions to the integral form of Maxwell's equations which are reduced to a set of simpler linear equations. The equations are then solved by the MoM technique, an advantage of which is that MoM is a "source" method, meaning that only the structure in question is quantised, rather than the surrounding free space as with "field" methods. Boundary conditions do not have to be set and memory requirements scale in proportion to the size of the geometry in question and the required solution frequency. The problem is quantised into wires in the case of NEC.

## A.2 Finite difference

Finite difference engines are most usually represented in the finite-difference time domain (FDTD) form, whereby spatial quantisation is achieved by dividing the problem into cuboids. FDTD analysis generates $E$ and $H$ field solutions in alternating computational steps via quantisation grids, whereas the finite-difference frequency domain (FDFD) form requires solutions to simultaneous differential linear equations. Boundaries are quantised to cuboidal cell faces,resulting in a "staircase" approximation to the sloping boundaries. Quantisation errors for spherical or circular structures inevitably exist and re-quantisation at a smaller cuboid size for such regions is implemented in software to minimise the errors at the boundaries. This approach suits complex geometries since the size of the cuboids can be altered or transformed to suit the problem geometry.

## A.3 Finite element method

The time domain finite element method (TDFEM) uses the time-domain form of Maxwell's equations whereas the more common frequency domain FEM (FDFEM) form uses the frequency-domain form. The problem to be analysed is quantised into numerous discrete polygons bounded by elements, and scaling of the polygons is used to improve the accuracy of the quantising. The mesh of polygons is simplified into a set of simultaneous differential linear equations, whereby currents flowing along each edge of the polygon give rise to a field within the polygon. Neighbouring polygons have an influence on the sum field calculated. Structures which contain conductors and

dielectrics can be easily modelled.

## A.4 Transmission line matrix

The Transmission Line Matrix (TLM) approach performs time-domain analysis on a single quantised grid. The nodes of the grid are interconnected by virtual transmission lines. Excitations at specific grid nodes propagate to adjacent grid nodes through the transmission lines at each time step. Each node is connected to its neighbouring nodes by a pair of orthogonally polarised transmission lines. Lossy media can be modelled by introducing loss into the transmission line equations or by loading the nodes with lossy stubs. The TLM method can readily model complex nonlinear materials. Impulse responses and the time-domain behaviour of systems are determined explicitly.

FDTD and TLM methods are suitable for implementation on massively parallel machines. The disadvantages of the TLM and FDTD methods are that sizeable problems need a fine grid which then needs excessive computational power to solve. Nevertheless, both TLM and FDTD techniques are very powerful and are widely used. For many types of EM problems they represent the only practical methods of analysis.

# Appendix B

# Lumped component analysis

Figure (B.1) shows the equivalent circuit normally adopted for a conventional two-coil Tesla transformer [30] [31] [32]. The primary capacitor $C_1$ is charged to a high voltage from a DC or AC source, in the latter case ensuring that the charging time is no more than a quarter of the AC period. The potential difference due to the charged capacitor is simultaneously developed across some form of closing switch, which is typically a two terminal, self-breaking spark gap (chapter three of [64]). Once the electric field across the spark gap is sufficiently high to promote gap breakdown, the gap "fires" and the capacitor discharges through the primary inductance $L_1$. Current flows back and forth through the inductor and the spark gap, to and from the capacitor, at a resonant frequency determined by the values of inductance and capacitance. The amplitude decays towards zero at a rate which is a function of the circuit losses; these are minimised by design but the operating circuit $Q$ is typically 10 - 20 and is dominated by circuit losses due to the primary spark gap and the transfer of energy out of the primary and into the secondary circuit. The primary circuit $Q$

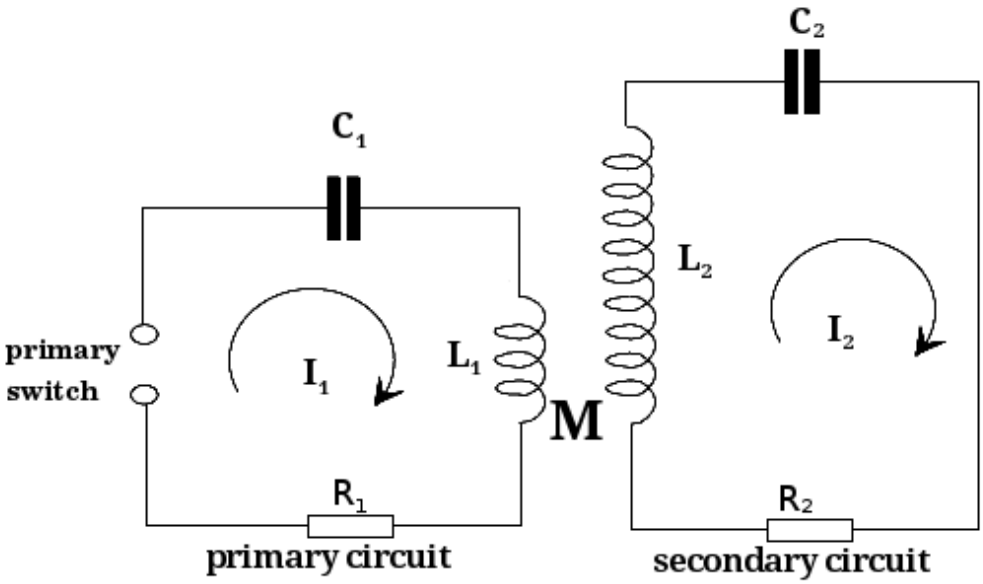


Figure B.1: Lumped equivalent circuit of a Tesla transformer

can be defined for small values of $R$ by (p. 409 of [120]):

$$Q = \frac{1}{R}\sqrt{\frac{L}{C}} = \frac{1}{\omega_0 RC} \tag{B.1}$$

where

$\omega$ is the resonant frequency

$L_1$, $C_1$, $R_1$, $L_2$, $C_2$, $R_2$ are the lumped component values in the primary and secondary circuits

Reduction of $R$ causes a decrease in $I^2R$ losses and an increase in $Q$. Large values of $L$ compared with small values of $C$ lead to an increase in $Q$. Comparison of the peak current $I_0$ at time $t$ to the value $I_1$ at $t$+$\frac{2\pi}{\omega}$ (one RF cycle later) allows the ratio of peak currents one cycle apart to be expressed as

$$\frac{I_1}{I_0} = e^{-\vartheta} \tag{B.2}$$

The logarithmic decrement $\vartheta$ of this current is sometimes referred to as the "ring down" and is given by (p. 408 of [120])

$$\vartheta = \frac{\pi R}{\omega_n L} = \frac{\pi}{Q} \cong \frac{1}{Q} \tag{B.3}$$

for resonators where $R$ is small but not zero. The exponentially decaying current that flows in the primary inductor generates a magnetic field whose flux cuts the windings of the secondary coil $L_2$ to a larger or smaller degree, depending on the geometry of the two windings. A voltage is induced in the secondary with a value determined by the mutual inductance $M$ between the two windings, and the rate of change of current in the primary. $M$ is a quantity that describes the degree to which the magnetic field generated by a current in the primary coil couples into the secondary coil. The coupling coefficient $k$ varies from zero, when none of the primary coil field intercepts the secondary winding, to a value of one when all the magnetic flux due to the primary coil is intercepted by the secondary winding.

The current in the secondary winding oscillates at a frequency determined by the secondary coil inductance $L_2$ and capacitance $C_2$ of the secondary circuit. If the resonant frequency of the secondary circuit equals that of the primary circuit, the Tesla transformer is said to be tuned. The secondary voltage $V_2(t)$ can then be expressed as [20]:

$$V_2\left(t\right) = \frac{V_1}{2}\sqrt{\frac{L_2}{L_1}}e^{-\frac{t}{T}}\left(\cos\frac{wt}{\sqrt{1-k}} - \cos\frac{wt}{\sqrt{1+k}}\right) \tag{B.4}$$

where the coupling coefficient is

$$k = \frac{M}{\sqrt{L_1 L_2}} \tag{B.5}$$

and

$$T = \left( \frac{4L_1 L_2}{R_2 L_1 + R_1 L_2} \right) \tag{B.6}$$

A Tesla transformer design can be optimised to achieve the highest secondary voltage possible, with the maximum voltage gain being [30]

$$G_{max} = \left[ \frac{V_2(t)}{V_1} \right]_{max} = \frac{2k}{\sqrt{(1-T)^2 + 4k^2 T}} \sqrt{\frac{L_2}{L_1}} \tag{B.7}$$

and the coupling coefficient being

$$k = \sqrt{\frac{\alpha^2 (1+T)^2 - (1-T)^2}{4T}} \tag{B.8}$$

in which

$$\alpha = \frac{1+2m}{1+2m+2m^2} \tag{B.9}$$

$k$ can be eliminated from equation (B.7) to give

$$G_{max} = \left[ \frac{V_2(t)}{V_1} \right]_{max} = \sqrt{\frac{\alpha^2 (1+T)^2 - (1-T)^2}{\alpha^2 T (1+T)^2}} \sqrt{\frac{L_2}{L_1}} \tag{B.10}$$

Equation (B.10) achieves $G_{max}$ when $T < 1$ in order to define $k$, and an integer value is chosen for $m$ in order to define $\alpha$.

Another way to optimise a Tesla transformer design is to minimise the time taken to transfer the total initial charge present on $C_1$ to $C_2$. Complete transfer of the charge implies the developed voltage $V_2$ is a

maximum and high if $C_2$ << $C_1$. This is achieved by adjusting $k$ so that (p. 285ff. of [20] and [30])

$$\frac{w_2}{w_1} = \frac{a+2b+1}{a} = \frac{\sqrt{1+k}}{\sqrt{1-k}} \tag{B.11}$$

and

$$k = \frac{c^2 - a^2}{c^2 + a^2} \tag{B.12}$$

in which

$$c = a + 2b + 1 \quad b = 1, 2, 3 \ldots \tag{B.13}$$

Setting $T$ = 1 and a value of $k$ via equation (B.12) sets a maximum voltage across the secondary and complete energy transfer from the primary capacitor $C_1$. The values chosen for $a$ and $c$ set the value of the coupling coefficient $k$ and the number of cycles required for complete energy transfer, shown in table (B.1). The value of $k$ employed in the experimental Tesla transformer used in this thesis is highlighted and at the resonant frequency of 136 $kHz$, the Tesla transformer takes 7.4$\mu s$ to complete 1 cycle. The spark gap used was estimated to have quenched after approximately 90 $\mu s$, which equates to a little more than 12 cycles and two notches. Section (4.2) modelled the circuit parameters of $k$, switch times and so on and the resultant beat envelope, containing two notches, was shown in figure (4.6). Investigation of that figure reveals 12 cycles, suggesting a small error in the estimated spark gap conduction period. Had the spark gap performance resulted in a sufficiently short conduction period, operation with $k$ = 0.6 would have been possible and table (B.1) shows

| a | c | $k$ | notch | cycles | a | c | $k$ | notch | cycles |
|---|---|---|---|---|---|---|---|---|---|
| 1 | 2 | 0.6 | 1 | 1.0 | 1 | 4 | 0.882 | 2 | 2.0 |
| 2 | 3 | 0.385 | 1 | 1.5 | 2 | 5 | 0.724 | 2 | 2.5 |
| 3 | 4 | 0.280 | 1 | 2.0 | 4 | 7 | 0.508 | 2 | 3.5 |
| 4 | 5 | 0.220 | 1 | 2.5 | 5 | 8 | 0.438 | 2 | 4.0 |
| 5 | 6 | 0.180 | 1 | 3.0 | 7 | 10 | 0.342 | 2 | 5.0 |
| 6 | 7 | 0.153 | 1 | 3.5 | 8 | 11 | 0.308 | 2 | 5.5 |
| 7 | 8 | 0.133 | 1 | 4.0 | 10 | 13 | 0.257 | 2 | 6.5 |
| 8 | 9 | 0.117 | 1 | 4.5 | 11 | 14 | 0.237 | 2 | 7.0 |
| 9 | 10 | 0.105 | 1 | 5.0 | 13 | 16 | 0.205 | 2 | 8.0 |
| 10 | 11 | 0.095 | 1 | 5.5 | 14 | 17 | 0.192 | 2 | 8.5 |
| 11 | 12 | 0.087 | 1 | 6.0 | 16 | 19 | 0.170 | 2 | 9.5 |
| 12 | 13 | 0.08 | 1 | 6.5 | 17 | 20 | 0.161 | 2 | 10.0 |
| 13 | 14 | 0.074 | 1 | 7.0 | 19 | 22 | **0.146** | **2** | **11.0** |
| 14 | 15 | 0.069 | 1 | 7.5 | 20 | 23 | 0.139 | 2 | 11.5 |

Table B.1: Values of $k$ to guarantee 100% energy transfer from [72]

that complete energy transfer would have been achieved in just 1 cycle.

# Appendix C

# Distributed analysis

Chapter five of [40], chapter five of [41] and chapter seven of [42] all present thorough examinations of lossy transmission lines and transmission line resonators, on which this appendix is based unless otherwise identified. Figure (C.1) shows a short segment $dz$ of a standard transmission line model, orientated up the $z$ axis. The standard model is an infinite series of such segments with the values of the components specified per unit length. In this analysis the model refers to the secondary winding of a Tesla transformer formed as a resonant quarter wavelength tall helical transmission line, mounted vertically and earthed to a ground plane and terminated at its upper end in a capacitive topload. Per length $dz$, $R$ and $L$ refer to the series resistance and inductance of the transmission line, $C$ to its shunt capacitance and $G$ to its shunt conductance. In the case of a Tesla transformer secondary coil the shunt conductance $G$ is likely to be high compared with a typical coaxial cable or two-wire transmission

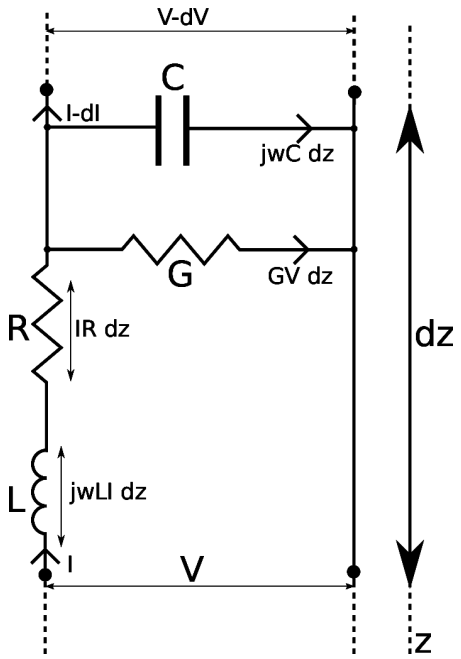


Figure C.1: A transmission line lumped-equivalent model

line because, under non-sparking conditions*, the high voltage present across the Tesla transformer secondary coil causes leakage currents to flow on the surface of the resonator and under sparking conditions, the line is effectively shunted by a dynamic impedance due to the formation of a spark channel or channels.

The voltage at an arbitrary point along the transmission line can be found via the superposition of forward and reflected voltage wavefronts. The maximum superposition voltage is given by

$$V_{max} = |V^{+}| + |V^{-}| \tag{C.1}$$

*a Tesla transformer whose output voltage is not sufficiently high to promote the formation of distinct spark channels, because the output terminal “toploaд” is below the corona inception voltage [20] [87]

and the minimum voltage by

$$V_{min} = |V^+| - |V^-| \tag{C.2}$$

where $V^+$ indicates a voltage wave propagating in the $^+z$ "forward" direction i.e. upwards, from the base of the resonator towards the topload. $V^-$ indicates a voltage wave propagating in the opposite ("backward") direction, having been reflected due to the complex impedance of the topload, back toward the resonator base.

The complex voltage reflection coefficient $\Gamma = \Gamma e^{j\theta}$ is defined [38] [39] as

$$\Gamma = \frac{reflected\,wave\,complex\,amplitude}{forward\,wave\,complex\,amplitude} \tag{C.3}$$

The reflection coefficient at the grounded base of the resonator is therefore

$$\Gamma_{base} = \frac{V^-_{base}}{V^+_{base}} \rightarrowtail \frac{reflected}{forward} \tag{C.4}$$

and that at the top of the resonator is similarly

$$\therefore \Gamma_{top} = \frac{V^-_{top}}{V^+_{top}} \rightarrowtail \frac{reflected}{forward} \tag{C.5}$$

Figure (C.2) shows a helical transmission line of length or *height* $\mathcal{H}$. The reflection coefficient at a position $z$ away from the base (and hence distance $d$ from the topload) can be found (p. 210ff. of [40]) as:

$$\frac{\Gamma_{top}}{\Gamma} = \frac{\Gamma_{base}}{\Gamma_{top}} e^{+(2\gamma\mathcal{H}-z)} \tag{C.6}$$

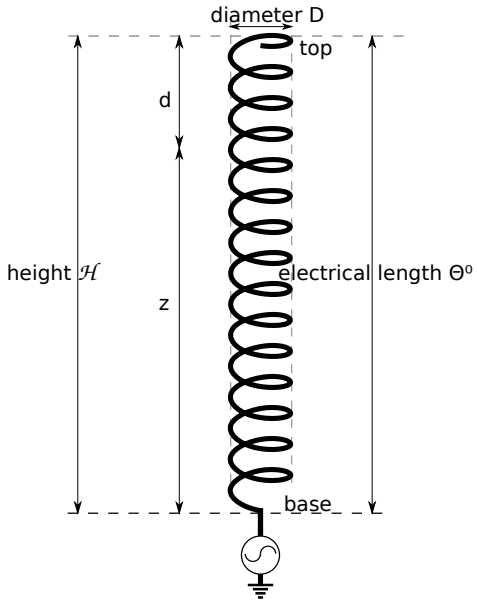


Figure C.2: Helical transmission line reflection coefficient

$$\therefore \Gamma = \Gamma_{base} e^{-2\gamma d} \tag{C.7}$$

where

$\gamma$ is the complex propagation constant, given by $\alpha + j\beta$, determining how rapidly the amplitude of a wave is attenuated along the length of the line, in which

$\alpha$ is the attenuation constant describing the exponential decay of a wave propagating along the transmission line

$\beta$ is the phase constant $\frac{2\pi}{\lambda} = \omega\sqrt{L_s C_s}$ describing how the phase of the wave changes as a function of $z$ (p. 180 of [40]

The velocity factor of the helical transmission line resonator is [75]

$$\mathbb{V} = \frac{1}{\left[\sqrt{1 + 20D^3 s^{-\frac{5}{2}} \lambda_0^{-\frac{1}{2}}}\right]} \tag{C.8}$$

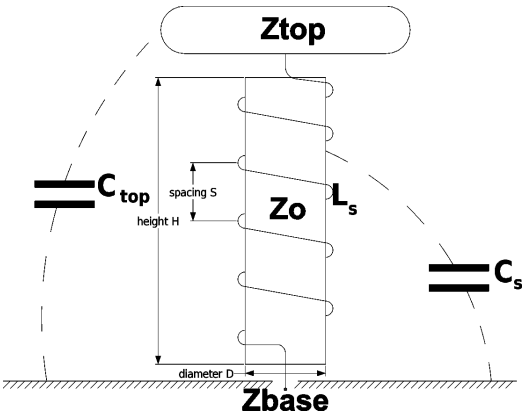


Figure C.3: Some concepts for resonator transmission line analysis

where

D is the diameter of the helix

s is the pitch of the winding

$\lambda_0$ is the wavelength at the resonant frequency

For a quarter wavelength resonant transmission line, $Z_{0_{average}}$ is derived from the Schelkunoff [108] [109] average characteristic impedance for a half wave dipole antenna (p. 384ff. and p. 587 of [42], [75] and p. 236 and p. 414ff. of [108]):

$$Z_{0_{average}} = \left(\frac{60}{\mathbb{V}}\right)\left(\ln\left(\frac{4\mathcal{H}}{D}\right) - 1\right) \tag{C.9}$$

where

$\frac{\mathcal{H}}{D}$ is the ratio of the resonator's height to its diameter and

$\mathbb{V}$ is the velocity factor for the transmission line

The general case for $VSWR$ is given by [†]

[†] and for completeness, $\Gamma$ in terms of $VSWR$ can be found from $\Gamma = \frac{VSWR-1}{VSWR+1}$

$$VSWR = \frac{|E|_{max}}{|E|_{min}} = \frac{1 + |\Gamma|}{1 - |\Gamma|} \tag{C.10}$$

The voltages present at the ends of the secondary resonator are separated in phase by $90°$. If the resonator was lossless, $VSWR$ would be infinite and the base and top reflection coefficients would be equal. In a lossy case, the $VSWR$ at the top and the base are different, due to the loss mechanisms discussed in appendix (D) which affect the propagating wavefront. Assuming that resonator losses are low,

$$\frac{1}{VSWR_{base}} = \frac{1}{VSWR_{top}} + \alpha l \tag{C.11}$$

In the case of the Tesla transformer secondary coil resonator, a capacitive topload is utilised in order to assist with voltage grading, in which case the $VSWR$ for the topload tends towards a very high value, such that

$$VSWR_{base} \cong \frac{1}{\alpha l} \tag{C.12}$$

Under conditions where the Tesla transformer secondary coil is ringing down due to external losses, but not to the presence of a connected load, the shunt conductance $G$ is low and

$$\alpha l = \frac{R_{loss}}{2Z_{0_{average}}} \tag{C.13}$$

An expression for resonator loss in terms of *physical geometry* and $Z_0$ for helical resonators derived from [75] and given in [121] is

$$\alpha l = \frac{7.8125 \left(\frac{\mathcal{H}}{D}\right)^{\frac{1}{5}}}{d_{wire} Z_0 \sqrt{f}} \tag{C.14}$$

where

$d_{wire}$ = conductor diameter in inches

$f$ = frequency in $MHz$

$\frac{\mathcal{H}}{D}$ = aspect ratio of the helical resonator

The electrical length of the resonant line is [121]

$$\Theta^{\circ} = \beta l = \frac{360\mathcal{H}}{\mathbb{V}\lambda_0} \tag{C.15}$$

where, for a coil terminated with a topload, $\Theta$ must be < 90 degrees in order to still achieve resonance. The topload reflection coefficient is

$$\Gamma_{top} = \frac{V_s^-}{V_s^+} = \frac{Z_{top} - Z_{0_{average}}}{Z_{top} + Z_{0_{average}}} = |\Gamma_{top}|\angle\Phi_{top}^{\circ} \tag{C.16}$$

where $Z_{top}$ and $Z_{0_{average}}$ are complex values. Reducing the $\frac{\pi}{2}$ resonator length ($\frac{\lambda}{4}$, or $\Theta$ = 90$^o$) by a distance $d$ shortens the *electrical* length by $\phi$ degrees. The reflection coefficient of the topload capacitance can be found from [40]

$$\Gamma = |\Gamma|\angle\phi_{top} = \frac{Z_L - Z_{0_{average}}}{Z_L - Z_{0_{average}}} \tag{C.17}$$

A toroid topload is a pure capacitive reactance, $Z_{top} = X_{top}$ and so

$$Ctop = \frac{1}{\omega X_{top}} \tag{C.18}$$

and it is straightforward to find the capacitance required to bring the line into resonance since

$$Z_{top} = \frac{\left(\Gamma_{top} Z_{0_{average}}\right) + Z_{0_{average}}}{1 - \Gamma_{top}} \tag{C.19}$$

The preceding equations define the physical characteristics of a resonator (its diameter and height, the diameter of the conductor from which it is wound and the toploaded capacitance required). The design process used for the secondary coil and toploaded discussed in chapter (5) follows:

- Determine the velocity factor $\mathbb{V}$ using equation (C.8) for a given coil height $H$ and coil diameter $D$ and pitch $s$ (from number of turns $n$ and wire diameter $d_w$).
- Find the average characteristic impedance $Z_{0_{average}}$ (equation (C.9)) from the velocity factor $\mathbb{V}$ and the coil $\frac{\mathcal{H}}{d}$ (aspect ratio).
- Find the toploaded capacitance required to bring the coil into resonance.
- Find $\alpha l$ (equation (C.13)) from the coil's $\frac{\mathcal{H}}{d}$ ratio, resonant frequency, conductor diameter and average characteristic impedance $Z_{0_{average}}$.
- Find $VSWR$ (equation (C.12)) from $\frac{1}{\alpha l}$.

The result establishes the voltage ratio between the induced voltage from the primary circuit and the voltage present at the top of the resonator. Foreshortening the electrical length of the resonant transmission line by an amount $\phi$, then adding capacitance in the form of a toploaded so that $\theta + \phi$ again equals $90°$, brings the coil and toploaded combination back into resonance. Addition of the toploaded also allows voltage grading to be achieved and so prevents electrical breakdown of

the air surrounding the topload/coil combination. This enables a high voltage to be generated.

The results for the 0% winding design used are presented in table (C.1), using parameters taken from table (5.1).

| parameter | result |
|---|---|
| $\frac{\mathcal{H}}{D}$ ratio | 4.94 |
| $d_w$ | 0.35 $mm$ |
| $n$ | 1600 |
| $s$ | 0.36 $mm$ |
| velocity factor $\mathbb{V}$ | 0.0017 |
| Average characteristic impedance $Z_{0_{average}}$ | 70 k$\Omega$ |
| propagation loss $\alpha l$ | 0.023 |
| $VSWR$ | 43 |

Table C.1: Secondary resonator design for the 0% winding

$VSWR \approx 43$ means that the maximum voltage at the top of the Tesla transformer secondary coil is 43 times the peak voltage induced in the base of the secondary coil from the primary circuit of the Tesla transformer.

# Appendix D

# Resonator loss mechanisms

Chapters (4) and (6) mentioned the influence of skin effect on RF resistance, the predominant mechanism responsible for energy loss from the "non-sparking" secondary coil of a Tesla transformer. Additional loss mechanisms are however present, and this appendix examines these during the period which starts when all of the energy from the primary has transferred to the secondary. During this period, currents circulate in the resonant system comprising the secondary winding and its topload, but no current flows from the topload through any other path (such as an ionised air channel, or load).

## D.1 Proximity effect in conductors

In addition to skin effect, frequency-dependent AC resistance occurs when the circular symmetry of current distribution in a round wire conductor is disturbed due to magnetic flux from adjacent conductors which carry currents (p. 36 of [33] and chapter twenty four of [43]). Detailed examinations are presented in [45] [122] [123]. Additional

work [124] suits the analysis of long solenoids whose turns are spaced closely to one another. A simple formula is presented in [125] for calculating RF skin and *proximity* effect resistance of a coil in terms of the coil radius, the number of turns and the radius and winding pitch of the circular conductor from which it is wound.

## D.2 Dielectric loss

A useful theoretical discussion is presented in section 8-15 of [39] and a practical discussion of dielectric loss mechanisms in chapter two of [126]. The loss tangent of a dielectric is related to dissipation factor ($DF$) (p. 140ff. of [120]) by

$$\tan\delta = DF = \frac{1}{Q} \tag{D.1}$$

The $Q$ of a capacitor is in part determined by the nature of the dielectric [101], while the dielectric material that a solenoid secondary is wound upon similarly has an effect on the coil $Q$. Various methods exist by which dielectric loss can be measured, for example the Schering bridge (p. 905 of [33]) or the split post dielectric resonator [127] [128].

## D.3 Ground loss resistance

When a resonant winding is operated against a finite conductivity ground plane, currents are induced which flow to and fro the base of the resonator where it connects to the ground plane, completing the circuit and causing Joule heating power dissipation. Good conductors such

as copper have high conductivities in the region of $10^7$ $S/m$ whereas those of typical ground planes are much lower (e.g. the conductivity of concrete is approximately 2.3 $S/m$ [4]). The Joule loss appears as an increase in the input impedance of the winding and the total resistive loss mechanism becomes

$$R_{loss} = R_{wire} + R_{ground} \tag{D.2}$$

which highlights the importance of achieving a low impedance ground plane in establishing low loss conditions.

## D.4 Electromagnetic radiation from a Tesla transformer

External loss mechanisms of a non-sparking Tesla transformer secondary coil are those which occur via the fields surrounding the secondary. These additional mechanisms exist in the case of a solenoid which is *not* isolated from its surroundings:

- magnetic induction fields around the secondary coil coupling into conducting objects in the vicinity of the Tesla transformer and the induced currents therein dissipating power as $I^2R$ in those objects
- electric fields around the secondary coil coupling into dielectric materials in the vicinity of the Tesla transformer and dissipating power as dielectric hysteresis losses
- electromagnetic radiation propagating into the far field

In a helical cavity filter, magnetic field coupling from the resonant helix induces currents in the walls of the conductive bounding cavity which give rise to $I^2R$ losses, since the conductive material from which the cavity is constructed must have non-zero resistivity. Intuitively, a solenoid not bounded by a cavity will yield a higher $Q$ than an identical solenoid operated inside a cavity. A field analysis of helical resonators carried out by Miley and Beyer [129] shows that an optimum $Q$ is achieved if the ratio of the cavity radius to the helix radius is infinite i.e. when there is no cavity. Similarly, the same conditions apply to a resonant secondary coil in a Tesla transformer.

This section is inspired by [130] and discusses whether radiation losses reduce significantly the $Q$ of the resonant secondary coil in a Tesla transformer. The IEEE [131] define an electrically small antenna (ESA) as

> "an antenna whose dimensions are such that it can be contained within a sphere whose diameter is small compared to a wavelength at the frequency of operation".

Wheeler [132] stated that an ESA is in the form of a capacitor or *inductor* which is tuned to resonance by an opposite reactance and defined an ESA as a structure which fits inside a sphere whose radius $r$ is $\frac{\lambda}{2\pi}$. It is clear that a Tesla transformer's secondary coil fits this description. Kraus [107] recognised that an ESA of $\frac{\lambda}{10}$ presents an approximately linear or triangular current distribution which simplifies mathematical analyses. Some Tesla transformer secondary coils have a fundamental resonance of hundreds of $kHz$ with the higher-order modes ($f_3$, $f_5$, $f_7$ etc.) reaching up to a few $MHz$. One example of a physically large Tesla transformer was in

Tesla's original Colorado Springs experiments [25] (see figure (2.2)) which utilised a winding approximately 2.5 $m$ in diameter by 3 $m$ tall with a fundamental frequency of approximately 95 $kHz$ ($\lambda \approx 3000$ $m$). It is clear that the dimensions are of the order of $\frac{\lambda}{1000}$ and it was an ESA even though the structure itself was physically large. The 0.5 $m$ tall experimental secondary windings used in this thesis are clearly electrically small since, for any mode frequency of less than (say) 1 $MHz$ where the wavelength is $\lambda$ = 300 $m$, the coil needs to have a maximum dimension of less than $\frac{\lambda}{2\pi} \approx 48$ $m$ to be considered as electrically small.

Electric and magnetic fields surrounding an antenna are defined by three boundaries [133]. In each case $D$ represents the largest linear dimension of the structure of an antenna, expressed in the same units as $\lambda$ (and as an example, for a 1 $m$ tall vertical conductor connected to an orthogonal 1 $m$ long horizontal conductor, $D$ = 1.414 $m$). The boundaries represent areas where one field mode dominates the other field modes present.

The "reactive near-field" [131] [134] occupies a spherical volume with a radius given by

$$r = \frac{\lambda}{2\pi} \tag{D.3}$$

for certain types of ESA. Some energy is always contained within this reactive near-field region as a magnetic induction field associated with alternating currents, and an electric induction field associated with alternating voltages. In this region, which for the Tesla transformer discussed in this thesis equates to a spherical volume of 351 $m$ radius, inductive coupling into nearby structures can occur and

hence power can be lost.

The next region which surrounds the antenna is the radiating near-field (also known as the Fresnel region or zone) which extends to a distance given by

$$r = \frac{2D^2}{\lambda} \tag{D.4}$$

In the case of an ESA this region is insignificant in its effect, or non-existent [133]. For the experimental Tesla transformer secondary coils used in this study, $\frac{2D^2}{\lambda}$ is approximately 2.5 x $10^{-3}$ $m$, suggesting that the radiating near-field region of the secondary coil is contained within the volume described by the secondary/topload combination. Since the secondary is electrically small, the premise that the radiating near-field is non-existent is supported.

The radiating far-field (also known as the Fraunhofer region) extends from the $\frac{2D^2}{\lambda}$ range to infinity. The $E$ and $H$ field vectors in this far field region are in-phase and develop real (rather than reactive) power and hence can do work at a distance (e.g. accelerate electrons in the conductors of a distant antenna and a radio wave can be received). Seybold (p. 46 of [134]) stated that for ESAs where $D \ll \lambda$, the distance for the radiating far-field boundary should be taken as equal to the reactive near-field boundary.

It can be seen therefore that a Tesla transformer secondary coil generates fields which can couple to objects upto several metres away, dissipate power in those objects and hence lose circulating energy. This is clearly a mechanism by which the coil $Q$ can be reduced. Figure (D.1) helps to illustrate the different ranges at which field types dominate.

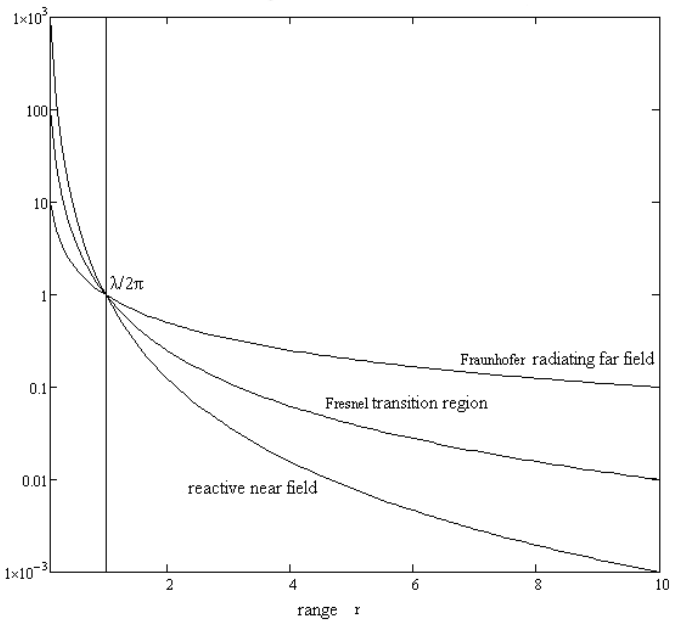


Figure D.1: Field decay as a function of distance

### D.4.1 Radiation efficiency

The various secondary winding losses contribute to an overall equivalent loss mechanism which can be termed a loss resistance. An ESA has an equivalent LCR circuit [132] as shown in figure (D.2) but labelled as an equivalent circuit for a Tesla transformer secondary.

The values of $L_{sec}$ and $C_{sec}$ represent the inductance and capacitance of the secondary winding/topload combination. Considering antenna efficiency for ESAs, the radiation resistance of an ESA (that part of the input impedance which is real and appears to be a load in which radiated EM power appears to be dissipated) is very low and a small fraction of the total real input impedance. Loss mechanisms in larger structures may be negligible but in ESAs they are more significant [107] and limit the radiation efficiency $\eta$:

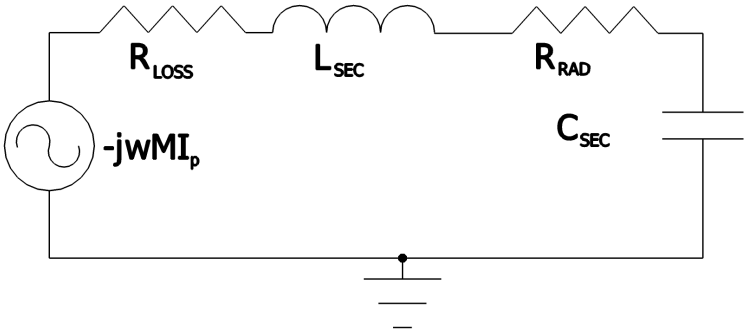


Figure D.2: Lumped equivalent circuit of an ESA/Tesla transformer secondary

$$\eta = \frac{R_{rad}}{R_{rad} + R_{loss}} \tag{D.5}$$

where

$R_{rad}$ is the radiation resistance representing a power dissipation mechanism caused by the transfer of energy from the antenna into the far field

$R_{loss}$ is an equivalent resistance which accounts for that power not radiated into the far field but instead is dissipated as Joule heating in the conductor, or as dielectric loss (hysteresis) heating

Since $P = I^2R$, the concepts of loss resistance and radiation resistance [107] can be used to express efficiency as shown in equation (D.5). For efficient power transfer, an antenna needs to have a value of $R_{rad}$ which matches the system impedance $Z_0$ (typically 50 $\Omega$) and a value for $R_{loss}$ which is small compared with $R_{rad}$. In the case of an ESA this is often not the case and in the case of a Tesla transformer, it is designed to

dissipate power in a connected load rather than lost via EM radio wave propagation. Kraus [100] observed that "the terminal impedance of such a small helix would be sensitive to frequency and the radiation efficiency would be low".

Formulae which express radiation resistances of ESAs are described in many references but the most pertinent for the case of a Tesla transformer secondary coil is from Kandoian and Sichak [75]:

$$R_{rad} = \left[\frac{25.3\mathcal{H}}{\lambda}\right]^2 \tag{D.6}$$

where

$\mathcal{H}$ = coil height

$\lambda$ = wavelength

expressed in the same units. For the experimental coil where $\mathcal{H} \approx 0.5\ m$, $f_1$ = 137 $kHz$ and $\lambda$ = 2200 $m$, $R_{rad}$ is approximately 33 $\mu\Omega$. Compared with the RF or even DC resistance of approximately 100 $\Omega$ or 200 $\Omega$ (see table (5.1)), equation (D.5) demonstrates that radiation efficiency is extremely low:

$$\eta = \frac{33\,\mu\Omega}{33\,\mu\Omega + 200\,\Omega} \times 100\% = 0.000016\% \tag{D.7}$$

Another formula for calculating $R_{rad}$ of ESAs given by Kraus [3] states that the radiation resistance of a helix of height $\mathcal{H} \ll \lambda$ is given by:

$$R_{rad} = 395\left(\frac{2}{\pi}\right)^2 \mathcal{H}_\lambda^2 \tag{D.8}$$

which yields a radiation resistance of $10.5\ \mu\Omega$ for the $f_1$ mode. Higher-order mode frequencies also result in very low calculated values for $R_{rad}$, e.g. the $f_7$ mode was measured to be approximately 1 $MHz$ which would result in a value for $R_{rad}$ of 1.8 $m\Omega$.

A normal-mode helical antenna (NMHA) [75] [107] is an antenna which has a structure very similar to a Tesla transformer secondary coil. Kraus [107] stated that the radiation resistance of an NMHA is

$$R_{rad} = 160\mathcal{H}_{\lambda}^{2}\ \Omega \tag{D.9}$$

which yields a value for $R_{rad}$ of 8 $\mu\Omega$ for the $f_1$ mode frequency.

Any of the calculations of $R_{rad}$ yield small values of tens or hundreds of $\mu\Omega$ for wavelengths of hundreds of $kHz$, showing a Tesla transformer resonant secondary winding to be a poor EM radiator.

# References


[1] P. Vizmuller. *Filters with Helical and Folded Helical Resonators*. Artech House, 1987.
(8 citations on 7 pages: 2, 33, 34, 38, 40, 53, and 54)

[2] P. Nicholson. Tesla Secondary Simulation Project. http://abelian.org/tssp/, 2008.
(5 citations on 5 pages: 4, 7, 66, 107, and 113)

[3] J. D. Kraus. *Antennas*. McGraw-Hill, 2nd edition, 1988.
(7 citations on 7 pages: 4, 50, 54, 55, 85, 115, and 144)

[4] A. Voors. 4nec2. http://www.qsl.net/4nec2/, 2012.
(2 citations on 2 pages: 4 and 138)

[5] N. Kyriazis. nec2c. http://www.qsl.net/5b4az/pages/nec2.html, 2013.
(2 citations on 2 pages: 5 and 69)

[6] N. Kyriazis. xnec2c. http://www.qsl.net/5b4az/pages/nec2.html, 2013.
(1 citation on page 5)

[7] J. Vreeken. nec2c-rxq. http://sharon.esrac.ele.tue.nl/users/pe1rxq/, 2012.
(1 citation on page 5)

[8] Feko. http://www.feko.info, 2012.
(1 citation on page 5)

[9] Gnuplot. http://www.gnuplot.info/, 2012.
(1 citation on page 5)

[10] Linux Mint. http://www.linuxmint.com, 2013.
(1 citation on page 6)

[11] Linear Technology. LTspice IV.
http://www.linear.com/designtools/software/, 2013.
(1 citation on page 6)

[12] Octave. http://www.gnu.org/software/octave/, 2013.
(1 citation on page 6)

[13] Qucs. http://qucs.sourceforge.net, 2012.
(1 citation on page 7)

[14] S. Hyde. RFSim99.
http://www.microwavers.org/software/RFSim99.exe, 1999.
(1 citation on page 7)

[15] LyX. http://www.lyx.org/, 2012.
(1 citation on page 8)

[16] JabRef. http://jabref.sf.net, December 2011.
(1 citation on page 8)

[17] F. Ferzak. *Nikola Tesla Collected Articles and Lectures*, volume 1. KOHA, 2000.
(1 citation on page 10)

[18] J.D. Craggs and J.M. Meek. *High Voltage Laboratory Technique*. Butterworths Scientific Publications, 1954.
(5 citations on 5 pages: 10, 15, 31, 39, and 49)

[19] C. R. J. Hoffmann. A Tesla transformer high-voltage generator. In *Rev. Sci. Instrum.*, volume 46, pages 1–4, 1975.
(2 citations on 2 pages: 10 and 22)

[20] W. J. Sarjeant and R. E. Dollinger. *High Power Electronics*. TAB Professional and Reference Books, 1989.
(9 citations on 8 pages: 10, 15, 19, 23, 99, 123, 125, and 128)

[21] R. Lomas. *The Man Who Invented the Twentieth Century: Nikola Tesla, Forgotten Genius of Electricity*. New Headline Book Publishing, 2000.
(6 citations on 5 pages: 10, 11, 12, 13, and 14)

[22] T. Valone. *Harnessing the Wheelwork of Nature: Tesla's Science of Energy*. Adventures Unlimited Press, 2002.
(3 citations on 2 pages: 10 and 11)

[23] M.J. Seifer. *Wizard: The Life and Times of Nikola Tesla: Biography of a Genius*. Carol Publishing Group, 1996.
(3 citations on 3 pages: 10, 11, and 14)

[24] Wikipedia. Nikola Tesla. https://upload.wikimedia.org/wikipedia/commons/d/d4/N.Tesla.JPG, 2013.
(1 citation on page 12)

[25] N. Tesla. *Colorado Springs Notes, 1899-1900*. Nolit, 1978.
(3 citations on 3 pages: 13, 14, and 140)

[26] Wikipedia. Colorado Springs Notes. https://upload.wikimedia.org/wikipedia/commons/e/e5/Tesla_colorado_adjusted.jpg, 2013.
(1 citation on page 13)

[27] H. B. Rockman. *Intellectual Property Law for Engineers and Scientists*. Wiley-IEEE, 2004.
(1 citation on page 14)

[28] J. R. Reed. Analytical expression for the output voltage of the triple resonance Tesla transformer. *Review of Scientific Instruments*, 76(10):104702, 2005.
(1 citation on page 14)

[29] A. C M De Queiroz. The triple resonance network with sinusoidal excitation. In *Electronics, Circuits and Systems, 2007. ICECS 2007. 14th IEEE International Conference on*, pages 1143–1146, Dec 2007.
(1 citation on page 14)

[30] M. Denicolai. Optimal performance for Tesla transformers. *Review of Scientific Instruments*, 73(9):3332–3336, 2002.
(5 citations on 5 pages: 15, 19, 121, 124, and 125)

[31] B. L. Goodlet. High-voltage testing equipment. In *Journal of the Institute of Electrical Engineers*, 1934.
(3 citations on 3 pages: 15, 26, and 121)

[32] W. Smythe. *Static and Dynamic Electricity*. McGraw-Hill, 1950.

(3 citations on 3 pages: 15, 99, and 121)

[33] F.E. Terman. *Radio Engineer's Handbook*. McGraw-Hill Handbooks. McGraw-Hill Book Company, Incorporated, 1943.

(6 citations on 6 pages: 15, 40, 43, 56, 136, and 137)

[34] A. C M De Queiroz. Multiple resonance networks. *Circuits and Systems I: Fundamental Theory and Applications, IEEE Transactions on*, 49(2):240–244, 2002.
(1 citation on page 16)

[35] A. C M De Queiroz. Generalized LC multiple resonance networks. In *Circuits and Systems, 2002. ISCAS 2002. IEEE International Symposium on*, volume 3, pages III–519–III–522 vol.3, 2002.
(1 citation on page 16)

[36] A. C M De Queiroz. A simple design technique for multiple resonance networks. In *Electronics, Circuits and Systems, 2001. ICECS 2001. The 8th IEEE International Conference on*, volume 1, pages 169–172 vol.1, 2001.
(1 citation on page 16)

[37] S. S. Attwood. *Electric and Magnetic Fields*. Wiley and Sons, 1941.
(1 citation on page 16)

[38] D. K. Cheng. *Field and Wave Electromagnetics*. Addison-Wesley, 1983.
(4 citations on 4 pages: 16, 17, 84, and 129)

[39] J. D. Kraus and K. R. Carver. *Electromagnetics*. McGraw-Hill, 1973.
(7 citations on 7 pages: 16, 18, 44, 57, 84, 129, and 137)

[40] R. B. Adler, L. J. Chu and R. M. Fano. *Electromagnetic Energy Transmission and Radiation*. Wiley and Sons, 1960.
(7 citations on 7 pages: 16, 54, 115, 127, 129, 130, and 133)

[41] S. Ramo, J.R. Whinnery, and T. Van Duzer. *Fields and Waves in Communication Electronics*. J. Wiley, third edition, 1993.
(13 citations on 10 pages: 16, 17, 18, 44, 47, 50, 51, 57, 99, and 127)

[42] E. C. Jordan and K. G. Balmain. *Electromagnetic Waves and Radiating Systems*. Prentice-Hall, 1968.
(4 citations on 4 pages: 16, 18, 127, and 131)

[43] F.W. Grover. *Inductance Calculations*. Van Nostrand Company, 1947.
(5 citations on 5 pages: 17, 52, 56, 58, and 136)

[44] R. Lundin. A handbook formula for the inductance of a single-layer circular coil. *Proceedings of the IEEE*, 73(9):1428–1429, 1985.
(1 citation on page 17)

[45] B.M. Novac, I.R. Smith, and M.C. Enache. Accurate modeling of the proximity effect in helical flux-compression generators. *Plasma Science, IEEE Transactions on*, 28(5):1353–1355, 2000.
(2 citations on 2 pages: 17 and 136)

[46] J. Luo, B.M. Novac, I.R. Smith, and J. Brown. Accurate modelling of high-voltage pulsed transformers. In *Pulsed Power Symposium, 2006. The Institution of Engineering and Technology*, pages 74–78, 2006.
(2 citations on 2 pages: 17 and 49)

[47] R.A. Abd-Alhameed and P.S. Excell. The complete surface current distribution in a normal-mode helical antenna using a Galerkin solution with orthogonal sinusoidal basis functions. In *Computation in Electromagnetics, 2002. CEM 2002. The Fourth International Conference on (Ref. No. 2002/063)*, 2002.
(1 citation on page 17)

[48] D. W. Knight. Practical continuous functions for the internal impedance of solid cylindrical conductors. http://www.g3ynh.info/zdocs/comps/Zint.pdf, April 2013.
(1 citation on page 17)

[49] J. F. Corum and K. L. Corum. *TCTutor: A personal computer analysis of spark-gap Tesla coils*. Corum & Associates, Inc., 8551 State Route 534, Windsor, Ohio 44099, USA, 1988.
(1 citation on page 17)

[50] J. F. Corum and K. L. Corum. *Vacuum Tube Tesla Coils*. Corum & Associates, Inc., 8551 State Route 534, Windsor, Ohio 44099, USA, 1987.
(2 citations on 2 pages: 17 and 25)

[51] C. A. Balanis. *Antenna Theory: Analysis and Design*. Wiley and

Sons, 1997.
(1 citation on page 18)

[52] K. Fleder. The Bergeron method.
http://www.ti.com/litv/pdf/sdya014, October 1996.
(1 citation on page 18)

[53] D. H. Sloan. A Radiofrequency High-Voltage Generator. In *Phys. Rev*, volume 47, 1935.
(4 citations on 4 pages: 19, 38, 40, and 51)

[54] M.C. Scott, J.P. O'Loughlin, and R.P. Copeland. A 350 kV dual resonant transformer for charging a 40 pF PFL at kilo-hertz rep-rates. In *Pulsed Power Conference, 1995. Digest of Technical Papers., Tenth IEEE International*, volume 2, pages 1466–1471 vol.2, 1995.
(2 citations on 2 pages: 19 and 23)

[55] S.A. Scott K.D. Skeldon and A.I. Grant. A high potential Tesla coil impulse generator for lecture demonstrations and science exhibitions. In *American Journal of Physics*, volume 65, 1997.
(1 citation on page 20)

[56] K.D. Skeldon. Development of a portable Tesla coil apparatus. In *European Journal of Physics*, volume 21, 2000.
(1 citation on page 20)

[57] Yu.A. Andreev, Yu I. Buyanov, A. M. Efremov, V.I. Koshelev, B.M. Kovalchuk, K.N. Sukhushin, V. A. Vizir, and V. B. Zorin. High-power ultrawideband electromagnetic radiation generator. In *Pulsed Power Conference, 1997. Digest of Technical Papers. 1997 11th IEEE International*, volume 1, pages 730–735 vol.1, 1997.
(2 citations on 2 pages: 22 and 31)

[58] E. A. Abramyan. Transformer type accelerators for intense electron beams. *Nuclear Science, IEEE Transactions on*, 18(3):447–455, 1971.
(1 citation on page 23)

[59] M. T. Buttram and G. J. Rohwein. Operation of a 300-kV, 100-Hz, 30-kW average power pulser. *Electron Devices, IEEE Transactions on*, 26(10):1503–1508, 1979.

(1 citation on page 23)

[60] G.J. Rohwein. A three megavolt transformer for PFL pulse charging. *Nuclear Science, IEEE Transactions on*, 26(3):4211–4213, 1979.
(1 citation on page 23)

[61] G. N. Glasoe and J. V. Lebacqz. *Pulse Generators*. McGraw-Hill, 1948.
(4 citations on 3 pages: 23, 25, and 80)

[62] P. Sarkar, S.W. Braidwood, I.R. Smith, B.M. Novac, R.A. Miller, and **R.M. Craven**. A compact battery-powered half-megavolt transformer system for EMP generation. *Plasma Science, IEEE Transactions on*, 34(5):1832–1837, 2006.
(3 citations on 3 pages: 23, 24, and 30)

[63] P. Sarkar, I.R. Smith, B.M. Novac, R.A. Miller, and **R.M. Craven**. A high-average power self-break closing switch for high repetition rate applications. In *Pulsed Power Symposium, 2006. The Institution of Engineering and Technology*, pages 62–65, 2006.
(2 citations on 2 pages: 23 and 80)

[64] I. Vitkovitsky. *High Power Switching*. Van Nostrand Reinhold, 1987.
(2 citations on 2 pages: 25 and 121)

[65] TCML. Tesla Coil Mailing List. http://www.pupman.com, 2013.
(2 citations on 2 pages: 28 and 41)

[66] D. McCauley. *DRSSTC: Building the modern day Tesla Coil*. Eastern Voltage Research, 2006.
(1 citation on page 29)

[67] P. Sarkar, B.M. Novac, I.R. Smith, R.A. Miller, **R.M. Craven**, and S.W. Braidwood. A high repetition rate battery-powered 0.5 MV pulser for ultrawideband radiation. In *Power Modulator Symposium, 2006. Conference Record of the 2006 Twenty-Seventh International*, pages 592–595, 2006.
(1 citation on page 30)

[68] F.J. Agee, C.E. Baum, W.D. Prather, J.M. Lehr, J.P. O'Loughlin,

J.W. Burger, J.S.H. Schoenberg, D.W. Scholfield, R.J. Torres, J.P. Hull, and J.A. Gaudet. Ultra-wideband transmitter research. *Plasma Science, IEEE Transactions on*, 26(3):860–873, 1998.
(1 citation on page 30)

[69] T.H. Martin. A nominal one-megavolt, pulsed power generator. *Nuclear Science, IEEE Transactions on*, 18(3):104–105, 1971.
(1 citation on page 31)

[70] R. K. Golka. Long arc simulated lightning attachment testing using a 150 kW Tesla coil. In *IEEE Int. Symp. on Electromagnetic Compatibility*, San Diego, USA, Oct 1979.
(1 citation on page 31)

[71] **R.M. Craven**. Design improvements in Tesla coil performance. In *Pulsed Power '97 (Digest No: 1997/075), IEE Colloquium on*, pages 38/1–38/3, 1997.
(1 citation on page 31)

[72] M. Denicolai. Tesla transformer for experimentation and research. Licentiate thesis, Helsinki University of Technology, 2001.
(2 citations on 2 pages: 31 and 126)

[73] A.I. Zverev. *Handbook of Filter Synthesis*. Wiley-Interscience, 1967.
(6 citations on 6 pages: 32, 33, 46, 51, 83, and 107)

[74] W. W. Macalpine and R. O. Schildknecht. Coaxial resonators with helical inner conductor. In *Proc. IRE*, pages 2099–2105, 1959.
(5 citations on 3 pages: 32, 38, and 51)

[75] A. Kandoian and W. Sichak. Wide-frequency-range tuned helical antennas and circuits. In *IRE International Convention Record*, volume 1, pages 42–47, 1953.
(11 citations on 11 pages: 32, 33, 38, 51, 54, 85, 130, 131, 132, 144, and 145)

[76] P. Vizmuller. *RF Design Guide*. Artech House, 1995.
(3 citations on 3 pages: 32, 33, and 38)

[77] Pasternack Enterprises. GSM bandpass filter catalogue, 869

MHz to 894 MHz. 2012 (3/3). http://www.pasternack.com, 2012.
(1 citation on page 32)

[78] R. Denton. Cavity filter for the APT weather satellites on 137 MHz band. http://www.wxsat.org, 2012.
(1 citation on page 35)

[79] Harper Collins. *Collins English Dictionary: complete & unabridged*. Harper Collins, 2006.
(1 citation on page 38)

[80] T.L. Simpson. Effect of a conducting shield on the inductance of an air-core solenoid. *Magnetics, IEEE Transactions on*, 35(1):508–515, 1999.
(1 citation on page 43)

[81] D. W. Knight. Solenoid inductance calculation. http://www.g3ynh.info/zdocs/magnetics/Solenoids.pdf, January 2013.
(1 citation on page 43)

[82] R. G. Medhurst. H.F. resistance and self-capacitance of single-layer solenoids. Technical report, General Electric Company, February 1947.
(2 citations on 2 pages: 43 and 50)

[83] D. W. Knight. The self-resonance and self-capacitance of solenoid coils. http://www.g3ynh.info/zdocs/magnetics/appendix/self-res.html, April 2013.
(1 citation on page 44)

[84] K. Chang. *Encyclopedia of RF and Microwave Engineering, 6-Volume Set*. Wiley-Interscience, 2005.
(2 citations on 2 pages: 44 and 50)

[85] F.E. Terman. *Electronic and Radio Engineering*. McGraw-Hill Electrical and Electronic Engineering series. McGraw-Hill, 1955.
(4 citations on 4 pages: 46, 47, 108, and 109)

[86] A. C M De Queiroz. Capacitance calculations. http://www.coe.ufrj.br/~acmq/tesla/capcalc.pdf, February 2012.

(1 citation on page 48)

[87] E. Kuffel and W. S. Zaengl. *High Voltage Engineering - Fundamentals*. Pergamon Press, 1984.
(4 citations on 3 pages: 49, 99, and 128)

[88] G. Grandi, M.K. Kazimierczuk, A. Massarini, and U. Reggiani. Stray capacitances of single-layer solenoid air-core inductors. *Industry Applications, IEEE Transactions on*, 35(5):1162–1168, 1999.
(2 citations on 2 pages: 49 and 50)

[89] D. Kajfez and E.J. Hwan. Q-factor measurement with network analyzer. *Microwave Theory and Techniques, IEEE Transactions on*, 32(7):666–670, 1984.
(1 citation on page 49)

[90] A.H.W. Beck. *Space-charge waves and slow electromagnetic waves*, chapter 3. Pergamon Press, 1958.
(3 citations on 2 pages: 51 and 52)

[91] J.R. Pierce. *Travelling Wave Tubes*. Van Nostrand, 1950.
(4 citations on 3 pages: 52, 53, and 54)

[92] S. Sensiper. Electromagnetic wave propagation on helical structures (a review and survey of recent progress). *Proceedings of the IRE*, 43(2):149–161, 1955.
(3 citations on 3 pages: 52, 53, and 54)

[93] P. Klock and R. Mittra. On the solution of the brillouin (k-b) diagram of the helix and its application to helical antennas. In *Antennas and Propagation Society International Symposium, 1963*, volume 1, pages 99–103, 1963.
(1 citation on page 53)

[94] J. R. Wallington. Absorptive harmonic filters using helical transmission lines. In *Microwave Conference, 1969. 1st European*, pages 194–197, 1969.
(2 citations on page 53)

[95] A. R. Neureuther, P. Klock, and R. Mittra. A study of the sheath helix with a conducting core and its application to the helical antenna. *Antennas and Propagation, IEEE Transactions on*,

15(2):203–210, 1967.
(1 citation on page 53)

[96] P. Klock. A study of wave propagation of helices. Technical Report 68, Antenna Laboratory, University of Illinois, Urbana, Ill. USA, contract AF33(657)-10474, March 1963.
(1 citation on page 53)

[97] J.R. Pierce. Theory of the beam-type traveling-wave tube. *Proceedings of the IRE*, 35(2):111–123, 1947.
(2 citations on 2 pages: 53 and 54)

[98] K.L. Corum and J.F. Corum. RF coils, helical resonators and voltage magnification by coherent spatial modes. In *Telecommunications in Modern Satellite, Cable and Broadcasting Service, 2001. TELSIKS 2001. 5th International Conference on*, volume 1, pages 339–348 vol.1, 2001.
(2 citations on 2 pages: 53 and 54)

[99] J. R.Pierce and P.K Tien. Coupling of modes in helixes. In *Proceedings of the IRE*, pages 1389–1396, September 1954.
(1 citation on page 54)

[100] J.D. Kraus. The helical antenna. *Proceedings of the IRE*, 37(3):263–272, 1949.
(2 citations on 2 pages: 54 and 144)

[101] F. Frungel. *High Speed Pulse Technology*. Academic Press, 1965.
(3 citations on 3 pages: 76, 99, and 137)

[102] Applied Kilovolts. KS series high voltage modules. http://www.exelis-ps.com/product.cfm?prod=ks, 2012.
(1 citation on page 78)

[103] D. Kajfez. Q-factor measurement with a scalar network analyser. *Microwaves, Antennas and Propagation, IEE Proceedings*, 142(5):369 –, 1995.
(3 citations on 2 pages: 83 and 90)

[104] G. L. Matthaei, L. Young & E. M. T. Jones. *Microwave Filters, Impedance-Matching Networks, and Coupling Structures*. McGraw-Hill, 1964.

(1 citation on page 83)

[105] F. E. Terman and J. M. Pettit. *Electronic Measurements*. McGraw-Hill, 1952.
(2 citations on 2 pages: 83 and 84)

[106] C. Wu, K. Zhang, G. Wei, and J.D. Xu. Applying critical-points method in the presence of phase shift due to feed line. *Progress In Electromagnetics Research M*, 5:15–23, 2008.
(1 citation on page 83)

[107] J. D. Kraus and R. Marhefka. *Antennas for all Applications*. McGraw-Hill, 2001.
(7 citations on 6 pages: 84, 115, 139, 142, 143, and 145)

[108] S. Schelkunoff. *Antennas: Theory and Practice*. Chapman and Hall, 1952.
(3 citations on 2 pages: 84 and 131)

[109] S.A. Schelkunoff. *Electromagnetic Waves*. Van Nostrand Company, 1944.
(2 citations on 2 pages: 85 and 131)

[110] R. W. Anderson. S-parameter techniques for faster, more accurate network design. Application note, Hewlett Packard, 1968.
(1 citation on page 90)

[111] F. Caspers. CERN accelerator school: RF for accelerators. In *CERN Accelerator School*, 2010.
(2 citations on 2 pages: 90 and 91)

[112] J.E. Aitken. Swept-frequency microwave Q-factor measurement. *Electrical Engineers, Proceedings of the Institution of*, 123(9):855–862, 1976.
(1 citation on page 90)

[113] J. Bird. *Electrical Circuit Theory and Technology, Second Edition*. Newnes, 2003.
(1 citation on page 99)

[114] **R.M. Craven**, I.R. Smith and B.M. Novac. A study of resonator designs for the two-coil Tesla coil. In *UK pulsed power symposium*. Loughborough University, UK, paper P.3, March

2011.
(1 citation on page 112)

[115] **R.M. Craven**, I.R. Smith and B.M. Novac. Optimizing the secondary coil of a Tesla transformer to improve spectral purity. *Plasma Science, IEEE Transactions on*, 42(1):143–148, 2014.
(1 citation on page 112)

[116] **R.M. Craven**, I.R. Smith and B.M. Novac. Quality factor measurements of air-cored solenoids. In *Electronics Letters*. The IET, in preparation.
(1 citation on page 112)

[117] **R.M. Craven**, I.R. Smith and B.M. Novac. Novel secondary windings for Tesla transformers. In *UK pulsed power symposium*. Loughborough University, UK, accepted for inclusion March 2014.
(1 citation on page 112)

[118] **R.M. Craven**, I.R. Smith and B.M. Novac. Improvements to secondary windings of Tesla transformers. In *IEEE International Power Modulator and High Voltage Conference (IPMHVC)*, Santa Fe, New Mexico, USA, submitted for inclusion June 2014.
(1 citation on page 112)

[119] T. H. Hubing. Survey of numerical electromagnetic modelling techniques. http://www.cvel.clemson.edu/pdf/tr91-1-001.pdf, 1991.
(2 citations on 2 pages: 117 and 118)

[120] F. Langford-Smith. *Radio Designer's Handbook*. Iliffe and Sons, 1957.
(3 citations on 3 pages: 122, 123, and 137)

[121] K.L. Corum and J.F. Corum. Application of transmission line resonators to high voltage RF power processing: history, analysis and experiment. In *Proceedings of the 19th Annual Southeastern Symposium on System Theory: SSST*, 1987.
(2 citations on 2 pages: 132 and 133)

[122] H. B. Dwight. *Electrical Coils and Conductors: their Electrical Characteristics and Theory*. McGraw-Hill, 1945.

(1 citation on page 136)

[123] P. Sarkar, B.M. Novac, I.R. Smith, and G. Louverdis. 2D modelling of skin and proximity effects in Tesla transformers. In *IEEE International Power Modulators and High Voltage Conference, Proceedings of the 2008*, pages 268–271, 2008.
(1 citation on page 136)

[124] E. Fraga, C. Prados, and D. X. Chen. Practical model and calculation of AC resistance of long solenoids. *Magnetics, IEEE Transactions on*, 34(1):205–212, 1998.
(1 citation on page 137)

[125] G. S. Smith. Proximity effect in systems of parallel conductors. *Journal of Applied Physics*, 43(5):2196–2203, 1972.
(1 citation on page 137)

[126] L. L. Langton. *Radio-Frequency Heating Equipment*. Pitman and Sons, 1949.
(1 citation on page 137)

[127] Agilent. Split post dielectric resonators for dielectric measurements of substrates. http://cp.literature.agilent.com/litweb/pdf/5989-5384EN.pdf, February 2013.
(1 citation on page 137)

[128] J. Krupka and R. N. Clarke. Split post dielectric resonator technique for precise measurements of laminar dielectric specimens - measurement uncertainties. In *13th International Conference on Microwaves, Radar and Wireless Communications*, volume 1, pages 305–308, 2000.
(1 citation on page 137)

[129] D. Miley and J. Beyer. Field analysis of helical resonators with constant-bandwidth filter application. *Parts, Materials and Packaging, IEEE Transactions on*, 5(3):127–132, 1969.
(1 citation on page 139)

[130] D. Atkins. IGDS Msc in EMC and RF communications: Electrically Small Antennas. Master's thesis, University of York, March 2004.
(1 citation on page 139)

[131] IEEE. Standard definitions of terms for antennas, 1993.
(2 citations on 2 pages: 139 and 140)

[132] H.A. Wheeler. Small antennas. *Antennas and Propagation, IEEE Transactions on*, 23(4):462–469, 1975.
(2 citations on 2 pages: 139 and 142)

[133] IEEE. Standard test procedures for antennas, 1980.
(2 citations on 2 pages: 140 and 141)

[134] J. S. Seybold. *Introduction to RF Propagation*.
Wiley-Interscience, 2005.
(2 citations on 2 pages: 140 and 141)

End Note

The electronic PDF version of this thesis contains internal “clickable” hyperlinks between the various chapters and sections and so on. All references are similarly hyperlinked; the end of each reference entry shows the “back references”, which hyperlink back to the referring page(s) where the reference is cited. All URLs were verified correct as of January 2014.